POLITECNICO DI MILANO

Corso di Laurea Magistrale in Ingegneria Biomedica

Scuola di Ingegneria Industriale e dell'Informazione

Dipartimento di Elettronica, Informazione e Bioingegneria

Tesi di Laurea Magistrale

DEVELOPMENT AND ASSESSMENT OF A PERICARDIAL TRANSCATHETER VALVE

Adviser: Prof. Alberto REDAELLI

Co-Adviser: Prof. Gaetano BURRIESCI

Thesis by:

Benedetto D'ANTICO 781440

Simone MAZZOLA 784180

Academic Year 2012 -2013

CONTENTS

Index of figures

Sommario

Summary

Introduction

State of the art

Materials and Methods

Results and Discussions

Conclusion and Future Developments

Index of Tables

Sommario

Summary

Results and discussions

Ringraziamenti

La prima persona a cui va il mio ringraziamento è mia nonna Francesca. Senza di Lei non sarei la persona che sono oggi e probabilmente il professionista che sarò domani. Le cose più importanti che ho imparato da Lei sono state il valore del denaro e la possibilità di ottenere ciò che si vuole dalla vita a patto di volerlo e impegnarsi a fondo. A lei va il mio ringraziamento più grande per avermi regalato una mamma da sogno che mi ha educato, sostenuto e ha fatto di tutto per farmi studiare e farmi seguire la strada che volevo prendere. Lei mi ha sempre aiutato e mi è stata vicina in tutto il mio percorso, specialmente nei momenti difficili. Spero di continuare ad imparare da lei ogni giorno. Sei grande mamma!!

Agli amici più stretti che mi sono stati vicini sin da piccolo e che mi accolgono con calore ogni volta che ritorno a casa: Antonio e mio cugino Angelo per primi.

Ai nuovi amici che ho trovato a Milano e che hanno reso questi 5 anni valevoli dello sforzo compiuto per arrivare fin qui. Ogni, Pier Carlo, Alessia, Chiara e Juliana a cui va il mio saluto fino in Brasile.

Alle persone che ho conosciuto a Londra e che hanno contribuito a rendere ancor più speciale una città che per me già lo era. A Simone con cui ho condiviso 6 mesi tra i più belli della mia vita nonché giornate interminabili in laboratorio e in ufficio. Al Prof. Redaelli e Prof. Burriesci che hanno permesso il realizzarsi di questa indimenticabile esperienza.

Alle nuove persone che incontrerò e che mi vorranno bene e alla Donna che saprà amarmi e volermi bene perché se sono quello che sono devo ringraziare anche chi ancora non conosco perché il pensiero di incontrarli mi prepara ad essere quello che sarò.

E come dicono gli Inglese, last but not least, a Me stesso.

Benedetto D’Antico

Ringraziamenti

Desidero ringraziare innanzitutto i Prof. Burriesci e Redaelli che hanno permesso il concretizzarsi di questa indimenticabile esperienza in terra inglese, fruttuosa sia dal punto di vista culturale/universitario sia dal punto di vista umano e per avermi infuso grande interesse nel settore cardiovascolare.

Un pensiero (nostalgico) và a tutti gli amici conosciuti a Londra, alla Callan School e in ufficio/dipartimento che hanno allietato le nostre serate londinesi.

Un grazie speciale lo dedico a Benedetto, per avermi insegnato ad amare Londra e per aver condiviso le gioie e le fatiche durante questi mesi di lavoro.

Un grazie INFINITO ai miei genitori, Giancarlo e Graziella, per avermi sempre sostenuto durante tutto il percorso di studi, dalle scuole elementari ad ora, sia praticamente sia finanziariamente. Un grazie non meno importante anche per la vostra assoluta generosità e per i valori che mi avete insegnato e che continuerete ad insegnarmi.

Grazie a tutti i parenti che mi sono stati vicini in questi anni, a Lara, a Pietro e alle due cucciole Talisa e Noemi, che mi mostrano ogni giorno i valori della spensieratezza e della gioia per le piccole cose quotidiane, valori che noi adulti abbiamo purtroppo perso.

Grazie anche ai compagni di corso conosciuti al Poli e agli amici di tutti i giorni.

Come potrei dimenticarmi poi della mia Debora…..grazie per non avermi mai fatto pesare i 6 mesi di lontananza, grazie dell'amore che ogni giorno mi dimostri e che proseguirà fino all'infinito. Grazie per farmi sentire importante e amato ogni secondo.

Simone Mazzola

Sommario

1 Introduzione

Il cuore ha quattro camere (atrio destro, ventricolo destro, atrio sinistro e ventricolo sinistro) e quattro valvole (tricuspide, polmonare, mitrale e aortica) (Figura 1); la valvola aortica si trova tra il ventricolo sinistro e l' aorta. Durante la sistole del ventricolo sinistro (contrazione), la pressione al suo interno aumenta fino a superare la pressione sistolica nell'aorta. A questo punto della sistole, la valvola aortica si apre, il sangue esce dal ventricolo sinistro e fluisce nella circolazione sistemica attraverso l'aorta. Successivamente, durante la diastole, la pressione nel ventricolo sinistro diminuisce e la pressione in aorta forza la valvola aortica nella posizione chiusa [3].

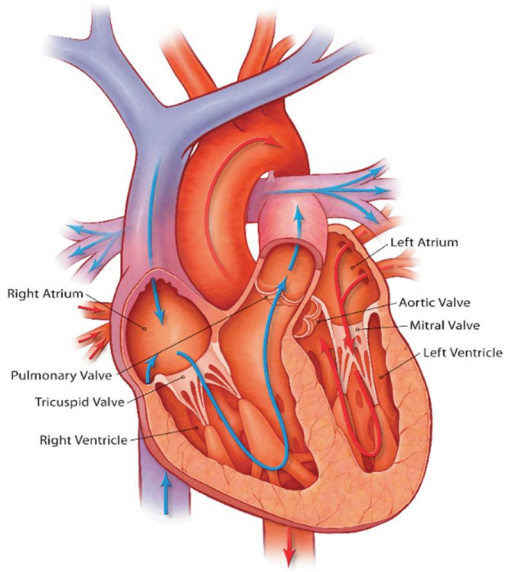

Figura 1: Anatomia del cuore umano in cui vengono mostrate le quattro camere (atrio sinistro e destro e ventricolo sinistro e destro) e le quattro valvole principali (mitrale, tricuspide, aortica e polmonare). La valvola aortica si trova tra il ventricolo sinistro e l'aorta.

La maggiore incidenza di valvulopatia degenerativa dovuta alla maggiore aspettativa di vita è uno dei motivi dell'alto tasso di patologie a carico della valvola aortica nei paesi sviluppati.La chirurgia a cuore aperto convenzionale per la sostituzione di valvole

cardiache prevede la sternotomia parziale o completa con circolazione extra-corporea e arresto cardiaco. La sostituzione della valvola aortica mediante chirurgia a cuore aperto è associata ad elevata mortalità (dal 10% al 50%) nei pazienti ad alto rischio con gravi comorbidità [13].

Negli ultimi anni si è verificato un deciso miglioramento delle tecniche chirurgiche al fine di estendere il trattamento ad un numero sempre maggiore di pazienti anziani con gravi comorbidità, cioè pazienti ad alto rischio per la chirurgia di sostituzione valvolare tradizionale. Una grande varietà di procedure chirurgiche minimamente invasive sono state sviluppate dai vari gruppi di ricerca negli ultimi anni [17]. In generale, lo scopo di queste tecniche è quello di minimizzare il trauma chirurgico globale evitando sternotomia, circolazione extracorporea, arresto cardiaco e impiantando perciò la protesi nel cuore pulsante. L'impianto di valvola aortica transcatetere (TAV) è un nuovo approccio, recentemente introdotto come alternativa alla chirurgia tradizionale per la sostituzione della valvola aortica stenotica. Viene eseguito inserendo la valvola sostitutiva (biologica o sintetica) in situ accedendo attraverso il sistema vascolare. La valvola viene crimpata all'interno di un catetere (montata su uno stent a palloncino espandibile, su uno stent autoespandibile, o su entrambi) e, attraverso un filo guida, posizionata correttamente, monitorando il tutto tramite dispositivi di imaging [1]. Una volta raggiunta la posizione intracardiaca corretta, la valvola viene nuovamente espansa fino al raggiungimento del suo diametro finale (con sufficiente forza radiale per evitare perdite paravalvolari e migrazione della valvola) al fine di ripristinare la sua funzionalità.

Mentre i risultati in termini di sopravvivenza e di miglioramento dei sintomi sono simili tra i gruppi di pazienti che si sottopongono a sostituzione TAV sia con valvole CoreValve sia con valvole Edwards Sapien (Figura 2), si sono osservate differenze notevoli nelle

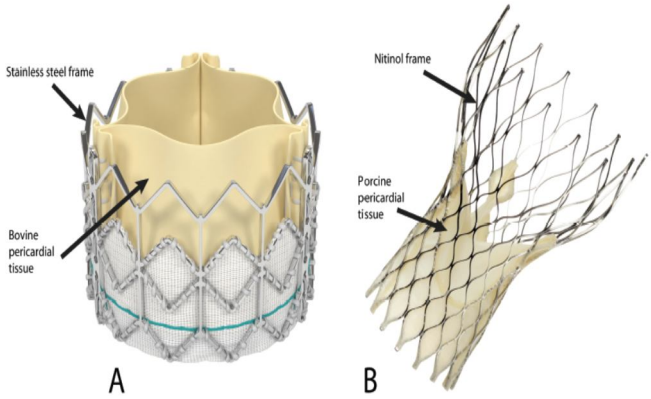

Figura 2 A: Valvola Edward Sapien completamente espansa. Figura 2B: Medtronic Core Valve completamente espansa

complicanze osservate in pazienti trattati con le due valvole.

La possibilità di regolare la posizione della valvola durante l'inserimento della CoreValve offre un netto vantaggio rispetto alla valvola Sapien. A causa dell'auto-espansione dello stent in Nitinol della CoreValve, essa può essere espansa in più fasi, consentendo regolazioni fini della posizione durante le fasi di espansione e della messa in posizione. Al contrario, la valvola Sapien viene rapidamente espansa con un palloncino a singola espansione che non consente di riposizionarla durante o dopo l'espansione.

I primi risultati di test clinici e sperimentali di sostituzione valvolare percutanea sono promettenti; tuttavia, la tecnica è ancora nella fase iniziale del suo sviluppo con inconfutabili problemi che devono essere risolti, come le perdite paravalvolari (PVL), il cui tasso risulta essere molto più alto dopo TAVI rispetto alla sostituzione chirurgica convenzionale della valvola aortica.

Scopo di questo lavoro è quello di realizzare nuove valvole con stent in Nitinol che superino le problematiche appena descritte, valutare gli indici valvolari ottenuti e confrontarli con quelli delle valvole attualmente in commercio. Inoltre, un'analisi computazionale è stata eseguita per analizzare la dinamica di apertura e di chiusura dei lembi valvolari. Questo tipo di analisi integrerà le osservazioni cliniche e sperimentali con lo studio degli sforzi sulla superficie dei foglietti valvolari.

2 Materiali e Metodi

Le valvole da noi realizzate sono costituite da uno stent in Nitinol prodotto da UCL e da foglietti valvolari con alette di contenimento integrati in un unico modello.

Stent e leaflets saranno in primo luogo descritti per quanto riguarda forma e materiale; seguirà poi la descrizione della nuova TAV.

2.1 Stent

Lo stent è stato sviluppato da UCL con la collaborazione dell'Ospedale UCLH ed è stato per la prima volta impiantato in un modello ovino nel Maggio del 2013 [2]. Il materiale

utilizzato per la sua realizzazione è il Nitinol: a causa della sua natura autoespandibile, può essere espanso in fasi che consentano regolazioni fini durante le fasi di espansione. Il design auto-espandibile offre molti altri potenziali vantaggi rispetto a un dispositivo espandibile a palloncino. Infatti una valvola aortica percutanea autoespandibile può minimizzare il verificarsi di perdite paravalvolari e consentire il trattamento di pazienti con insufficienza aortica. In secondo luogo, evitando il trauma causato dal palloncino sui lembi della valvola, il design autoespandibile può teoricamente prolungare la durata della valvola. Tre diverse dimensioni dello stent sono state realizzate: 23 mm, 26 mm e 29 mm. In questa tesi focalizzeremo la nostra attenzione sulla taglia 26 millimetri.

Quattro diverse prospettive dello stent da 26 millimetri sono rappresentate in Figura 3.

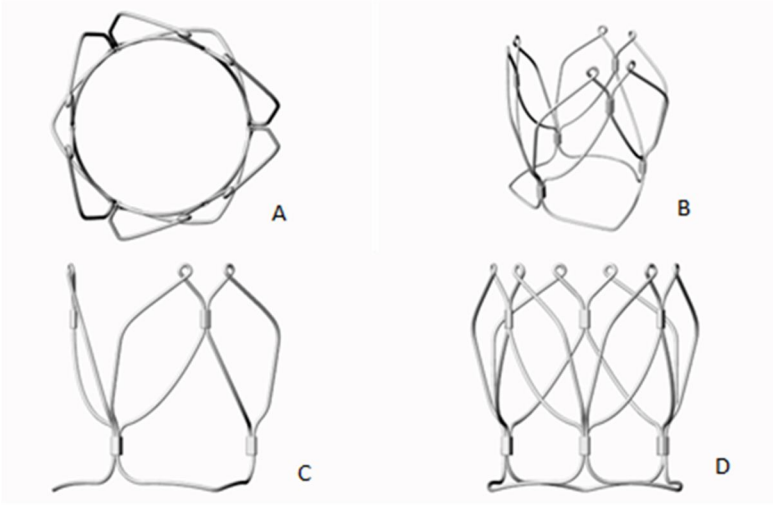

Figura 3: Stent 26 mm da diverse prospettive

2.2 Leaflets

2.2.2 Materiali

I leaflets sono stati realizzati in pericardio, un materiale composito costituito da una matrice amorfa di proteine e polisaccaridi in complessi macromolecolari idratati e contenente fasci multidirezionali di fibre di collagene ed elastiche aventi direzioni preferenziali [38]; tale materiale è biocompatibile ed emocompatibile.

Inoltre, un nuovo pericardio decellularizzato è stato utilizzato per la realizzazione di altre valvole con la stessa geometria di quelle realizzate in pericardio standard. Tale tessuto proviene da un'azienda del settore, intenzionata a testare il proprio tessuto su di una valvola aortica.

2.2.3 Forma

La forma utilizzata per la valvola precedentemente realizzata da UCL era composta da due parti separate: i leaflets e le ali (Figura 4). Tale configurazione ha richiesto la cucitura delle ali al profilo dei leaflets.

Figura 4A : forma delle ali

Figura 4B : forma leafltes

Per la realizzazione delle nostre valvole abbiamo scelto di utilizzare una forma con entrambe le parti integrate (disponibile presso il Dipartimento di Ingegneria Meccanica UCL), composta cioè dai leaflets nella parte interna e dalle ali nel profilo esterno.

Il modello utilizzato è mostrato in Figura 5.

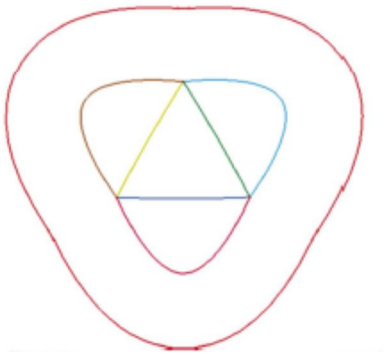

Figura 5: Modello di leafltes e ali: i tre triangoli al centro della figura rappresentano i leaflets mentre la forma più esterna rappresenta le ali.

Al fine di acquisire pratica con tale forma, abbiamo innanzitutto realizzato dei leaflets in pelle di daino, semplicemente posizionando la forma dei leaflets fatta di carta sul tessuto e suturando lungo la forma. Mediante immersione in acqua è stato possibile rimuovere la carta e ottenere la forma desiderata. Successivamente è stato utilizzato il pericardio.

Per effettuare un taglio più preciso e per evitare i problemi correlati alla difficoltà di maneggiare tale tessuto, è stato necessario realizzare un supporto in plastica utilizzando il taglio laser.

Il supporto in plastica viene visualizzato in Figura 6.

Figura 6: Supporto in plastica realizzato mediante taglio laser

Al fine di ottenere la forma dei leaflets in pericardio, una pezza del tessuto è stata posta tra due supporti di plastica; ago e filo sono stati utilizzati per tracciare la forma dei leaflets (Figura 7).

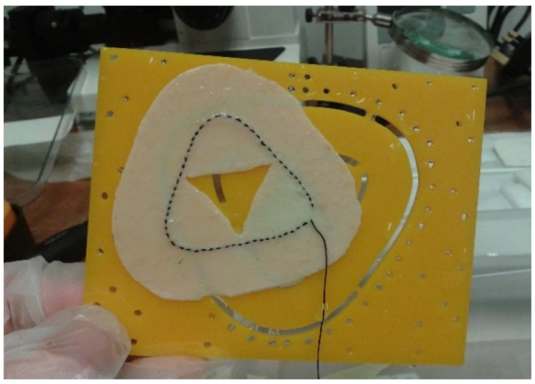

Figura 7: leaflets in pericardio ottenuti dopo la cucitura

2.3 Realizzazione della Valvola

La forma dei leaflets è stata piegata sullo stent e cucita con ago e filo per ottenere la valvola. Con riferimento ai leaflets in pericardio decellularizzato, i passaggi seguiti per la realizzazione delle valvole sono così riassumibili:

• è stato posato il tessuto su uno stampo in silicone che rappresenta il negativo della valvola (Figura 8). Questo permette di mantenere la struttura ferma mentre viene suturata allo stent (Figura 9).

• con ago e filo è stato suturato ogni punto allo stent mediante un punto Asola. Questa sutura garantisce che, anche se il filo dovesse cedere in un punto, il difetto creatosi non venga propagato.

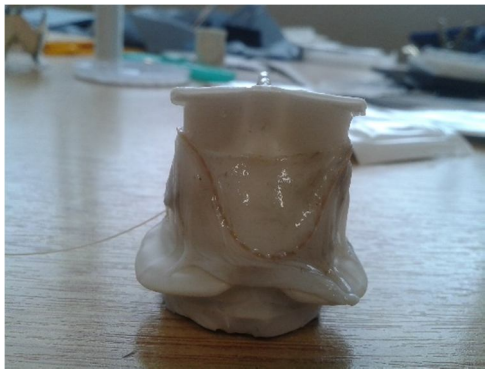

Figura 8: tessuto sullo stampo della valvola

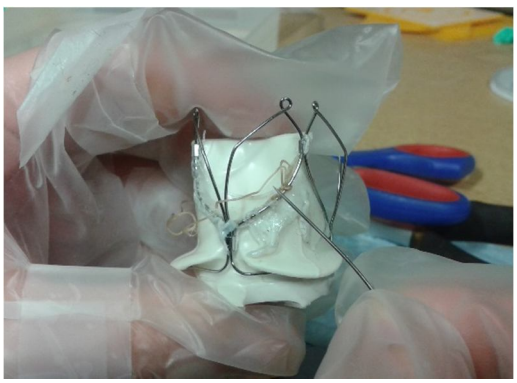

Figura 9: sutura del tessuto allo stent

Sono stati cosi ottenuti i lembi cuciti allo stent (Figura 10) e poi le ali (Figura 11) :

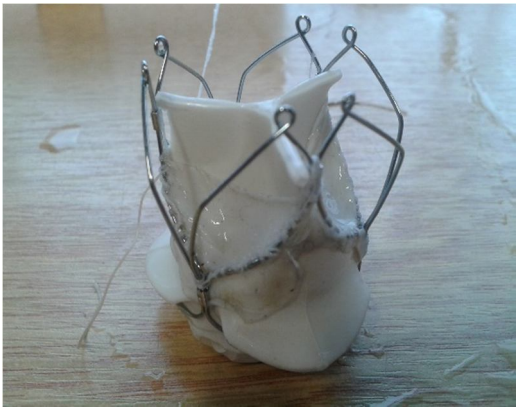

Figura 10: leaflets cuciti allo stent

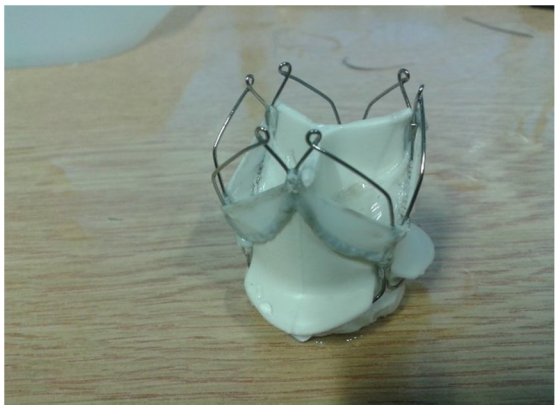

Figura 11: ali e leaflets cuciti allo stent

La valvola finale è rappresentata in Figura 12:

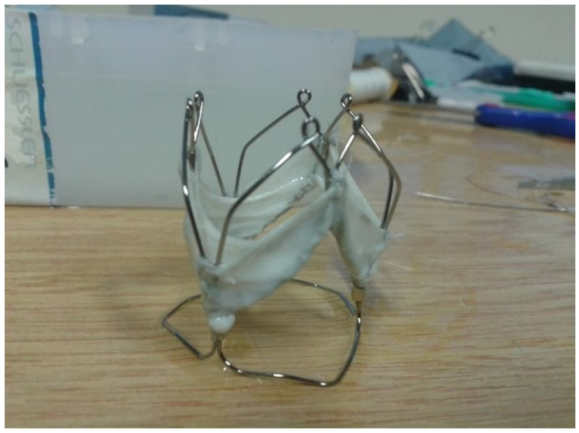

Figura 12: Valvola in pericardio decellularizzato con leaflets e ali

2.4 Proprietà meccaniche del tessuto

Al fine di ottenere le proprietà meccaniche dei tessuti utilizzati per realizzare i leaflets, il pericardio standard e il pericardio decellularizzato sono stati testati in laboratorio attraverso prove di trazione.

In Figura 13 e 14 sono rappresentati i grafici di sforzo e deformazione ottenuti dalla prova di trazione.

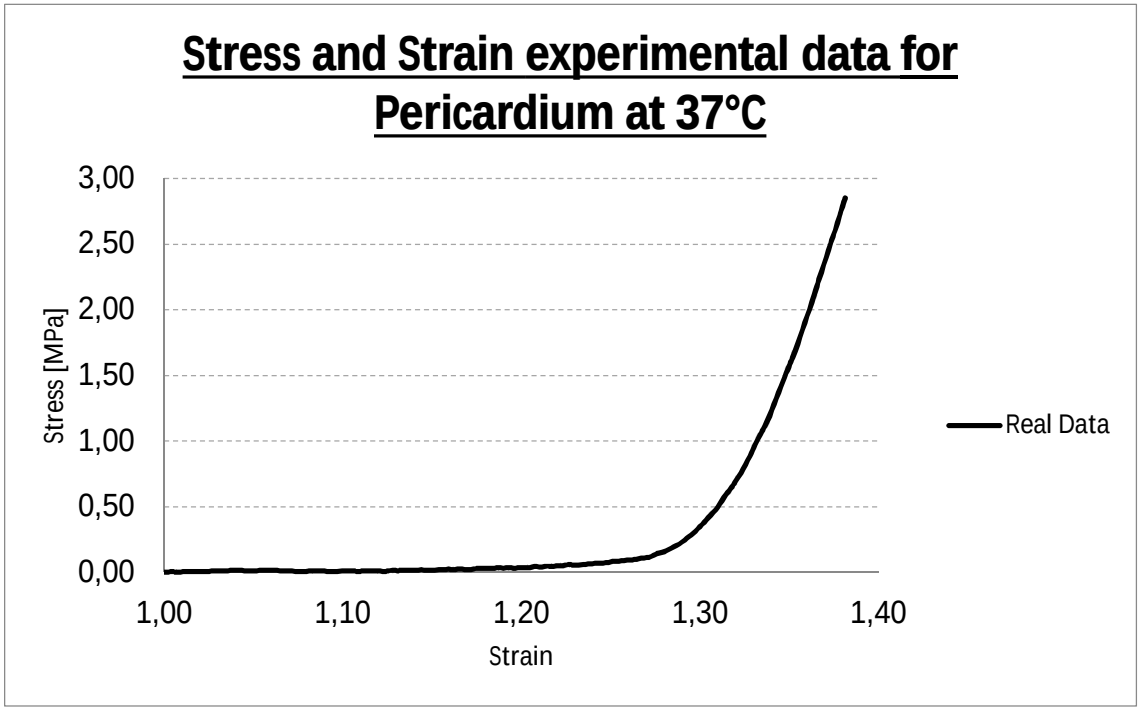

Figura 13: dati sperimentali del pericardio ottenuti a 37°C

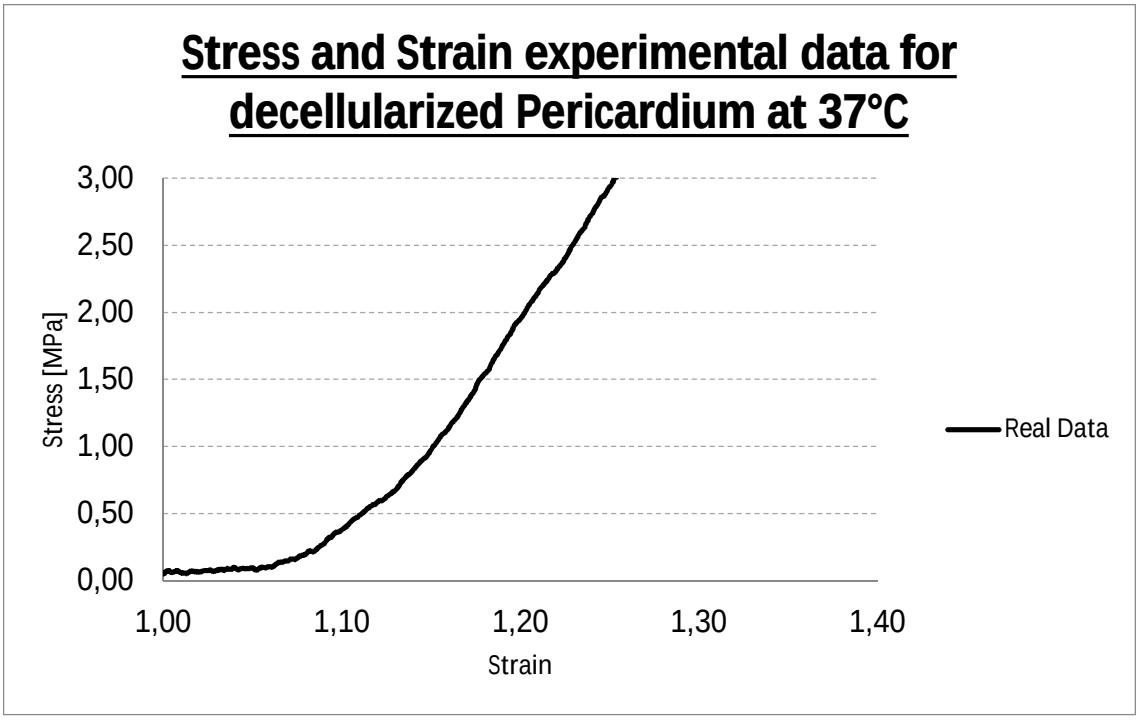

Figura 14 : dati sperimentali del pericardio decellularizzato ottenuti a 37°C

2.5 Banco prova

Al fine di testare la nostra valvola in un ambiente il più simile possibile al cuore umano e secondo lo standard ISO, è stato utilizzato il duplicator Pulse ViVitro, ampiamente utilizzato come sistema di prova idrodinamico cardiovascolare. Si compone di ViVitro Model Left Heart, di SuperPump e sistema di acquisizione dati ViViTest.

I componenti nel loro complesso consentono di valutare le prestazioni delle protesi valvolari cardiache nelle condizioni simulate. Sono state testate 3 valvole: una in pelle di daino per finalità di training e da cui non sono stati pertanto acquisiti i risultati, una in

pericardio standard e un'altra in pericardio decellularizzato. La stessa valvola pericardica è stata testata una seconda volta con i leaflets accorciati. Tali valvole sono poi state confrontate con altre valvole commerciali testate precedentemente sullo stesso banco prova dal gruppo di ricerca.

2.5 Analisi computazionale

Al fine di combinare prove sperimentali con analisi delle sollecitazioni sulla superficie dei leaflets, sono state eseguite simulazioni computazionali. Il codice ad elementi finiti utilizzato è stato Ls- Dyna.

In questa tesi le simulazioni numeriche riguardano:

• Simulazioni della sutura dei leaflet allo stent;

• Simulazioni di dinamica strutturale di apertura e chiusura dei lembi per analizzarne gli sforzi.

2.5.1 Simulazioni di sutura dei leaflet allo stent e simulazioni di dinamica

Come primo passo è stato necessario realizzare il collegamento dei leaflet con lo stent mediante dei fili. In seguito sono state eseguite simulazioni al fine di ottenere il posizionamento dei leaflet sullo stent utilizzando materiali, in una prima fase, non rappresentativi delle caratteristiche reali del pericardio.

Nei prossimi paragrafi saranno descritti i materiali, le geometrie del modello e il protocollo di simulazione adottato.

2.5.1.1 Materiali

Il primo materiale utilizzato per modellizzare i leaflets è stato il materiale elastico plastico termico, con una densità pari a 1000 Kg/m^3, coefficiente di Poisson pari a 0,495 e modulo di Young pari a 200 MPa. Partendo dal posizionamento ottenuto, una nuova simulazione è

stata eseguita con un materiale elastico plastico termico con modulo di Young pari a 2 MPa. Lo stent è stato considerato rigido mentre il materiale elastico plastico termico è stato attribuito ai fili, per la possibilità di assegnare proprietà termiche al fine di ottenerne l'accorciamento; in particolare, sono stati attribuiti ai fili elevati coefficienti di dilatazione termica e elevati (seppur negativi) coefficienti di generazione del calore.

Durante le simulazioni di dinamica i fili e lo stent sono stati rimossi e ai leaflet sono stati attribuiti i seguenti materiali:

- materiale elastico con modulo di Young pari a 2 MPa e coefficiente di Poisson pari a 0,495;
- materiale pericardio (i risultati ottenuti dalle prove di trazione sono stati interpolati con un modello Ogden, Figura 15);
- materiale pericardio decellularizzato (come per il pericardio, i risultati ottenuti dalle prove di trazione condotte sul pericardio decellularizzato sono stati interpolati con un modello Ogden, Figura 16).

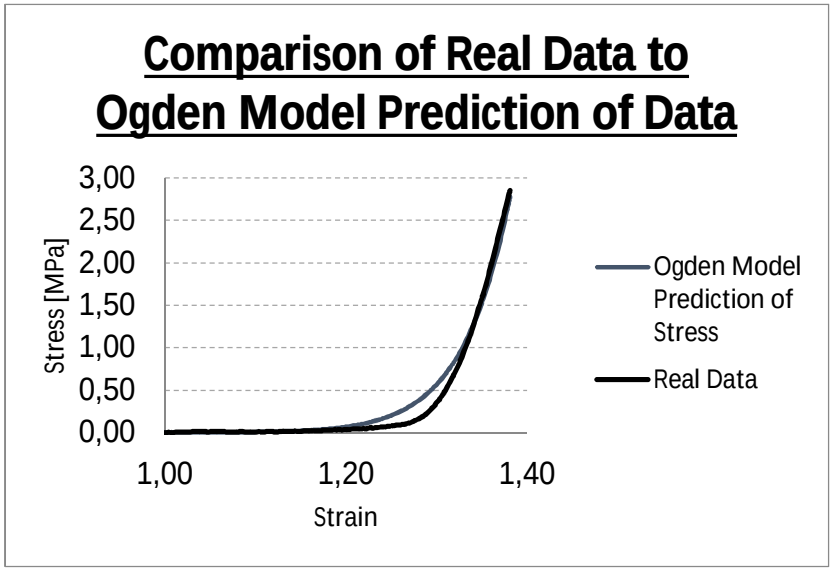

Figura 15 : interpolazione dei dati sperimentali ottenuti mediante modello di Ogden per pericardio standard

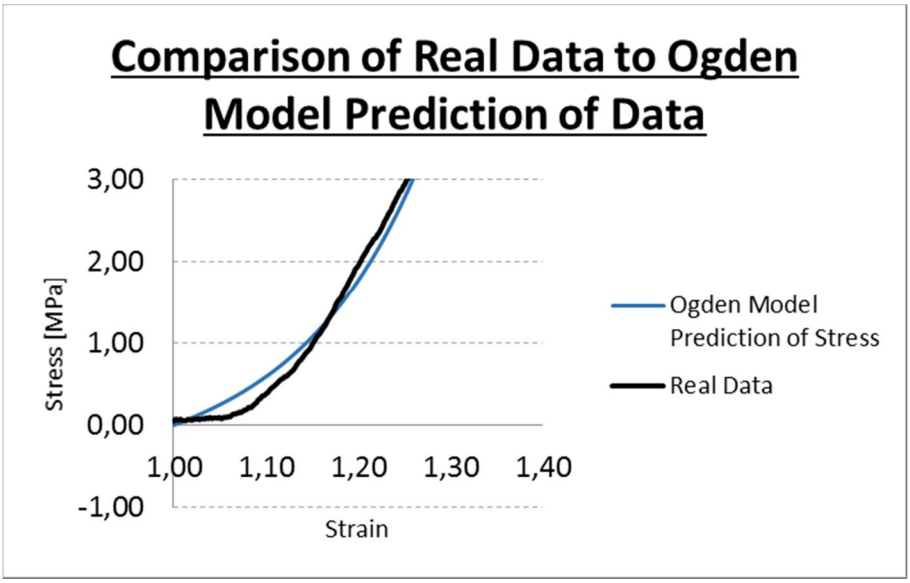

Figura 16 : interpolazione dei dati sperimentali ottenuti mediante modello di Ogden per pericardio decellularizzato

2.5.1.2 Geometria del modello

Il modello dei leaflets utilizzato per l'analisi computazionale è lo stesso utilizzato per la realizzazione delle valvole, ma privo delle ali (le finalità del modello computazionale sono la valutazione degli sforzi sulla superficie dei leaflets, Figura 17) .

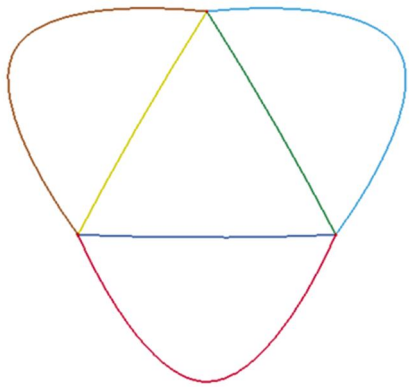

Figura 17: modello dei leaflets senza le ali, usato nel modello computazionale

Per quanto riguarda lo stent, è stato rappresentato solo il profilo su cui i leaflets sono cuciti (Figura 18). Nel modello computazionale, infatti, lo stent è solo un riferimento per il

posizionamento dei lembi durante la simulazione di sutura. Perciò, la geometria rappresenta solo tre cuspidi e non considera l'intera complessità dello stent utilizzato nella realizzazione delle valvole.

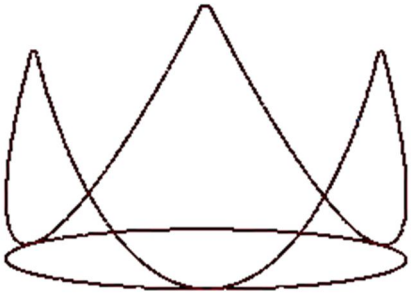

Figura 18: profilo di stent utilizzato nel modello di calcolo.

Sia per i leaflets sia per il modello di stent, la geometria è stata discretizzata in elementi triangolari con dimensione pari a 1 mm; questa scelta è stata considerata la migliore al fine di massimizzare il rapporto tra accuratezza e tempi di calcolo. Le mesh ottenute sono rappresentate in Figura 19.

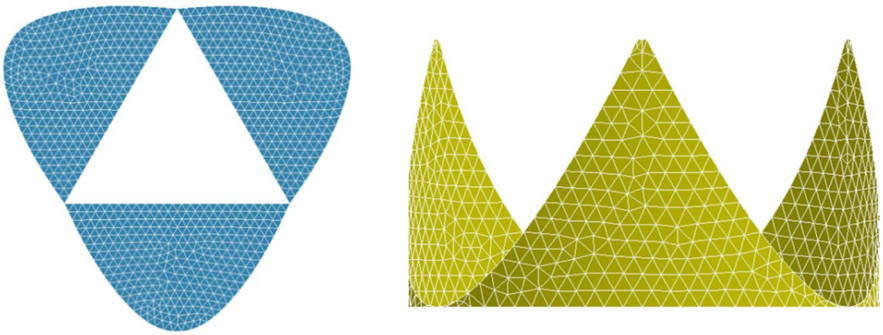

Figura 19 : leaflets e stent discretizzati in elementi triangolari

Lo spessore assegnato allo stent è stato pari a 0,4 mm mentre per i leaflets sono stati realizzati due diversi modelli: il primo con spessore pari a 0,4 mm e rappresentativo del pericardio e il secondo con spessore pari a 0,1 mm e rappresentativo del pericardio decellularizzato, molto più sottile del pericardio standard.

2.5.1.3 Protocollo di simulazione

Il primo passo per simulare la sutura tra i leaflets e lo stent è stato collegare la geometria dello stent con la geometria dei leaflets mediante dei fili. Per fare questo, abbiamo scelto elementi solidi tetraedrici (Figura 20).

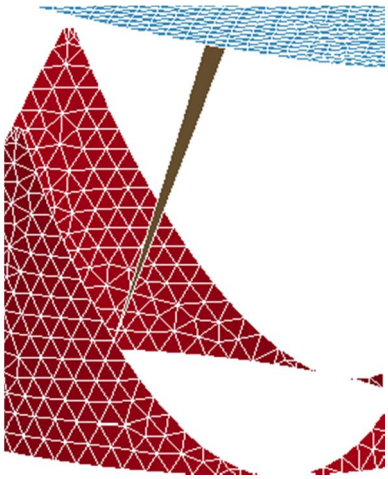

Figura 20: esempio di filo che collega stent e leaflets insieme

Il posizionamento ottenuto con la simulazione ha mostrato un notevole gap tra i leaflet e lo stent, come mostrato di seguito (Figura 21).

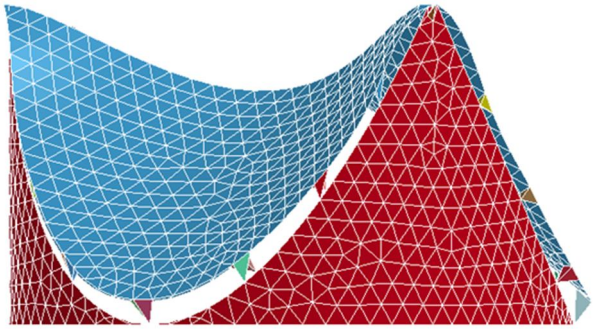

Figura 21: il primo posizionamento mostra un divario tra stent e leaflets

Per ottimizzarne la configurazione, un'altra simulazione è stata eseguita a partire dalla geometria ottenuta. Così, sono stati esportati gli elementi e le coordinate nodali e una nuova simulazione è stato eseguita impostando un modulo di Young per i leaflets pari a 2 MPa.

Il posizionamento ottenuto da questa simulazione è mostrato in Figura 22.

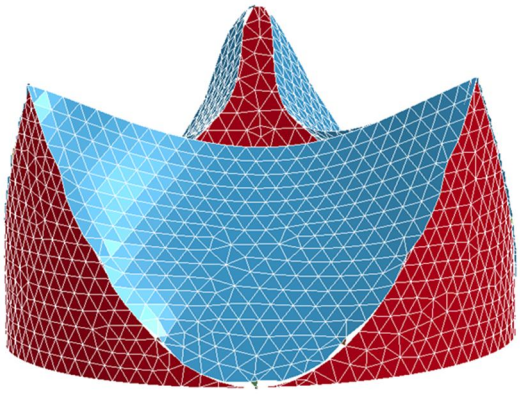

Figura 22: posizionamento finale dei leaflets

Il posizionamento della valvola mostrato nella Figura 22 è rappresentativo della forma nominale della valvola. Tuttavia, le valvole impiantate nel corpo e le valvole testate in laboratorio sono sempre compresse alla parete. A questo scopo abbiamo scelto di rappresentare, in modo semplificato, la valvola in due ulteriori diverse configurazioni: quella assunta una volta posizionata in una radice aortica da 23 mm (valvola Crimp23) e quella assunta se posizionata in una radice aortica da 21 mm (valvola Crimp21).

Partendo dai posizionamenti ottenuti per le tre diverse configurazioni della valvola, gli elementi e le coordinate nodali sono stati esportati in nuovi file di input al fine di analizzare la dinamica di apertura e di chiusura dei foglietti valvolari; in particolare la curva di pressione utilizzata (rappresentata in Figura 23) raggiunge il valore diastolico pari a 0,01333 MPa (100 mmHg) in 0,3 s e rimane costante per 0,5 s quando raggiunge il valore sistolico pari a -0,001333 MPa (- 10 mmHg).

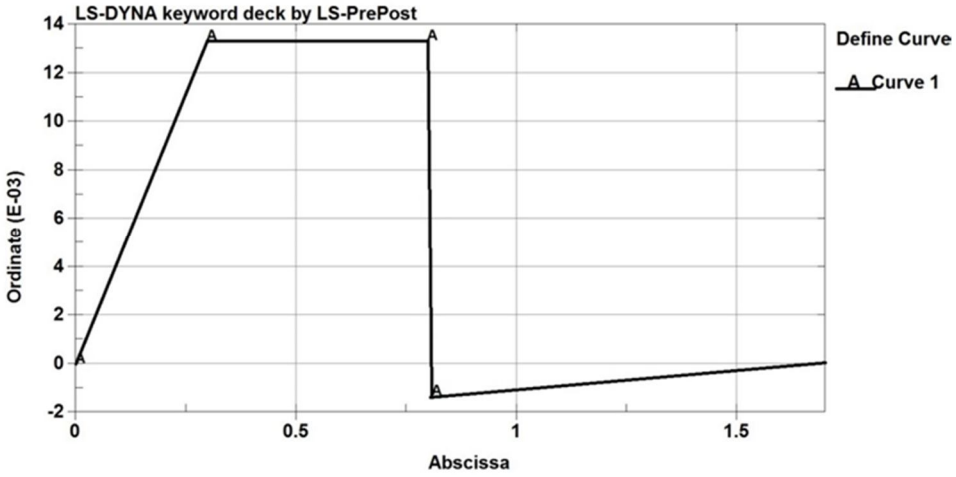

Figura 23 : Pressione tempo variabile applicata sui leaflets

3 Risultati e discussioni

3.1 Risultati sperimentali

Il confronto tra i diversi tipi di valvole e tra le stesse valvole posizionate nelle diverse radici aortiche è stato valutato al fine di confrontare le diverse cadute di pressione transvalvolare, le perdite di volume, la frazione totale di rigurgito, l'EOA, le perdite di energia totale e di iniezione, il volume di rigurgito a valvola chiusa e la sua perdita energetica. Nelle seguenti figure, sono mostrati alcuni dei confronti tra i diversi tipi di valvole (Figure 24-25-26-27), in particolare confrontiamo le valvole da noi realizzate con quelli commerciali. Tutti i risultati completi sono riportati nel capitolo Risultati e discussioni. Le valvole sono state testate in radici di diametro pari a 21 mm e 23 mm. Soltanto la valvola realizzata in pericardio decellularizzato non è stata testata nelle radici da 23 mm per problemi legati alla dimensione dei lembi valvolari, realizzati con una pezza fornitaci dall'azienda troppo piccola. Il test statistico tStudent è stato eseguito per la significatività dei dati.

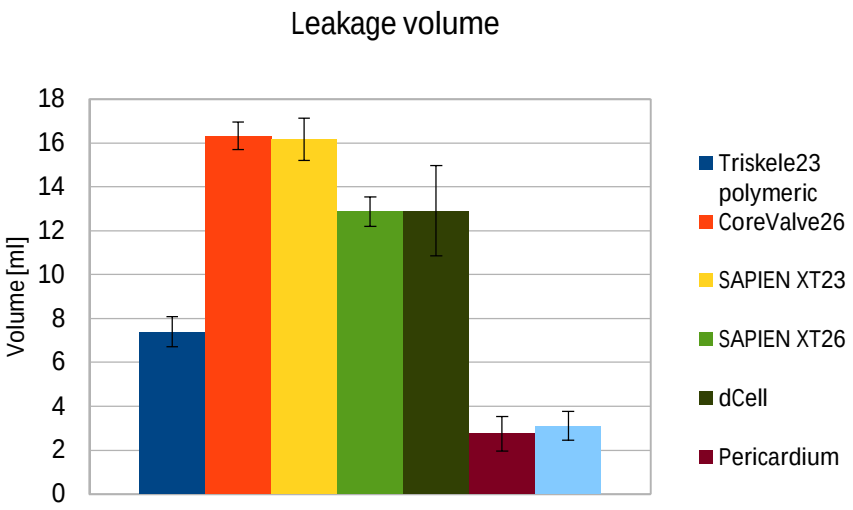

Figura 24: Leakage volume - 21 mm a CO = 5 l/min. Secondo il test tStudent, la differenza tra il valor medio delle valvole di controllo e quello delle valvole in pericardio è significativo con p uguale a 3.08%

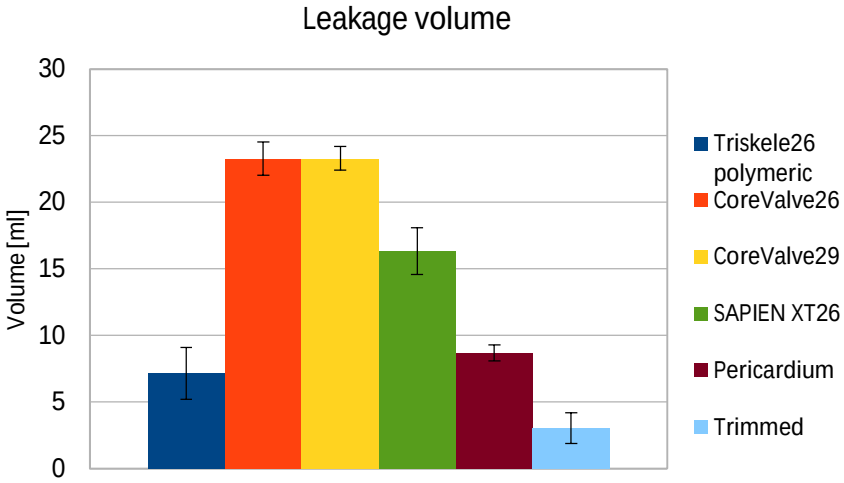

Figura 25: Leakage volume - 23 mm a CO = 5 l/min. Secondo il test tStudent, la differenza tra il valor medio delle valvole di controllo e quello delle valvole in pericardio è significativo con p uguale a 12.39%

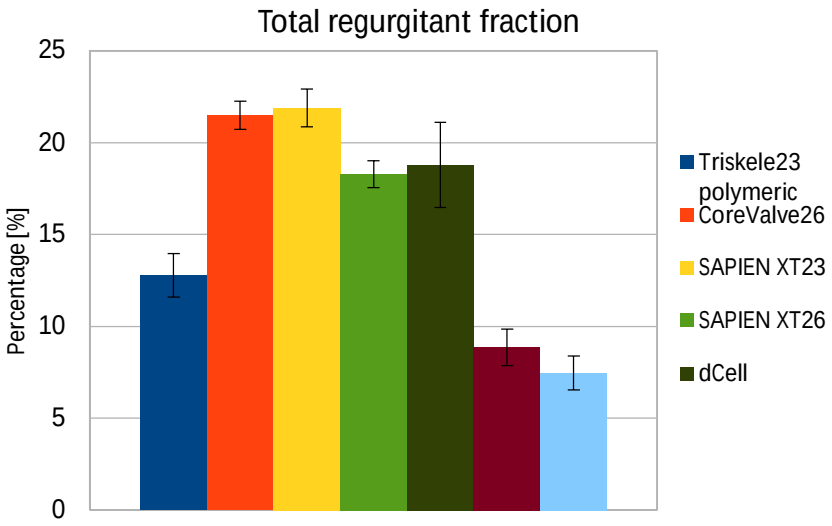

Figura 26: Total regurgitant fraction - 21 mm a CO = 5 l/min. Secondo il test tStudent, la differenza tra il valor medio delle valvole di controllo e quello delle valvole in pericardio è significativo con p uguale a 3.05%

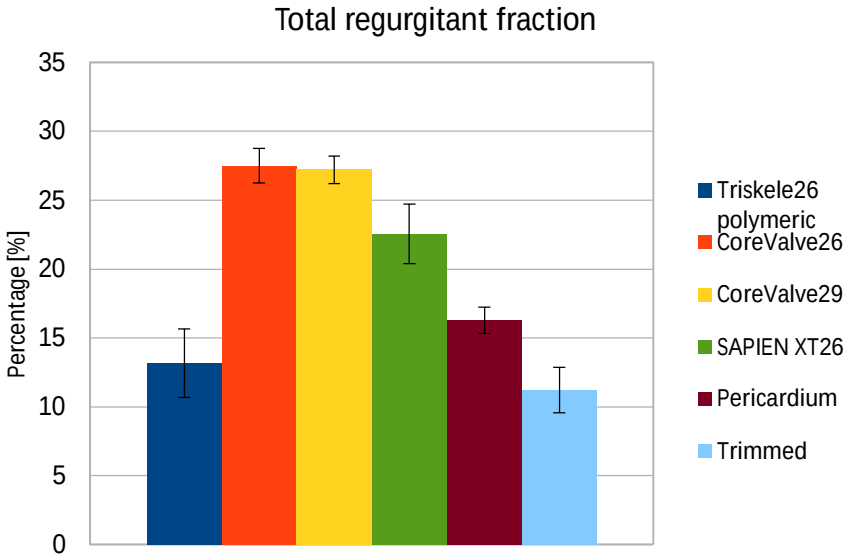

Figura 27: Total regurgitant fraction - 23 mm a CO = 5 l/min. Secondo il test tStudent, la differenza tra il valor medio delle valvole di controllo e quello delle valvole in pericardio è significativo con p uguale a 16.7%

Il rigurgito rappresenta il volume di fluido che tende a tornare nel ventricolo durante la fase diastolica del ciclo cardiaco. E' direttamente correlato alla dimensione della valvola e alla normale configurazione dei leaflets in assenza di pressione idraulica. Secondo alcuni studi [41], valvole bioprotesiche suine mostrano risultati in termini di rigurgito superiori rispetto a quelle bovine, beneficiando della loro relativamente chiusa configurazione dei leaflets.

Il rigurgito aortico ottenuto con valvola pericardica è il più basso in qualsiasi configurazione rispetto alle valvole commerciali, rappresentando un ottimo risultato ottenuto in questo lavoro. La valvola ha infatti un rigurgito di circa 2 ml contro i 16 ml di CoreValve26 e Sapien XT23 per entrambe le configurazioni di radice aortica (21 e 23 mm). Questo andamento si riflette anche sulla frazione totale rigurgitante poco superiore al 7% per le nostre valvole contro oltre il 20 % di Sapien e CoreValve26. La valvola dCell mostra un risultato comparabile con le valvole commerciali ma peggiore rispetto a quello della valvola in pericardio standard. Questo è dovuto a perdite nel tessuto dovute alla sua particolare consistenza soprattutto in prossimità delle suture con lo stent: in tali zone, sono presenti fori che consentono al sangue di tornare indietro al ventricolo quando la valvola è chiusa. Un'altra ragione è la presenza di un foro di dimensioni considerevoli in prossimità della zona di coaptazione dei leaflets (a causa della dimensione ridotta della pezza di pericardio fornitaci). Anche le ali attorno allo stent sono leggermente più piccole rispetto a quelle della valvola pericardica, causando ulteriori perdite di fluido.

Quasi tutti gli indici della nostre valvole mostrano prestazioni migliori rispetto a quelle delle valvole in commercio: caduta di pressione transvalvolare, perdite di volume, frazione totale di rigurgito, EOA, perdite di energia totale e di iniezione. Il volume perso a valvola chiusa e la sua rispettiva perdita energetica sono gli unici due indici rimasti uguali o peggiorati rispetto alle valvole in commercio. Il motivo principale è stata la lunghezza eccessiva dei leaflets per la valvola pericardica con lembi non accorciati e i lembi troppo corti per la valvola dCell.

3.2 Risultati computazionali

Analisi computazionali hanno dimostrato che gli sforzi ottenuti sulla superficie dei foglietti valvolari sono confrontabili con i valori riportati in letteratura [4] per la valvola pericardica. La valvola realizzata in pericardio decellularizzato presenta uno sforzo massimo medio sulla superficie dei lembi maggiore di quello presente sulla valvola pericardica, a causa delle diverse proprietà meccaniche del tessuto e del ridotto spessore del tessuto (Tabella 1). Per le stesse ragioni, le simulazioni computazionali hanno anche dimostrato diverse dinamiche di chiusura dei lembi tra valvole pericardica e valvola in pericardio decellularizzato; le simulazioni, infatti, hanno mostrato che i leaflets in pericardio decellularizzato hanno una fase di chiusura anticipata rispetto ai leaflets in pericardio standard.

Nel complesso, la valvola Crimp23 è maggiormente sollecitata rispetto alla valvola Crimp21 per tutti i tipi di materiale (Tabella 1).

	Valvola Crimp21	**Valvola Crimp23**
Elastic	0,289	0,313
Pericardium	0,287	0,437
Dcell Pericardium	0,990	1,250

Tabella 1 : Media degli sforzi principali massimi sulla superficie dei leaflets al tempo t = 0,34 s. Valori espressi in MPa

Nelle figure seguenti (Figure 28-29) sono mostrati gli sforzi principali massimi sulla superficie dei leaflets al picco di pressione per la valvola Crimp23 e per la valvola Crimp21, per entrambi i tipi di pericardio.

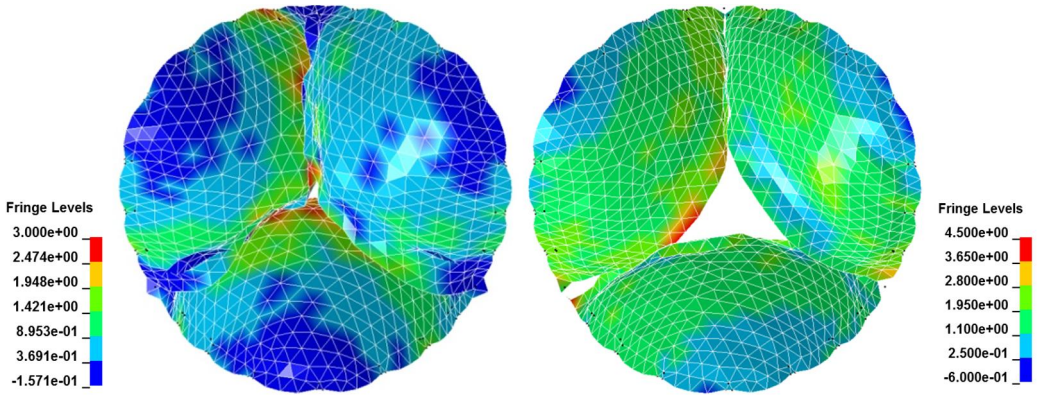

Figura 28 : Distribuzione delle sollecitazioni massime sulla superficie dei leaflets per la valvola Crimp23. Il materiale utilizzato è, rispettivamente, pericardio modellizzato con modello Ogden e pericardio decellularizzato modellizzato con il modello di Ogden.

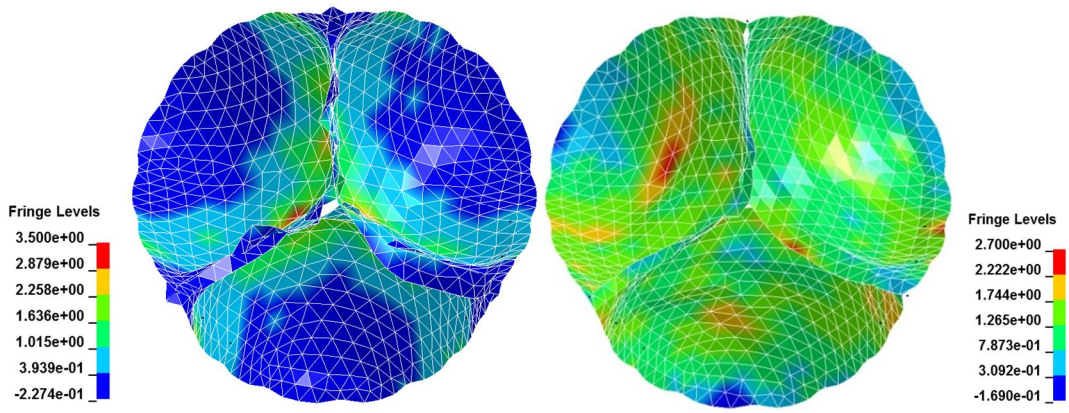

Figura 29 : Distribuzione delle sollecitazioni massime sulla superficie dei leaflets per la valvola Crimp21. Il materiale utilizzato è, rispettivamente, pericardio modellizzato con modello Ogden e pericardio decellularizzato modellizzato con il modello di Ogden.

L'analisi delle altezze di coaptazione (calcolate come distanza assiale tra i noduli di Aranzio e l’annulus aortico) ha suggerito che posizionando la valvola in una radice aortica con diametro pari a 21 mm, l’altezza di coaptazione aumenta rispetto al posizionamento in una radice aortica con diametro pari a 23 mm, e di conseguenza l’area di coaptazione; ciò potrebbe portare a migliori performance valvolari, rendendola meno insufficiente [48]. Questa osservazione testimonia l’importanza di utilizzare valvole di dimensioni e design adatte all’anatomia del paziente.

4 Conclusioni

In questa tesi, è stata sviluppata una nuova generazione di valvole cardiache al fine di migliorare la funzione emodinamica e ridurre l'energia assorbita durante il ciclo operativo rispetto alle valvole attualmente in commercio. Le performance delle valvole pericardiche e dCell suggeriscono che il disegno della valvola utilizzato è molto promettente per lo sviluppo di valvole cardiache con potenziale applicazione clinica. Quasi tutte le nostre valvole hanno mostrato performance superiori rispetto alle valvole commerciali; solo il volume di rigurgito nella fase di chiusura dei lembi e la conseguente perdita di energia sono uguali o peggiori rispetto al gruppo di controllo.

Per merito della natura auto-espandibile dello stent, la valvola può essere espansa in fasi che consentano regolazioni fini durante le fasi di apertura. Al contrario, valvole quali la Sapien sono rapidamente espanse mediante palloncino che non ne consente il riposizionamento.

L'uso di un tessuto biologico per i leaflets si è dimostrato importante al fine di migliorare la biocompatibilità e può essere meglio tollerato rispetto ad un materiale polimerico. Per il pericardio decellularizzato i vantaggi sono ancora più grandi a causa proprio della mancanza delle cellule.

Summary

1 Introduction

The heart has four chambers (right atrium, right ventricle, left atrium, and left ventricle) and four valves (tricuspid, pulmonary, mitral, and aortic valves) (Figura 30). The aortic valve is located between the left ventricle and the aorta.

During left ventricular systole (contraction), the pressure in the left ventricle increases until it rises just above the systolic pressure in the aorta. At this point in systole, the aortic valve opens and blood exits the left ventricle into the systemic circulation via the aorta. Thereafter, during left ventricular diastole (relaxation), the pressure in the left ventricle drops, and the pressure in the aorta forces the aortic valve back into its closed position [3].

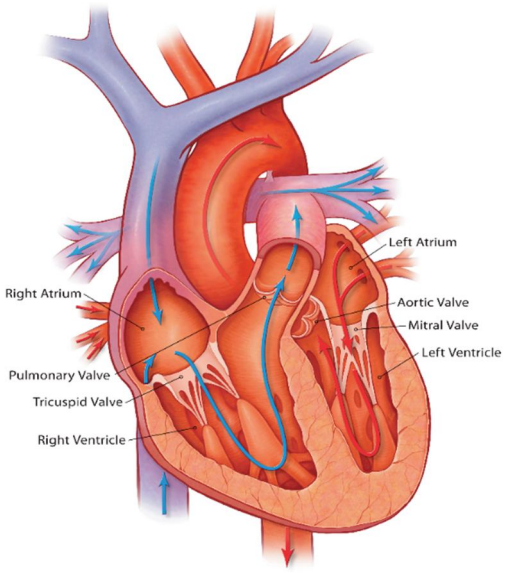

Figure 30 Anatomy of the human heart demonstrating the four chambers (left and right atria, and left and right ventricles) and the four main valves (mitral, tricuspid, aortic and pulmonary). The aortic valve is located between the left ventricle and aorta.

The high prevalence of valvular heart diseases, together with its increase with ageing, indicate a high and increasing burden of valve diseases [6]. Increased incidence of degenerative valve disease due to longer life expectancy is one reason for high prevalence

of heart valve disease in developed countries.

Conventional open heart surgery for heart valve replacement consists of partial or complete sternotomy with extra-corporeal circulation and cardioplegic cardiac arrest. In aortic valve replacement, open heart surgery is associated with high mortality rate (ranging from 10% to 50%) in high-risk patients with severe comorbidities [13].

There has been a great improvement in therapeutic techniques in recent years to extend treatment to increasing number of elderly patients with severe comorbidities who are at high risk for traditional valve replacement surgery. A variety of minimally invasive surgical procedures have been developed by several groups in recent years [17]. In general, the aim of these techniques is to minimize the overall surgical trauma by avoiding sternotomy, extra corporal circulation, and cardiac arrest, by implanting the prostheses in the beating heart.

Transcatheter aortic valve (TAV) implantation is a new approach that has been recently introduced as an alternative to traditional surgery for the substitution of the stenotic aortic valve. It is performed by delivering the valve substitute (biological or synthetic) into position through the vascular system. The valve is crimped inside a catheter (mounted on a balloon-expandable stent, a self-expandable stent, or both) and threaded along a guide wire into the correct position, under conventional visual guidance [1].

Once the correct intracardiac position is reached, the valve is re-expanded to its final diameter (with enough radial force to prevent paravalvular leak and valve migration), restoring its functionality.

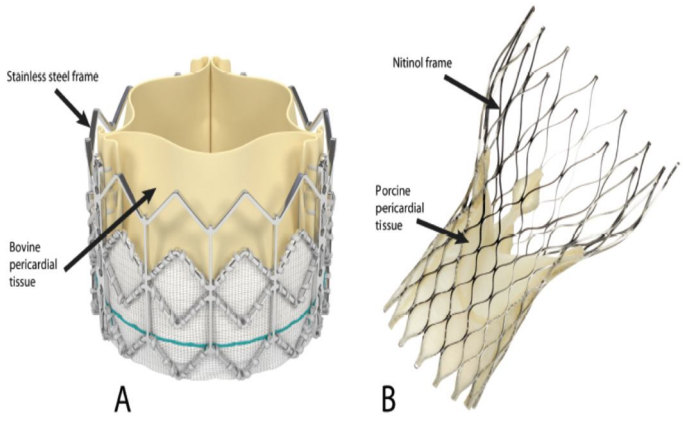

Figure 31A: Fully expanded Edwards Sapien Valve. Figure 31B: Fully expanded Medtronic Core Valve

While the outcomes in terms of survival and symptom improvement are similar between comparable patient groups who undergo TAV replacement with either the CoreValve or Edwards Sapien Valve (Figure 31), there are notable differences in complications seen in patients treated with the two valves. The ability to adjust the positioning of the valve during delivery gives the CoreValve a distinct advantage over the Sapien Valve. Due to the self-expanding nature of the Nitinol frame of the CoreValve, the CoreValve can be deployed in stages allowing for subtle adjustments in position during the deployment phases. In contrast, the Sapien Valve is rapidly deployed with a single balloon expansion that does not allow for repositioning either during or after deployment.

Early results of experimental and clinical trials of percutaneous valve replacement are promising; however, the technique is in the early stage of its development, with irrefutable potential problems that should be solved, such as paravalvular leak (PVL), that it's seen at a much higher rate after TAVI than after conventional surgical aortic valve replacement.

Aim of this work is to realize a new valve on a Nitinol stent that overcomes this problem and evaluating valves indexes, for comparing the valve with commercial ones, using a new stent design and leaflets shape and wings. Furthermore, a computational analysis has been performed in order to investigate the opening and closing dynamic of the leaflets. This kind of analysis could support clinical and experimental observations in order to study the stress fields during the systole and diastole.

2 Materials and Methods.

For the realization of the valve, we used the Nitinol stent manufactured by UCL and a leaflets shape with the wings profile integrated in a unique model.

Stent and leaflets will be firstly described regarding their material and shape and then will be described the new TAV.

2.1 Stent

The stent was developed by UCL with the collaboration of the Heart Hospital UCLH and for the first time implanted in a ovine model on May 2013 [2]. This stent is made of

Nitinol: due to the self-expanding nature of the Nitinol frame of the Stent, it can be deployed in stages allowing for subtle adjustments in position during the deployment phases. In contrast, other valves such as the Sapien Valve is rapidly deployed with a single balloon expansion that does not allow for repositioning either during or after deployment. The self-expanding design offers many others potential advantages over a balloon expandable device. First and most important, a self-expanding percutaneous aortic valve may minimize the occurrence of paravalvular leaks and enable the treatment of patients with aortic regurgitation. Secondly, by avoiding balloon trauma to the valve leaflets, the self-expanding design may theoretically prolong valve durability. Three different size of the stent was made: 23 mm, 26 mm and 29 mm. In this thesis, we focalize our attention on the 21, 23 and 26 mm sizes.

Four different views of the 26 mm stent are represented below (Figure 32).

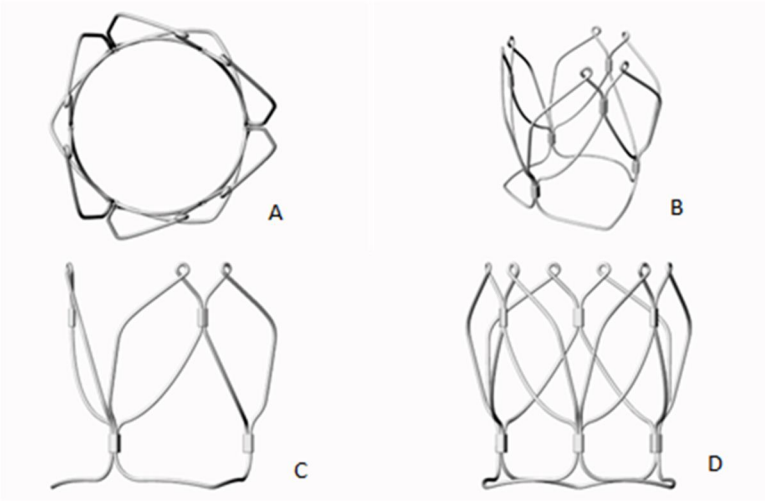

Figure 32: 26 mm stent from different views

2.2 Leaflets

2.2.2 Materials

The leaflets are made in pericardium, a composite material constituted by an amorphous matrix of proteins and polysaccharides in hydrated macromolecular complexes, containing

multidirectional bundles of collagen and elastic fibers having preferential directions [38]; it is bio-compatible and blood compatible.

Furthermore, a new decellularized pericardium has been used for the realization of other valves with the same geometry of the standard pericardium ones. This tissue has been provided by a company that was interested to utilize their tissue on a new aortic valve.

2.2.3 Shape

The shape used for previous valve made by UCL was composed of two separate parts: the leaflet and the wings (Figure 33 and 34). That configuration requested the stitching of the wings to the leaflets profile.

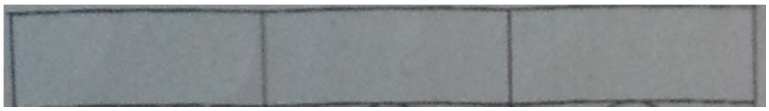

Figure 33: wings shape

Figure 34: leaflet shape

We chose to use a shape (available at the Department of Mechanical Engineering of UCL) composed by the leaflets shape in the inner part and the wings profile in the outer part. The model is shown in Figure 35.

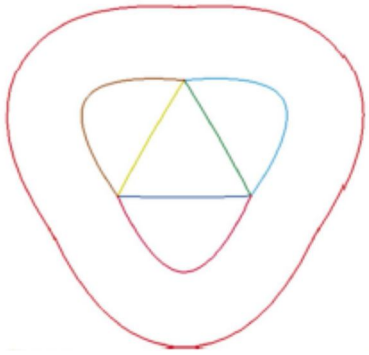

Figure 35: Model of leaflets and wings: the three triangles in the middle represent the leaflet whereas the shape around them represents the wings.

For training reason, we firstly realized deer skin shaped leaflets by simply positioning the paper shape on the tissue and suturing following the path. By water dipping it was possible to remove the paper and get the wanted shape. After that, the pericardium has been used.

In order to get a more precise cutting and to avoid problems correlated with the flexibility of the pericardium, it has been necessary to realize a plastic support by using the laser cutter. The CAD file drawn in Adobe Illustrator is shown below (Figure 36).

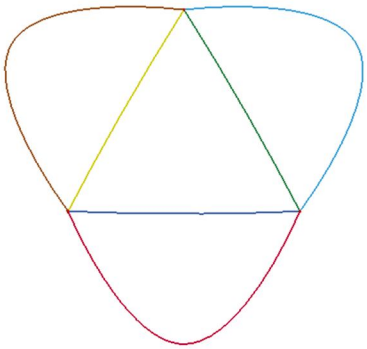

Figure 36: model realized in Adobe Illustrator

The obtained support is shown below (Figure 37)

Figure 37: Plastic model realized with laser cutting

In order to get the leaflet shape, a pericardium patch has been placed between two plastic supports and needle and thread have been used to track the desired leaflet shape (Figure 38).

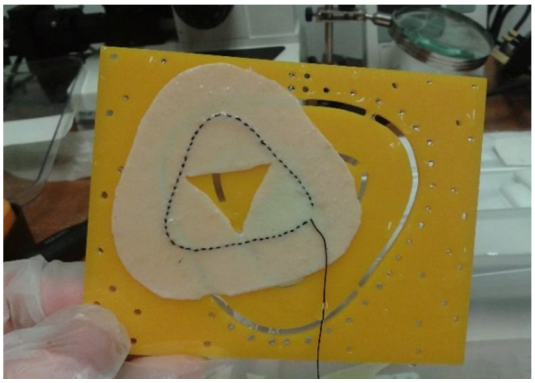

Figure 38: Pericardium leaflets obtained suturing with needle and thread

2.3 Enclosing: realization of the Valve

The leaflets shape has been folded on the stent and stitched to it with needle and thread in order to get the valve. With reference to the decellularized leaflets, the steps followed for the realization of the valves are summarized below:

- the tissue was folded on a silicon mold that represents the negative of the valve (Figure 39). This helps to keep the continuous structure stead while suturing it to the stent (Figure 40).
- needle and thread were used to suture every single stitch to the stent with an Asola suture. This suture guarantees that even if the thread has cut in one point, the slackness isn't propagated on.

Figure 39: tissue on the mold

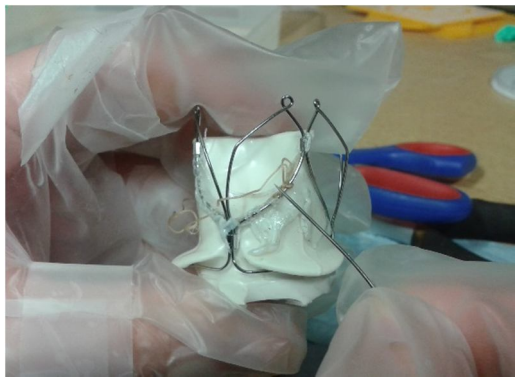

Figure 40: suturing of the tissue to the stent

We have first obtained the leaflets stitched to the stent (Figure 41) and then the wings (Figure 42).

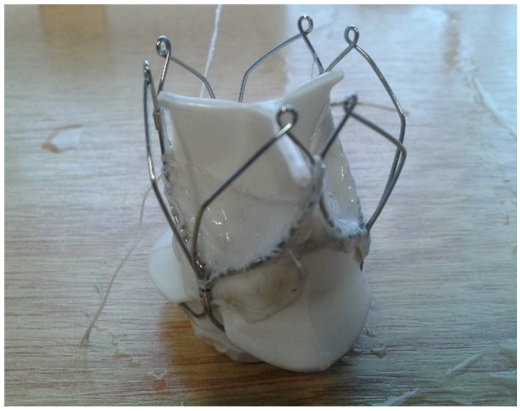

Figure 41: leaflets stitched to the stent

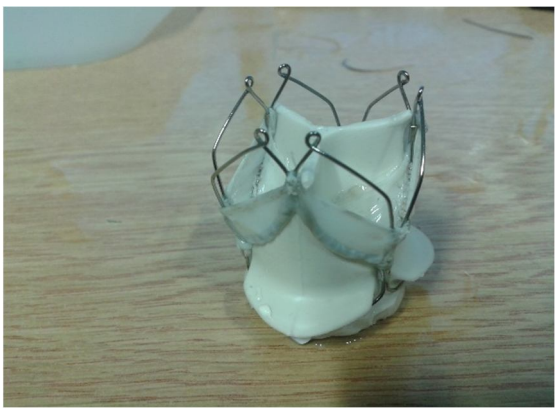

Figure 42: wings and leaflets stitched to the stent

Finally we got the final result depicted here (Figure 43):

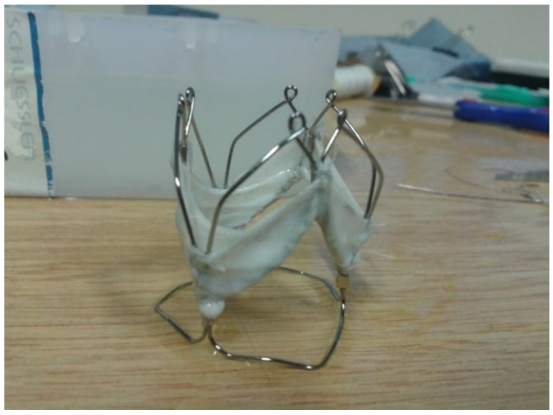

Figure 43: Valve with leaflets made of decellularized pericardium

2.4 Tissue properties

In order to get the material properties, standard pericardium and decellularized pericardium have been tested through tensile test in the Laboratory (see Figure 44).

Figure 44: Pericardial specimen during tensile test

In Figure 45 and 46 the stress and strain graphs obtained from the tensile tests are presented.

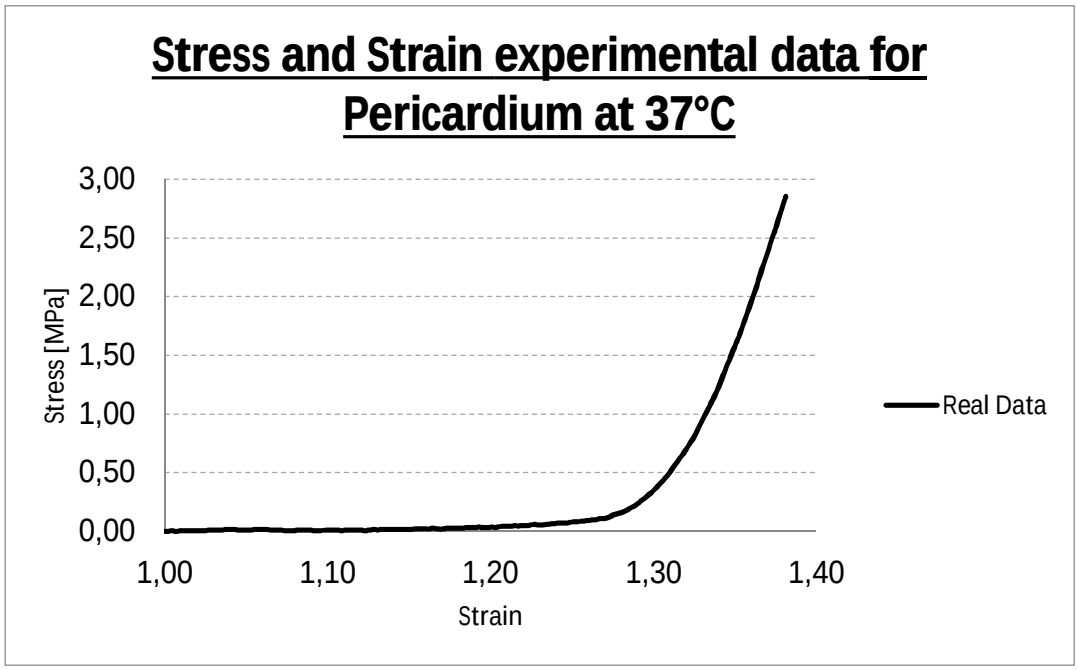

Figure 45: Pericardium experimental data at 37°C

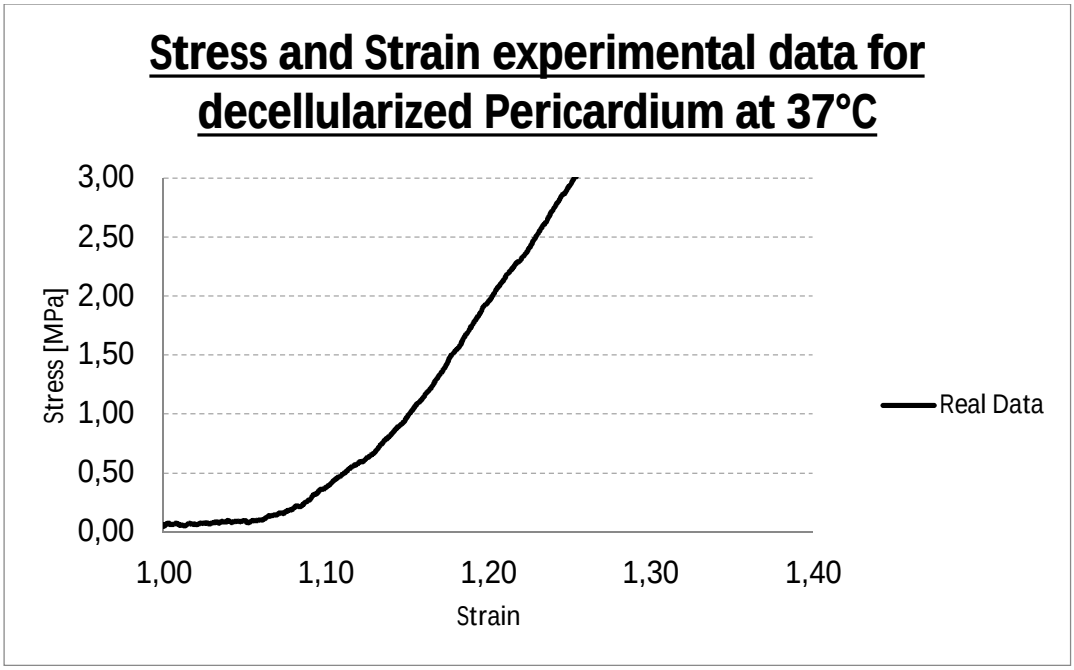

Figure 46: Decellularized pericardium experimental data at 37°C

2.5 Testing machine

In order to test our valve in an environment as closer as possible to the human heart and according to the ISO standard, we performed test on the ViVitro Pulse Duplicator that is widely used in vitro cardiovascular hydrodynamic testing system. It is composed of the ViVitro Model Left Heart, SuperPump and ViViTest data acquisition system.

ViVitro allows to assess the performance of prosthetic heart valves under simulated cardiac conditions.

Three valves have been tested: the first one was the deer skin valve and it was tested for training purpose therefore no data were collected, the second valve was the pericardial one and the third one was the decellularized pericardium valve. The same pericardial valve has been tested also with shorter leaflets (trimmed valve). Those valves have been compared with other commercial valves tested in the past on the same machine by the research group.

2.6 Computational analysis

In order to combine experimental tests with stress analysis on the surface of the leaflets, computational simulations have been run. The finite elements code used was Ls-Dyna.

In this thesis the numerical simulations involve:

- Simulation of the suturing of leaflets to the stent;
- Structural dynamic simulation of opening and closing of the leaflets in order to get stress fields.

2.6.1 Simulation of leaflets suturing and dynamic

As a first step it was necessary to simulate the positioning of the leaflets onto the stent, linking the leaflets with the stent through the threads. Thus, suturing simulations have been run in order to obtain the shortening of the threads; after that, dynamic simulations have been run in order to analyze the opening and the closing dynamic of the leaflets.

In the following paragraphs we are going to describe the materials and the geometries used for the leaflets, for the stent and for the threads. Furthermore, a detailed report of the simulation protocol will be described.

2.6.1.1 Materials

The elastic plastic thermal material was the first used to describe the leaflets, with a density chosen equal to 1000 Kg/m^3, Poisson's ratio equal to 0,495 and Young's modulus equal to 200 MPa. Starting from the positioning obtained with this configuration, in order to refine it, a new simulation has been run with identical material but with a Young's modulus equal to 2 MPa. For reasons of simplicity, the stent has been supposed rigid; regarding the material used for the threads, it was chosen to use an elastic plastic thermal material for the possibility to assign thermal properties to the elements; in particular a very high coefficient of thermal expansion and a very high (but negative in sign) coefficient of thermal generation have been assigned to the threads.

Once obtained the optimal positioning of the leaflets onto the stent, the materials assigned to the leaflets during the dynamic simulation were:

- elastic material with Young's modulus equal to 2 MPa and Poisson ratio equal to 0,495;
- pericardial material (an Ogden constitutive equation has been used to interpolate the experimental curves obtained from tensile tests, Figure 47).
- decellularized pericardial material (an Ogden constitutive equation has been used to interpolate the experimental curves obtained from tensile tests, Figure 48).

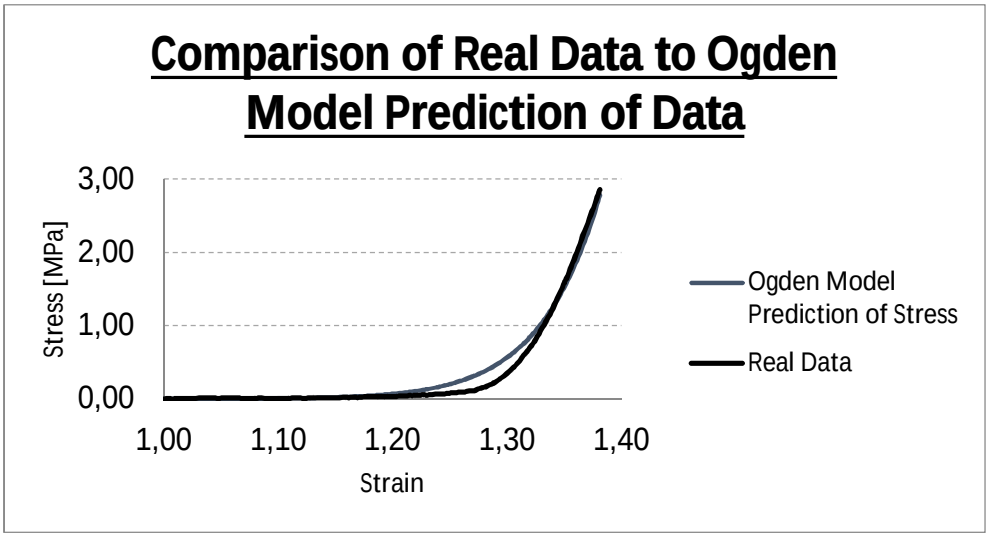

Figure 47: Pericardium experimental data and Ogden fitting

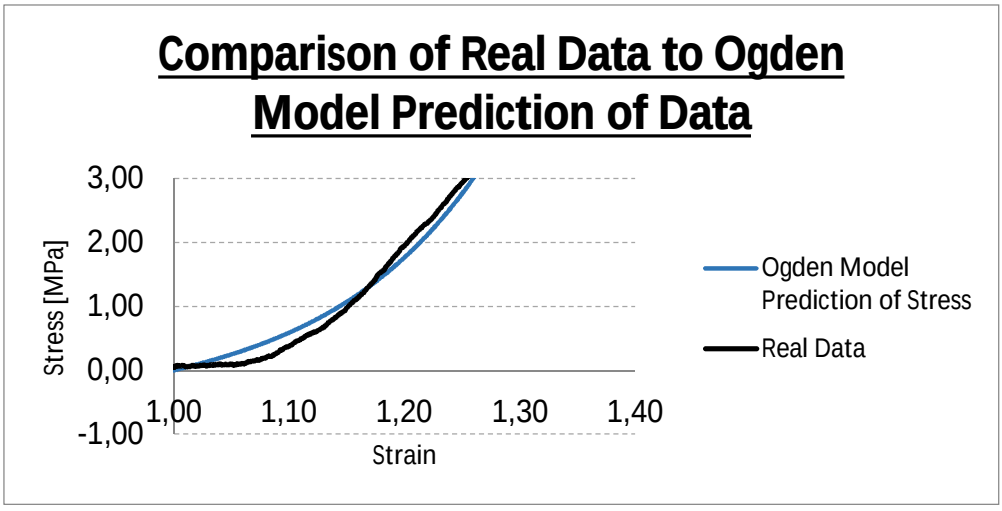

Figure 48: Decellularized pericardium experimental data and Ogden fitting

2.6.1.2 Model geometry

The model of leaflets selected for analysis was the same used for the realization of the valves but, due to the aim of the computational model that is the evaluation of stress fields on the surface of the leaflets, it has been chosen to omit the wings (Figure 49).

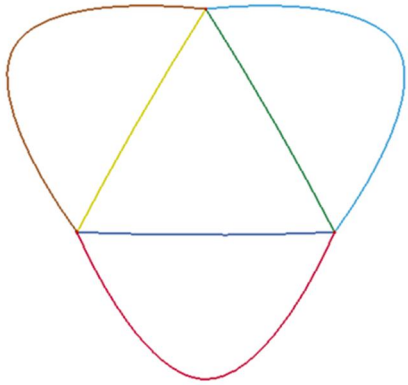

Figure 49: Leaflets model without wings. It has been used for the computational model

Regarding the stent, only the profile where the leaflets are stitched has been represented (Figure 50). In the computational model, in fact, the stent is just a reference for the positioning of the leaflets during the suturing simulation. Thus, the geometry involves only three cusps and doesn't consider the whole complexity of the real stent.

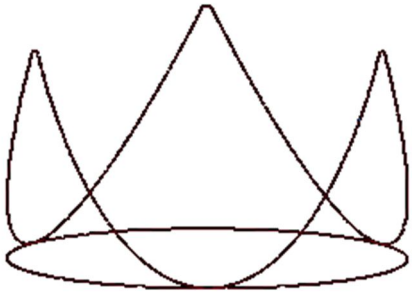

Figure 50: Stent profile used in the computational model. This is an exemplification of the real stent because only the shape of the leaflet was considered throughout the computational analysis.

For both the leaflets and the stent model, the structural domain was discretized into triangular elements with spacing equal to 1 mm; this choice has been considered the best in

order to maximize the ratio between accuracy and computational time. The meshes obtained are represented in Figure 51.

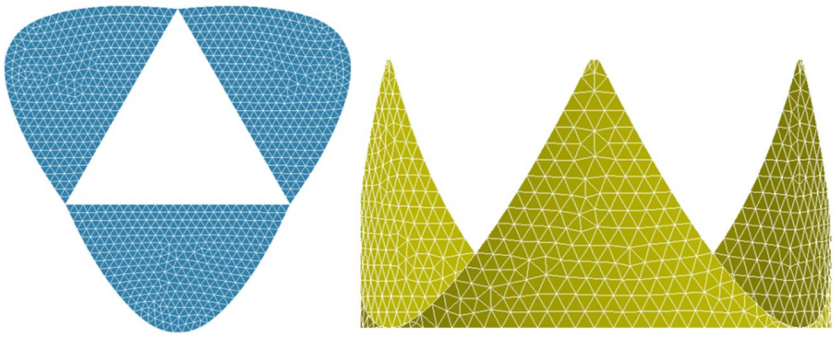

Figure 51: Leaflets and stent discretized in triangular elements

A shell thickness equal to 0,4 mm has been assigned to the stent whereas two different leaflets models have been realized: the first with a shell thickness equal to 0,4 mm (representative of the pericardium) and the second with a shell thickness equal to 0,1 mm (representative of the decellularized pericardium).

2.6.1.3 Simulation protocol

The first step in order to simulate the sutures between the leaflets and the stent was linking the stent geometry with the leaflets geometry. So, we chose tetrahedral solid elements (Figure 52).

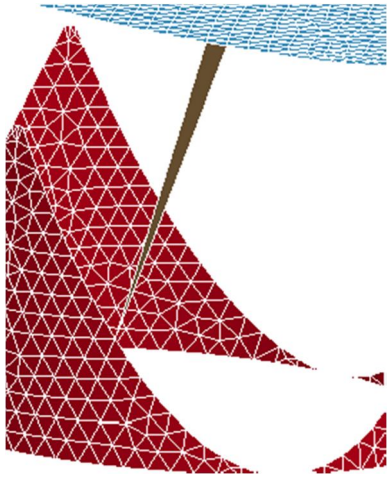

Figure 52: Example of thread that links stent and leaflets together

The positioning obtained with the simulation showed a significant gap between the leaflets and the stent (Figure 53).

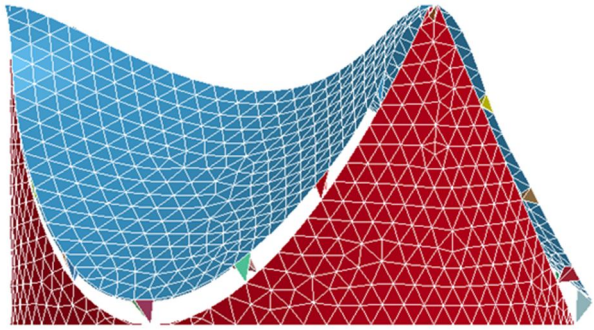

Figure 53: First positioning showing gaps between stent and leaflets

To optimize the shape, another simulation has been run starting from the geometry obtained from the previous one. Thus, the elements and the nodal coordinates have been exported and a new simulation was run, setting a Young's modulus for the leaflets equal to 2 MPa.

The positioning obtained from this simulation is shown in the Figure 54.

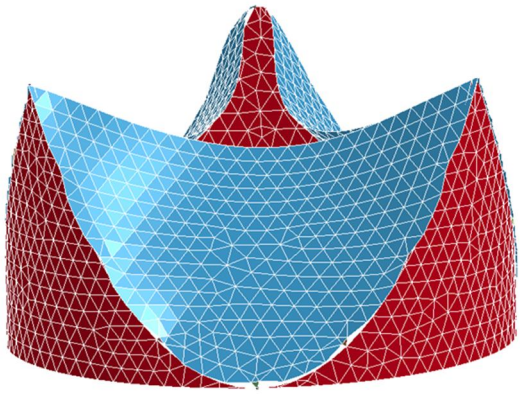

Figure 54: Final leaflets positioning

The positioning of the valve shown in the Figure 54 is representative of the valve's nominal shape. However, implanted valves in the body and tested valves in laboratory are always crimped against the walls: this means that the valve's disposition is quite different from the disposition assumed outside the aortic root. At this purpose, we have chosen to represent, in a simplified manner, the valve in other two different configurations: the one corresponding to a 23 mm root placement (Crimp23 valve) and the one corresponding to a 21 mm root placement (Crimp21 valve).

Starting from the positioning obtained with the suture simulations for all the valve's configurations (valve with nominal shape, Crimp23 and Crimp21), the elements and the nodal coordinates have been exported in new input files. The purpose was to analyze the opening and the closing dynamic of the valve. The threads and the stent have been removed and a pressure curve has been applied on the surface of the leaflets (Figure 55): in particular, it reached the diastolic value equal to 0,01333 MPa (100 mmHg) in 0,3 s and remained constant for 0,5 s when reached the systolic value equal to -0.001333 MPa (-10 mmHg).

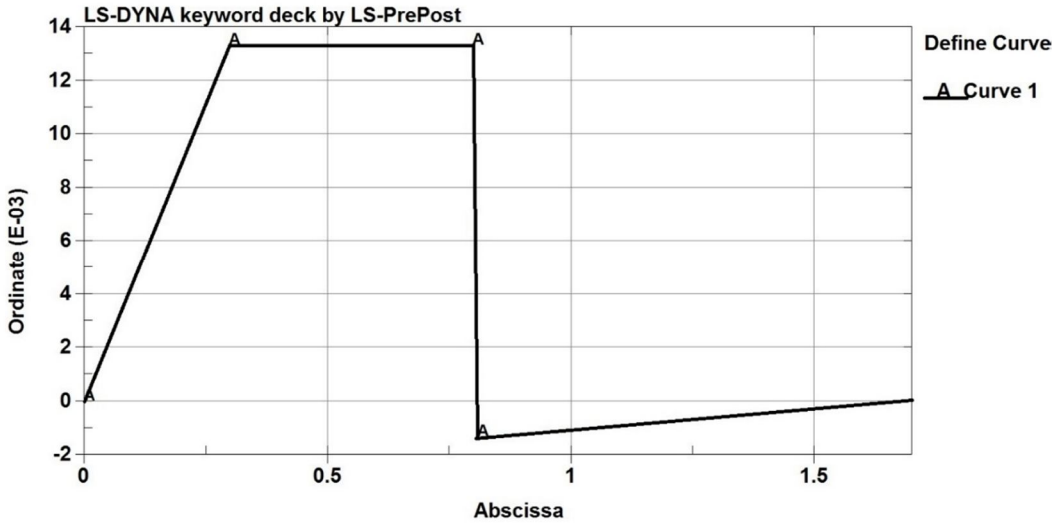

Figure 55: Time varying pressure applied to the leaflets

3 Results and Discussions

3.1 Experimental results

Comparisons between different types of valves and between the same valves placed in different root size have been assessed in order to compare transvalvular pressure drop, leakage volume, total regurgitant fraction, EOA and leakage, forward and total energy losses, closing regurgitant volume and its energy loss. In the following figures, some of the comparisons between different types of valves are shown (Figures 56-57-58-59); in particular we compared the valves realized with the commercial ones. All the complete results are shown in the Results and Discussions chapter. The valves have been tested in roots with diameter equal to 21 mm and 23 mm. Only the dCell valve haven't been tested in the root 23 due to the short length of its leaflets.

A tStudent test has been executed in order to check if the difference between the control valves' average and pericardium valve's average is significant.

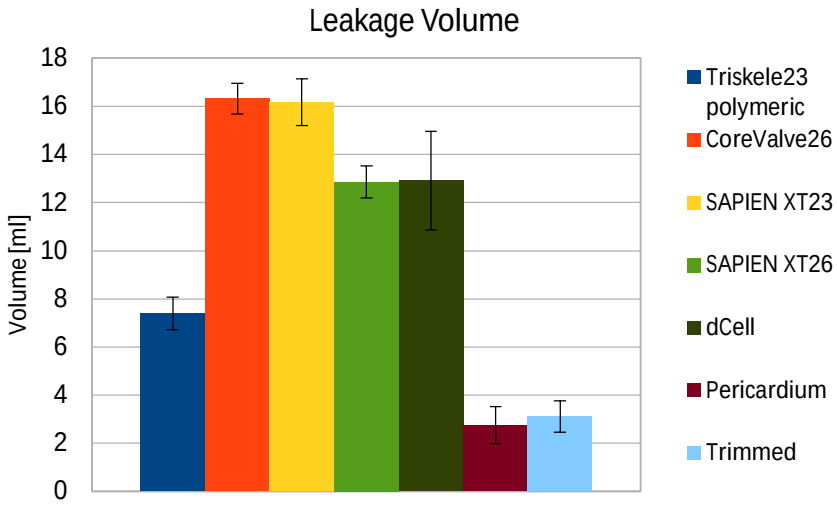

Figure 56: Leakage volume - 21 mm at CO = 5 l/min. According to a tStudent test, the difference between the control valves' average and pericardium valve's average is significant with p equal to 3.08%

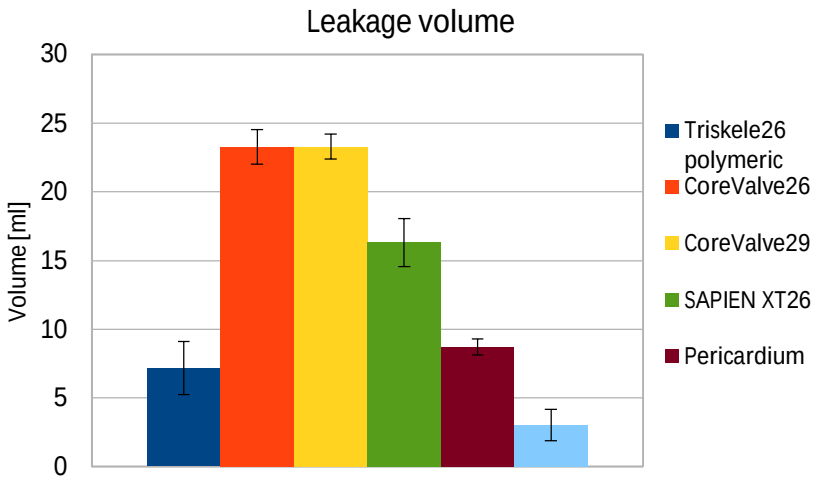

Figure 57: Leakage volume - 23 mm at CO = 5 l/min. According to a tStudent test, the difference between the control valves' average and pericardium valve's average is significant with p equal to 12.39%

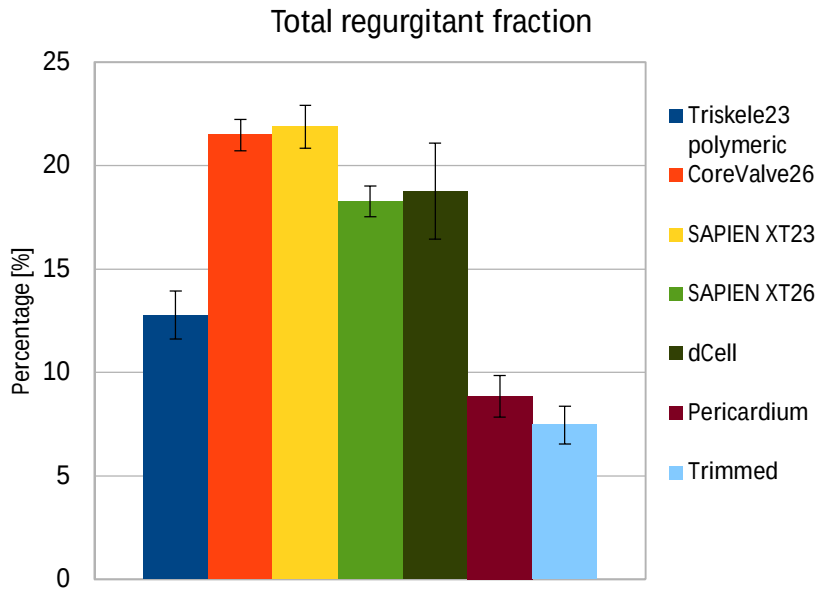

Figure 58: Total regurgitant fraction - 21 mm at CO = 5 l/min According to a tStudent test, the difference between the control valves' average and pericardium valve's average is significant with p equal to 3.05%

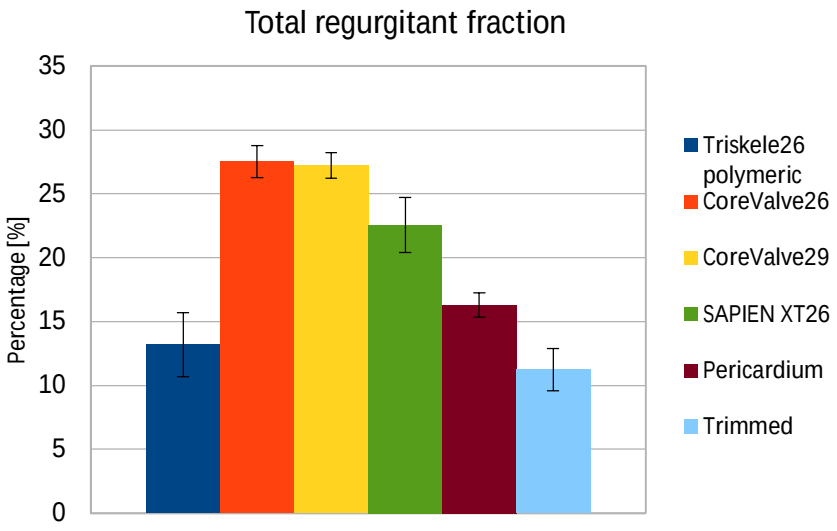

Figure 59: Total regurgitant fraction - 23 mm at CO = 5 l/min According to a tStudent test, the difference between the control valves' average and pericardium valve's average is significant with p equal to 16.7%

Regurgitation or leakage volume represents the amount of backward flow volume during the diastolic phase of a cardiac cycle. This is directly related to the valve size and the normal configuration of the leaflets in absence of a flow pressure. According to previous studies [41], porcine bioprosthetic valves have superior diastolic characteristics (e.g. regurgitation) benefiting from their relatively close leaflet configuration.

The aortic leaked obtained with pericardial valve is the lowest in any configuration compared with control valves. This is a very good achievement of this work. We have got leakage of about 2 ml for the pericardial valve against the 16 ml of CoreValve26 and Sapien XT23 for both root configurations This trade is also reflected on the Total Regurgitant Fraction equal to about 7% for our pericardium valves against more than 20% for Sapien and CoreValve26. The dCell valve has got comparable value with the control valve even if it has the same shape of the Pericardium Valve. This is due to some leakage in the tissue that we noticed during the experimental trials. In fact, close to the stitch, the tissue has holes that let the blood goes back when the valve is closed. Another reason was the presence of a hole in the middle of the valve when the leaflets are supposed to be closed (due to the dimension of the decellularized pericardium patch). Even the wings around the stent were slightly smaller than pericardium valve; thus, another portion of fluid escaped from there.

Almost all our valve's performance index have been improved compared to the commercial valve's performance indes: transvalvular pressure drop, leakage volume, total regurgitant fraction, EOA and leakage; forward and total energy losses are the ones with the best improvements. Closing regurgitant volume and its energy loss are the only two that are equal or worse than the control one. The main reason was the excessive leaflets length for the no-trimmed pericardium and the short leaflets length for the dCell valve.

3.2 Computational Results

Computational analysis have shown stress fields comparable with the values reported in literature [4] for pericardial valve. Decellularized pericardial valves have shown average of maximum stress on the surface of the leaflets higher than pericardial valve, due to the different mechanical properties of the tissue and the very low thickness of the fabric (Table 1). For the same reasons, computational simulations have also shown different closing dynamics between pericardial valves and decellularized pericardial valves; in fact, decellularized leaflets have a faster closing phase than pericardial leaflets.

Overall, the Crimp23 valve is more stressed than the Crimp21 valve for each material (Table 1).

	Crimp21 valve	Crimp23 valve
Elastic	0,289	0,313
Pericardium	0,287	0,437
Dcell Pericardium	0,990	1,250

Table 1: Average of maximum principal stresses on the surface of the leaflets at time t=0,34 s. Values expressed in MPa

In the figures below (Figures 60-61) the maximum stress on the surface of the leaflets are shown at the peak of pressure for the Crimp23 valve and for the Crimp21 valve for both pericardium and decellularized pericardium leaflets.

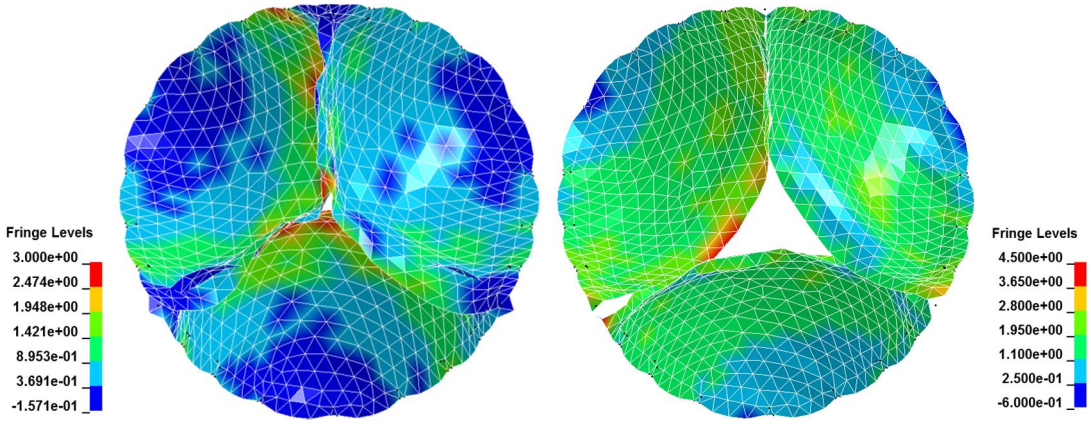

Figure 60: Maximum stress distribution on the surface of the Crimp23 valve's leaflets. The material are, respectively, pericardium fitted with Ogden model and decellularized pericardium fitted with Ogden model

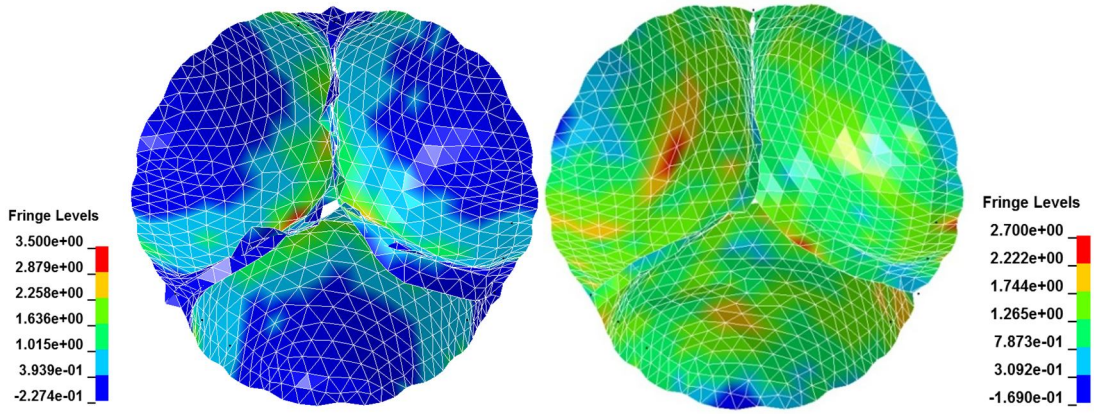

Figure 61: Maximum stress distribution on the surface of the Crimp21 valve's leaflets. The material are, respectively, pericardium fitted with Ogden model and decellularized pericardium fitted with Ogden model

The analysis of the coaptation heights (calculated as the axial distance between the nodules of Aranzio and the aortic annulus) suggested that positioning the valve in an aortic root with diameter equal to 21 mm increases the coaptation height and consequently the coaptation area than a positioning in a 26 mm aortic root; this could lead to better valve performance [48]. This observation proves the importance to implant valves with the correct sizes and the correct design for the patient.

4 Conclusions

In this thesis, a new generation of heart valves has been developed in order to improve the hemodynamic function and reduce the energy absorbed during the operating cycle. The enhanced hydrodynamic function of the pericardial and dCell valves suggests that the proposed valve design is a promising breakthrough in the development of heart valves with potential clinical application. Almost all our valve have shown better results than commercial valve; just the closing regurgitant volume and its energy loss are equal or worse than the control group. The main reason was the excessive leaflets length for the no-trimmed pericardium and the short leaflets lenght for the dCell valve. Furthermore, a new fully retrievable/repositionable TAV has been created thanks to the particular stent shape and material. Due to the self-expanding nature of the Nitinol frame of the Stent, it can be deployed in stages allowing for subtle adjustments in position during the deployment phases. In contrast, other valves such as the Sapien valve are rapidly deployed with a single balloon expansion that does not allow repositioning either during or after deployment. The self-expanding design offers many others potential advantages over a balloon expandable device such as minimizing the occurrence of paravalvular leaks and enabling the treatment of patients with aortic regurgitation. Secondly, by avoiding balloon trauma to the valve leaflets, the self-expanding design may theoretically prolong valve durability. The use of a biological tissue for the leaflets is important to improve biocompatibility: it can be better tolerate than polymeric material. For the decellularized pericardium the advantages are even bigger because of the cells absence.

Chapter 1: Introduction

The human heart has four chambers (right atrium, right ventricle, left atrium and left ventricle) and four valves (tricuspid, pulmonary, mitral and aortic valves) (Figure 1.1). The tricuspid valve is located between the right atrium and the right ventricle, the pulmonary valve between the right ventricle and the pulmonary artery, the mitral valve between the left atrium and the left ventricle and the aortic valve between the left ventricle and the aorta. The tricuspid and mitral valves are called atrio-ventricular valves since they are located between the atrium and the ventricle whereas the pulmonary and aortic valves are called arterio-ventricular valves since they are located between the artery and the ventricle. The aortic and pulmonary valves are also called semilunar valves because their leaflets have the shape of a half moon.

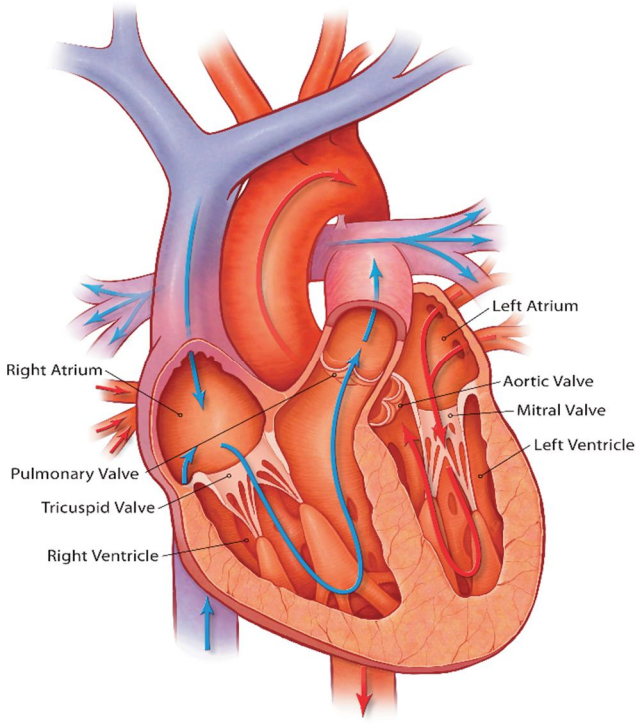

Figure 1.1 Anatomy of the human heart showing four chambers (left and right atria, left and right ventricles) and four main valves (mitral, tricuspid, aortic and pulmonary). The aortic valve is located between the left ventricle and aorta.

Atrio-ventricular valves are attached to the heart muscle (myocardium) by papillary muscles and fibrous cords and they are considered to be active structures responding to myocardial contractions. Semilunar valves, on the other hand, do not have direct attachment of the mobile part of the leaflet to the myocardium, and therefore they have been considered in the past to function passively in response to blood flow. All of the valves permit blood flow in one direction.

Oxygen-depleted blood returns from the body via venae cavae to the right atrium and through the tricuspid valve to the right ventricle. It then goes through the pulmonary valve to the pulmonary artery, and to the lungs. Oxygenated blood from the lungs returns via pulmonary veins to the left atrium and through the mitral valve to the left ventricle. It then goes through the aortic valve to the aorta, and finally to the whole body. The flow of blood is achieved by the pumping action of the heart. During ventricular ejection, aortic and pulmonary valves remain opened and mitral and tricuspid valves remain closed, whereas during ventricular filling, aortic and pulmonary valves remain closed and mitral and tricuspid valves remain opened [49]; in fact, the pressure in the left ventricle increases until it rises just above the systolic pressure in the aorta. At this point in systole, the aortic valve opens and blood exits the left ventricle into the systemic circulation via the aorta. Thereafter, during left ventricular diastole (relaxation), the pressure in the left ventricle drops, and the pressure in the aorta forces the aortic valve back into its closed position [3].

The 2 main structures we will focus our attention on are the aortic root and the aortic valve.

1.1 Aortic Root

The aortic root may be defined as the portion of the left ventricular outflow tract which supports the leaflets of the aortic valve, delineated by the sinotubular ridge superiorly and the bases of the valve leaflets inferiorly [5]. It comprises the sinuses, the aortic valve leaflets, the commissures, and the interleaflet triangles. The sinuses are expanded portions of the aortic root which are confined proximally by the attachments of the valve leaflets and distally by the sinotubular junction. They are named according to the coronary arteries arising from them, right, left, and non-coronary. The sinotubular junction, delineating the

superior aspect of the aortic root, is circular and composed of primarily elastic tissue, and it supports the peripheral attachments of the valve leaflets (Figure 1.2).

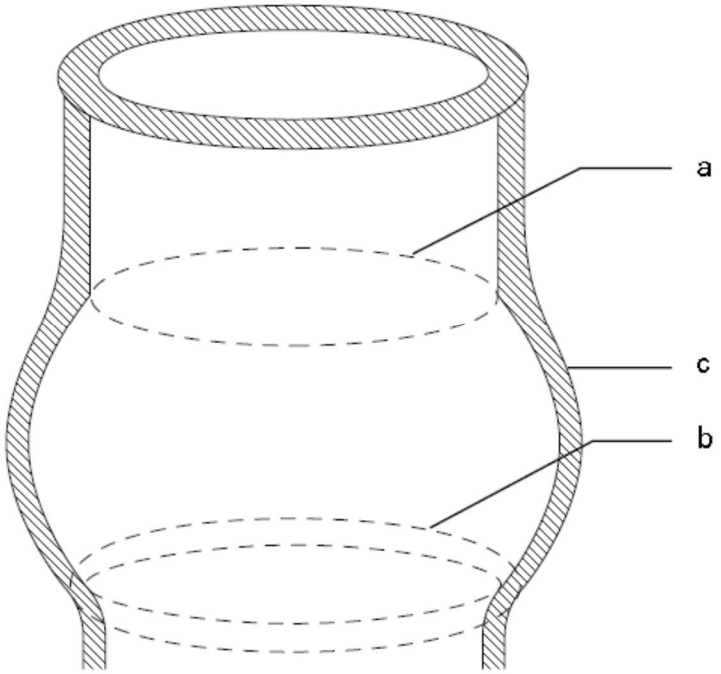

Figure 1.2 Representation of the aortic root

1.2 Aortic Valve

The aortic valve consists of three membranous leaflets and aortic sinuses. The valve is located between the left ventricle and the aorta and its function is to allow the blood to flow in one direction, from the ventricle to the aorta; thus, the aortic valve opens to allow blood to flow into the aorta and closes to prevent backflow into the ventricle. The valve opens and closes approximately 103,000 times each day and approximately 3.7 billion times in its life span. These opening and closing movements are achieved by the movement of its three leaflets.

1.2.1 Aortic Valve Leaflets

The valve leaflets are the portions of the aortic root which separate, hemodynamically, the aorta and the left ventricle. They are inserted into the wall of Root in a semilunar fashion. The term “annulus” is frequently used to describe the area of collagenous condensation at the point of leaflet attachment.

The posterior aspect of the aortic root (mainly non-coronary leaflet) is supported by fibrous tissue for approximately 55% of its circumference (membranous part of the septum to the left fibrous trigone), while the remainder is supported by ventricular muscle [5].

1.2.2 Aortic Valve Function

The function of the aortic valve has often been thought to be entirely passive, when the pressure generated by ventricular systole exceeds the pressure in the ascending aorta the valve leaflets open, and when left ventricular pressure decreases to less than aortic pressure they close. Aortic valve function is, however, much more complicated and the aortic root complex acts as an individual hemodynamic system. The upper portion of the aortic root is exposed to aortic pressure changes and therefore behaves as the rest of the vessel (it expands during systole allowing the leaflets to retract and open). The proximal part of Root complex, however, is exposed to ventricular pressure changes and it will expand as the ventricle fills and contracts during the peak of systole. It seems that sinuses serve an important physiological role in aortic valve function and their importance has been increasingly recognized by surgeons contemplating reconstruction of the aortic root [5].

1.3 Valvular heart disease

In the field of cardiovascular medicine, valvular heart disease is an important cause of morbidity and mortality worldwide.

The high prevalence of valvular heart diseases, together with its increase with ageing, indicate a high and increasing burden of valve diseases [6]. Increased incidence of degenerative valve disease due to longer life expectancy is one reason for high prevalence of heart valve disease in developed countries. Furthermore, emerging new forms of valve disease related to AIDS [7], new idiopathic disease such as antiphospholipid syndrome [8] and drugs such as ergot derivatives and appetite suppressant drugs have a role in the frequency of valvular heart disease [9]. Changes in the etiology and pathology of heart valve diseases have resulted in changes in patients' population such as old age, severe concomitant disorders and vulnerable general health condition. Hence, these changes have intensified the need for alternative less invasive therapeutic options. Moreover, improved reconstructive surgical techniques for congenital cardiac malformations, together with availability of cardiopulmonary bypass and intensive care facilities, have caused improved prognosis and growing number of long-term survivors of such conditions who are more susceptible to valve dysfunction in their later life [10]. Although conservative medical therapy for mild and asymptomatic cases of valve dysfunction may benefit them in the early stages, heart valve replacement therapy is a curative and standard treatment in severe symptomatic conditions. Valvular heart disease is the primary etiology or a secondary component in at least 30% of patients with surgical heart disease [11]. In 2006, there were 408,000 cardiac valve procedures (replacement and repair) performed worldwide, including 98,000 valve replacements in the United States and 195,300 in European countries [12].

1.3.1 Conventional heart surgery

Conventional open heart surgery for heart valve replacement consists of partial or complete sternotomy with extra-corporeal circulation and cardioplegic cardiac arrest. In aortic valve replacement, open heart surgery is associated with high mortality rate (ranging from 10%

to 50%) in high-risk patients with severe comorbidities [13] such as left ventricular failure, concomitant coronary artery disease with prior bypass surgery, chronic obstructive pulmonary disease, and advanced age [13]. A significant number of elderly patients with severe comorbidities cannot undergo open heart surgery because of high mortality rate. It has been estimated that about one third of the patients are in the high risk categories and do not receive surgery because of either excessive risk factors of open heart surgery or patient refusal due to fear of lifestyle changes after valve surgery [14]. Furthermore, in selected octogenarians who underwent an open heart procedure, reported mortality rate was up to 15%, which is significantly higher than overall mortality rate of 2% [15],[16]. Moreover, pre and postoperative complications in octogenarians are significantly higher than in younger patients, and 62% of them showed at least one nonfatal complication such as pulmonary problems, leg infection, and sternum complications [15].

1.4 Percutaneous techniques

There has been a great improvement in therapeutic techniques in recent years in order to extend treatment to increasing number of elderly patients with severe comorbidities who are at high risk for traditional valve replacement surgery. A variety of minimally invasive surgical procedures have been developed by several groups in recent years [17]. In general, the aim of these techniques is to minimize the overall surgical trauma by avoiding sternotomy, extra corporal circulation, and cardiac arrest, by implanting the prostheses in the beating heart. Minimally access surgical techniques include improved surgical procedures with the use of minimized incisions rather than traditional sternotomy, robotic aimed procedures for valve repair and replacement, and trans-apical access in which a combination of surgical and trans-catheter approaches are used. The trans-apical aortic valve replacement is one of the emerging procedures in recent years. In this new technique, the access to the aortic valve is achieved by left anterolateral minithoracotomy in the fifth intercostal space, then a balloon-expandable valve is delivered by trans-catheter systems [17]. The potential advantages of these techniques have been the psychological impact on patients, short hospitalization period, and better cosmetic outcome [17].

1.4.1 Implantation Techniques

Percutaneous heart valve replacement is performed by delivering the valve substitute (biological or synthetic) into position through the vascular system. The access is achieved by traditional cardiac catheterization techniques. The valve is crimped inside the catheter (mounted on a balloon-expandable stent, a self-expandable stent, or both) and threaded along a guide wire into the correct position, under conventional visual guidance [1]. Once the correct intracardiac position is reached, the valve is re-expanded to its final diameter (with enough radial force to prevent paravalvular leak and valve migration), restoring its functionality. Both ante-grade and retrograde approaches have been used to access the aortic valve in clinical trials (Figure 1.3).

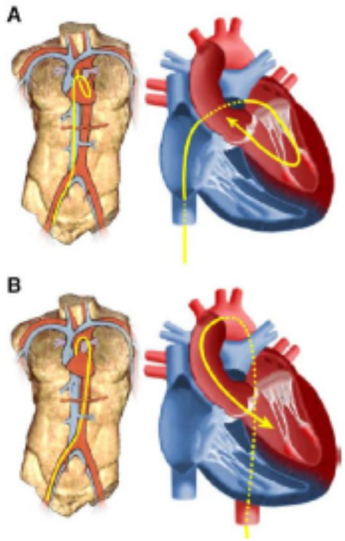

Figure 1.3: Percutaneous valve replacement approaches: (A) antegrade and (B) retrograde

The antegrade approach starts from the femoral vein and reaches the aortic valve after puncturing the interatrial septum, and crossing the mitral valve and the chordae tendinae. This approach has been very popular in the clinical experience; because of the greater dimensions and elasticity of the veins, it enables the passage of relatively large collapsed stents. However, its main limitations are the complexity of the procedure, which requires the presence of about three operators and the risk of damage to the anterior leaflet of the mitral valve [18][19]. The retrograde approach offers an easier and direct access to the

aortic valve from the femoral artery and in clinical trials has been proved to be much safer. However, this implantation procedure requires smaller collapsed valves, able to pass through the stiff and tortuous aortic vessels, and to cross the small gaps between the leaflets of calcified aortic valves [18]. Many patients might not be candidates for this method because of diseased or tortuous femoral arteries that could not accommodate such a large sheet size. In mitral position, percutaneous access can be achieved by the antegrade (via femoral or internal jugular vein) or the retrograde (via femoral artery) method, or a combination of both.

1.5 Transcatheter Aortic Valves (TAV)

Aortic valve disease, frequently aortic stenosis, is the most common valvular heart disease with increasing tendency with age due to degenerative calcification. The application of the percutaneous approach for the treatment of valve disease in aortic position is a more challenging area. Difficulties of vascular access due to complex anatomy, the size of delivery system and problems in secure positioning of the valve in the aortic annulus are some of the challenges in percutaneous aortic valve replacement therapy [19][20][21].

The first transcatheter aortic valve implantations performed in animals were conducted in 1992 by Dr. Andersen and colleagues. It would be another 10 years before Dr. Alan Cribier performed the first in-man TAV replacement procedure in France in 2002. In this first case, Dr. Cribier and his colleagues implanted a percutaneous heart valve that consisted of three bovine pericardial leaflets mounted within a tubular stainless steel balloon-expandable stent. Prior to implantation, the stent-valve was securely crimped onto a balloon catheter, which was subsequently advanced across the aortic valve. The balloon was then rapidly inflated and deflated, resulting in successful deployment of the first transcatheter aortic valve in man.

Since that first patient in 2002, there has been a rapid growth within the field of structural heart disease and transcatheter valve therapeutics. Five years after Cribier’s first case, TAV replacement (TAVR) was approved for use in Europe, and since then more than 40,000 patients have been treated worldwide with this technique, which is now indicated as a treatment strategy for both non-surgical patients and patients in high surgical risk groups.

The research and development of trans-catheter valves has evolved rapidly as a result of these early successes, and there are currently at least eight valves in commercial development. In the United States, two of these valves are available: the balloon expandable Edwards Sapien prosthesis *(Edward Lifesciences Inc: Irvine, CA;* Figure 1.4A*)* and the Medtronic self-expanding CoreValve ReValving System *(Medtronic Inc: Minneapolis, MN;* Figure 1.4B*).*

Both the Edwards-Sapien Valve and the Medtronic CoreValve are designed to function through a mechanism similar to a normally functioning human tricuspid aortic valve.

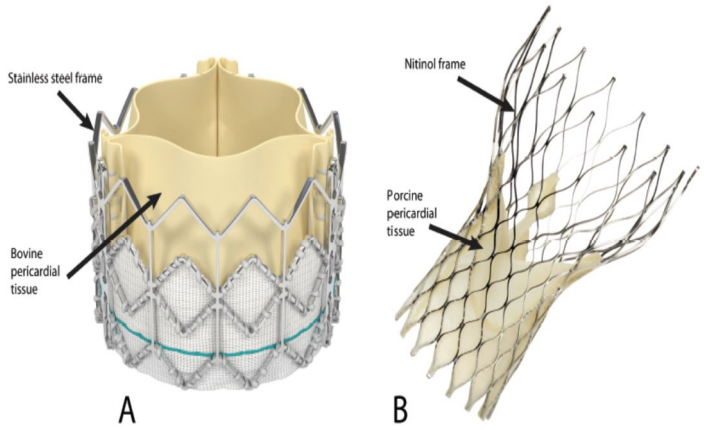

Figure 1.4A. Fully expanded Edwards Sapien Valve with its stainless steel frame and trileaflet construction made from bovine pericardial tissue. (Edward Lifesciences Inc: Irvine, CA.) 1.4B. Fully expanded Medtronic Core Valve with its Nitinol frame and trileaflet construction made from porcine pericardial tissue. (Medtronic, Inc.)

However, while both are trileaftlet in design with a metallic framework for support, their construction as well as preparation and delivery have significant differences. The integrated Edwards-Sapien transcatheter heart valve system is comprised of bovine pericardial tissue made from three identical sections of bovine pericardium that have been preserved in buffered glutaraldehyde to enable crosslinking of the tissue while preserving flexibility and strength. The valve tissue is affixed to a radiopaque stainless steel stent frame within a fabric cuff at its inflow aspect and to attachment bars on the commissural posts at its outflow aspect using polytetrafluoroethylene (PTFE) sutures to create a unidirectional trileaftlet tissue valve. Prior to delivery, the valve is tightly compressed using a crimping mechanism onto a balloon catheter. The compressed device is then inserted into a tip-deflecting catheter delivery system. Prior to delivery, aortic balloon valvuloplasty is performed, and thereafter the Sapien transcatheter heart valve system is

advanced up the aorta and placed across the native aortic valve. The balloon with the attached valve is then rapidly inflated and deflated, expanding and releasing the Sapien valve. The newly functioning valve is passively secured to the underlying native leaflets and to the aortic annulus as a result of this delivery. There are two sizes of the Sapien valve currently available: 23mm and 26mm in diameter.

In contrast to the Sapien valve, the CoreValve is a self-expanding valve with a Nitinol frame. Although the first generation CoreValve (first implanted in humans in 2004) was also made from bovine pericardium with an intra-annular valve function similar to that of the Sapien valve, the current generation CoreValve is made from porcine (not bovine) pericardium. The choice of porcine pericardium for the CoreValve may be due in part to suggested benefits that include diminished tissue thickness (thus allowing for a smaller sheath size), higher tensile strength, and tolerance to bending, as well as less tissue elongation providing for more consistent valve leaflet coaptation. The choice of Nitinol as opposed to stainless steel gives the CoreValve system the ability to be loaded onto a catheter delivery system that does not require a balloon and enables the valve to be gradually deployed in stages. The unique properties of Nitinol, a metal alloy of nickel and titanium, were first described by William Buehler and Frederick Wang during research at the Naval Ordnance Laboratory in 1962. Nitinol exhibits what is known as a martensitic transformation, which allows it to undergo a reversible, solid state transformation. As a result, at warmer temperatures (including body temperature), Nitinol forms a very strong, primitive cubic crystal structure referred to as austenite with a high radial strength. At colder temperatures, however, such as when placed in an ice water bath, Nitinol transforms into a complex monoclinic crystal structure known as martensite. At this lower temperature, Nitinol exhibits the property of superelasticity, giving it 10 to 30 times the elasticity of ordinary metal, enabling the CoreValve metal stent frame to be tightly compressed within the small delivery sheath required for the TAVR procedure. Lastly, Nitinol exhibits the property of shape memory such that the shape of the higher temperature austenite is “remembered” despite the deformed shape that occurs at the lower temperature, and thus, when it is deployed in the warmer temperature of the body, it regains its original configuration.

Chapter 2: State of the art

Early results of experimental and clinical trials of percutaneous valve replacement are promising; however, the technique is in the early stage of its development, with irrefutable potential problems that should be solved, such as paravalvular leak (PVL), that it's seen at a much higher rate after TAVI than after conventional surgical aortic valve replacement. With first-generation prostheses, the implants were associated with worse clinical outcomes; the most common types of presentation for the major complications were vascular dissection (62.8%), perforation (31.3%), and access-site hematoma (22.9%). More recent data have shown reductions in vascular complication rates following TAVI, "due to the combination of newer devices, smaller delivery systems, and the use of adjunctive techniques, combined with better screening and increased operator experience." [22]

2.1 Current Limitations, risks and solutions

There are some concerns about effectiveness, safety, durability, and technical difficulties of percutaneous heart valve replacement therapy, especially in aortic position [23].

However, percutaneous valve replacement therapy is in the early stage, and to establish a safe and successful percutaneous heart valve replacement therapy, the obstacles of current procedures should be overcome. One of the important problems of catheter-based techniques is the mismatch between the size of the femoral vessels of small children and the application devices that limit their application in these age groups [24]. The first-generation delivery catheters are in the order of 22 to 24F, requiring direct femoral, iliac, or axillary arterial access via surgical exposure if a retrograde approach is used. Although an antegrade transeptal approach may enable percutaneous femoral venous access with some of these devices, the large sheath size may still predispose to vascular injury [21]. Enormous advances in catheter delivery systems have been achieved to improve outcomes of transluminal intervention procedures for valve repair and replacements. The accuracy and feasibility of percutaneous procedures are related to choose an appropriate delivery system. Recently, *Attmann et al.* [25] reported 90% technical success of percutaneous

implantation of stented valve in pulmonary position in an animal model, by application of a commercially available endovascular stent–graft system for the treatment of thoracic aortic aneurysms *(Medtronic, Talent, Santa Rosa, CA)*, which had shown promising results in in vitro tests. Other frequent problems that were reported in transcatheter techniques are migration of a valved stent, paravalvular leakage, rhythm disturbance, hemodynamic instability, small aortic valve area, valve dysfunction after compression and re-expansion, and impairment of coronary flow and mitral function [26]. Developing improved delivery systems together with improved valved stent devices is necessary to overcome some of these complications. Another major problem encountered with percutaneous valve replacement is the impossibility of readjusting the position of a valved stent once fully deployed [27]. Deployment of the valved stent in the inappropriate position could lead to a fatal technical complication [28]. To address this problem, *Zegdi et al.* [29] introduced a novel transcatheter delivery method for repositioning of the valved stent. They successfully performed endovascular valve replacement in five sheep with failed bioprosthetic valve in the tricuspid position. With the use of this technique, they showed the feasibility of repositioning of the fully deployed valve before its definitive release. Moreover, researches are underway to develop repositionable devices for percutaneous implantation. These devices have potential advantages to be repositioned by contracting and re-expanding the anchors in other appropriate position [30]. Cerebral embolism is another complication of catheterization especially in aortic stenosis. *Meine and Harrison* [31] reported 22% risk of cerebral embolic events in retrograde catheterization in severe aortic stenosis. Among them, clinically apparent neurologic deficits were found in 3% of patients. The risk of embolism is also high in predilatation of stenotic aortic valve before insertion of percutaneous valved stent. To avoid any possible embolization, paravalvular leakage, reduced effective orifice areas [28], and risk of compromising coronary ostia with native valve leaflets in aortic position, resection of calcific valve has been considered by researchers. *Quaden et al*. [32] introduced a new method for aortic valve resection with the use of a high-pressure water stream scalpel, which was tested first on human calcified aortic leaflets in vitro. In this study, a pressure of 150 bar produced excellent resection results with a time of about 6 min per three leaflets. They minimized possible damage to surrounding tissues by applying an inflated polyethylene balloon. They also showed the feasibility of this technique by in vivo testing in an animal model. Recently, they reported the first endovascular resections of sclerotic aortic valves in a human. After deployment of

the aortic valve isolation chamber via the descending aorta, they resected the leaflets with an endoscopically guided laser scalpel via the right external carotid artery under endoscopic visualization [32]. Another concern in percutaneous valve replacement is the durability of valve substitutes. Currently, available percutaneous heart valves are tissue derived prostheses that are susceptible to several tissue degrading factors such as degeneration, calcification, and inflammation. There have been a few studies conducted to evaluate the durability of percutaneous valves in vivo. *Eltchaninoff et al.* [33] used a cylindrical stent carrying a three-leaflet equine pericardial valve for implanting in aortic position in sheep. Electron microscopy revealed inflammatory cells and focal calcification in different valves [33][34]. Recently, *Attmann et al.* [35] conducted an experimental study to examine the micropathology of percutaneous valve replacement. They implanted a self-expandable valved stent of bovine jugular vein into pulmonary position of nine sheep via femoral vein access. After 3 months, macro- and micropathology examinations of explanted valves showed massive calcification in the bovine jugular vein wall with increased number of T lymphocytes and slight fibrous overgrowth at the inflow of the two valved stents [35].

Consequently, further research is needed to develop materials with inflammation and calcification-resistant properties. This would offer one aspect for the future progress of percutaneous heart valves.

2.2 Comparison between CoreValve and Sapien

While the outcomes in terms of survival and symptom improvement are similar between comparable patient groups who undergo TAVR with either the CoreValve or Edwards Sapien Valve, there are notable differences in complications seen in patients treated with the two valves. One such difference between the CoreValve and Sapien Valve is the need for permanent pacemaker placement (PPM) after the procedure. The incidence of PPM placement after CoreValve ranges from 12.1 percent in the Italian registry up to 39 percent in other registries [3]. In contrast, the incidence of need for PPM in the PARTNER study with the Sapien Valve was 5.7 percent and 4.5 percent in groups A and B respectively, which was not different from those patients treated either medically or surgically. The increased incidence of PPM placement after the CoreValve procedure is due in part to the fact that the frame of the CoreValve extends below the aortic annulus and thus lays adjacent to the left bundle branch. As a result, the His bundle may be adversely affected during the expansion of the prosthesis due to the high radial force of the self-expanding Nitinol frame of the CoreValve. While the structure and design of the CoreValve leads to an increased need for PPM placement, it also allows for the valve to be more easily delivered and repositioned during delivery. In contrast to the Sapien Valve, which requires either a large 22 French or 24 French sheath for delivery, the CoreValve is able to be delivered through an 18 French sheath. Since the anatomy of many patients cannot accept a 22 or 24F sheath, the CoreValve can thus be used in many patients who otherwise would not have been able to tolerate the size of the Sapien delivery system [3].

As a result of the larger sheath size for delivery, there is an associated increase in vascular complications seen with the Sapien Valve. The primary vascular access for sheath placement and subsequent delivery of both the CoreValve and Sapien valve is via the femoral artery; however, due to the large sheath sizes required, alternative access sites are being investigated. These include direct left ventricular apical access for the Sapien Valve and both subclavian and direct aortic access for the CoreValve. The outcomes from these alternative access sites as compared to femoral access have not been fully evaluated; however, data from studies, including the trial that compared the transapical approach for TAVR with the Sapien valve against conventional SAVR, has raised concerns about these alternative approaches [3].

The ability to adjust the positioning of the valve during delivery gives the CoreValve a distinct advantage over the Sapien Valve. Due to the self-expanding nature of the Nitinol frame of the CoreValve, the CoreValve can be deployed in stages allowing for subtle adjustments in position during the deployment phases (Figure 2.1). In contrast, the Sapien Valve is rapidly deployed with a single balloon expansion that does not allow for repositioning either during or after deployment (Figure 2.2). The self-expanding design of the Core Valve prosthesis offers many others potential advantages over a balloon expandable device. First and most important, a self-expanding percutaneous aortic valve may minimize the occurrence of paravalvular leaks and enable the treatment of patients with aortic regurgitation. Secondly, by avoiding balloon trauma to the valve leaflets, the self-expanding design may theoretically prolong valve durability. Thirdly, the self-expanding upper segment of the valve may provide secure fixation in the ascending aorta. However, this was achieved by the use of general anesthesia and extra corporeal support and needs more clinical trials and long-term follow-ups to reveal the potential advantages of this technique [3].

Figure 2.1 and 2.2: Respectively, CoreValve and Sapien with the system used for the implantation

2.3 UCL's Stent

In 2013 it was designed and manufactured at the Department of Mechanical Engineering of UCL, a new fully retrievable/repositionable TAV with leaflets made of a novel synthetic functional nanocomposite polymer and with a stent patented by UCL (described in details in paragraph 3.2): the TRISKELE device. The valve is composed by a self-expanding Nitinol stent, polymeric leaflets and a sealing skirt (wings), as shown below (Figure 2.3).

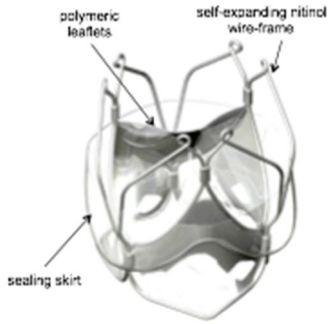

Figure 2.3: TRISKELE valve

In vitro comparative tests with first generation solutions have shown that the effective orifice area of the TRISKELE is similar to TAVI devices currently in the market, while the regurgitation fraction is improved, determining lower ventricular energy loss during cardiac cycle and better valve performance [2].

During the implant on ovine, the valve was collapsed in the delivery system and successfully implanted off-pump via brachiocephalic approach in orthotropic position, using continuous ultrasonic and fluoroscopic guidance. Dr Mullen successfully implanted and extracted three valves of different sizes (23 mm, 26 mm and 29 mm). Each valve was retrieved into the catheter and repositioned, after assessing their optimal positioning and hemodynamic performance (Figure 2.4).

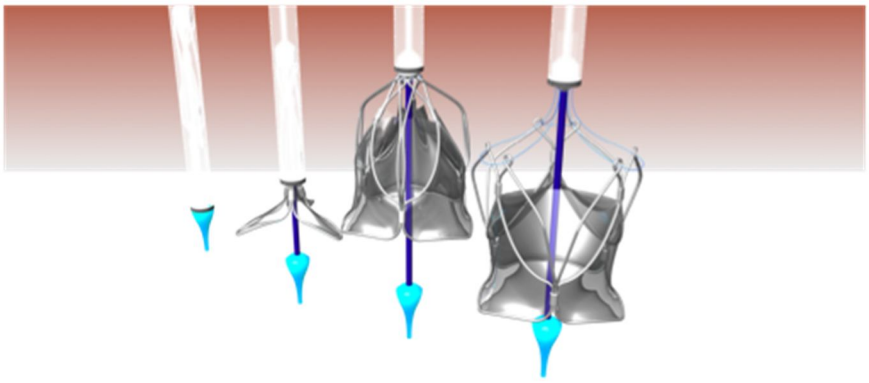

Figure 2.4 Opening of the stent from the catheter

No interference of coronary blood flow was observed for the two smallest sizes, more suitable for the animal anatomy, and good acute valve function with no significant regurgitation was confirmed for all devices.

Chapter 3: Materials and Methods

3.1 Goals of the work

The purposes of this work is to develop and assess a new heart valve (TAV) to reduce paravalvular leak (PVL) and evaluating valves indexes, in order to compare the valve with commercial ones, using the stent (described in the paragraph 3.2) and a model of leaflets and wings. Many parameters will be evaluated such as: Transvalvular pressure gradient, Closing Volume, Aortic Leakage and Aortic Regurge Fraction, Aortic Orifice Area (EOA), Transaortic Forward Energy Loss, Transaortic Closing Energy Loss, Transaortic Leakage Energy Loss, Transaortic Total Energy Loss. Furthermore, experimental data will be integrated with computational analysis: through computational models, stress fields on the surface of the leaflets will be calculated.

3.2 Stent

As explained in the paragraph 2.3, in 2013 a new fully retrievable/repositionable TAV was designed and manufactured at the Department of Mechanical Engineering of UCL, with leaflets made of a novel synthetic functional nanocomposite polymer and with a stent patented by UCL: the TRISKELE device.

The valves that we have realized are still composed of the TRISKELE's stent but we used pericardium instead of the composite polymer for the leaflets; moreover, in order to limit the fluid flow through the leaflets and the wings, we chose to use a geometry with them connected.

In the next paragraphs, we are going to describe the stent's properties and shape and the leaflets' materials and shape. After that, we will describe how we realized our valves and how we took the advantages from both structures.

3.2.1 Stent material: Nitinol (Ni-Ti)

Metallic alloys that tend to return to the original shape after large deflections have been appreciated since the 50s. They have been studied not only for their use in Aeronautical Engineering, because of their sufficient ductility, but also in medicine in the development of prostheses that replace long bones, in the study of surfaces and biofilms and in heart valve prostheses. They present a low modulus of elasticity (E) and excellent spring back when compared to other alloys (Figure 3.1).

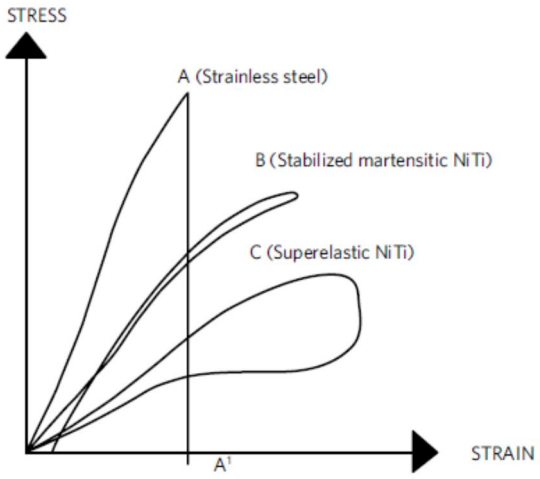

Figure 3.1: Stress and Strain diagram. A, B, C wires present different stiffness. A represents stainless steel behaviour; B represents stabilized martensitic wire (ex. Nitinol) and C represent superelastic wire**.**

Many of nickel-titanium alloys are commercialized as shape memory alloys, while others do not even show the effect of superelasticity and present characteristics of martensitic-stabilized alloys as the alloys originally known as Nitinol (*Unitek, Monrovia, CA, USA*).

In the ’80-‘90s of the last century, the attention turned towards super elasticity instead of the more complicated shape memory effect and towards medical applications, particularly implants. There appear to be three primary reasons for the sudden success. Perhaps most importantly, the medical industry itself has been driven towards less and less invasive medical procedures. This, in turn has created a demand for new medical devices that really

cannot be made with conventional materials. Other factors were the availability of micro-tubing and the ability to laser cut tubing with very high precision [36].

Probably the best illustration of all these points is the self-expanding stent. Nowadays, the term stent is reserved for devices used to scaffold or brace the inside circumference of tubular passages or lumens, such as the esophagus, biliary duct, and most importantly, a host of blood vessels including coronary, carotid, iliac, aorta and femoral arteries. Stenting in the cardiovascular system is most often used as a follow-up to balloon angioplasty.

Most stents today are 316L stainless steel and are expanded against the vessel wall by plastic deformation caused by the inflation of a balloon placed inside the stent. Nitinol stents, instead, are self-expanding: they are shape-set to the open configuration, compressed into a catheter, then pushed out of the catheter and allowed to expand against the vessel wall. Typically the manufactured stent diameter is about 10% greater than the vessel's in order to assure the stent anchors firmly in place.

The most important reason to use Nitinol for stents is that superelastic Nitinol has a flexibility 10-20 times greater than stainless steel; that is to say, one can observe devices to 'spring back ' with strains as high as 11% [37]. This in-site flexibility plays a role in some superficial stent applications such as the carotid and femoral arteries, where the vessels may be subject to outside pressures that would cause conventional stents to crush. Such deformations have been observed in stainless steel stents, and they can lead to serious consequences. Furthermore, modern medicine has been steadily driving towards less invasive procedures. Vascular diseases are repaired by passing wires and instruments percutaneously through needles into the femoral artery and onto the heart, brain, etc. These procedures require instruments and devices that can pass through very small openings and then elastically spring back into the desired shapes.

An additional unique attribute of Nitinol devices is that they can be deployed using the shape memory effect; this property derives from the two crystal structures that can be interconverted by changes in temperature or pressure. At temperatures between about 0 and 100 degrees Celsius, there are two important phases or crystal structures of NiTi that can be referred to as the high temperature and low temperature phase, or as austenite and martensite, respectively. The austenite phase has the symmetry of a cube and is characterized by hardness and rigidity.

When cooled, the austenite phase transforms to martensite, which is less symmetric and it can have 24 different relative orientations (called variants) of groups of atoms comprising the crystal. When pressure is applied to this low temperature phase, groups of atoms can change their relative orientation to accommodate the pressure, causing the material to be softer and more flexible than the austenite phase. Because martensite is also slightly denser than austenite (by LeChatelier's principle which states that an increase in pressure favors the denser phase of multiple phases at equilibrium), pressure can be used to convert austenite to martensite. The defects, which can be altered at the high temperature of a candle flame where NiTi is in the austenite phase, are used to create the shape to be "remembered" by forcing groups of atoms to have particular positions relative to one another [37].

Another important feature of superelastic materials is that they exhibit constant unloading stresses over large strains. Thus, the force applied by a superelastic device is determined by temperature, not strain as in conventional materials. Since body temperature is substantially constant, one can design a device that applies a constant stress over a wide range of shapes.

Another important advantage of Nitinol is the extremely good biocompatibility, in the meaning of very low foreign body reaction, due to the formation of a passive titanium-oxide layer (TiO_2), similar to that found on Ti alloys. This oxide layer serves two purposes:

• increases the stability of the surface layers by protecting the bulk material from corrosion;

• creates a physical and chemical barrier against Ni oxidation and modifies the oxidation pathways of Ni.

Several comparative studies have shown that in simulated physiological solutions NiTi is more resistant to chemical breakdown than 316L stainless steel, but less so than Ti-6AI-4V.

Furthermore, *Trepanier et al.* performed an in vivo study on passivated NiTi stents. Implantation of the material in rabbit paravertebral muscles and study of the inflammatory reaction for periods ranging from 3 to 12 weeks demonstrated good biological response to NiTi. Analysis of the fibrous capsule surrounding NiTi stents revealed a decrease of the thickness as a function of time.

For many of these reasons, Nitinol has been chosen as the constructive material for the UCL's Stent.

3.2.2 Stent: Shape

The stent was developed at UCL with the collaboration of the Heart Hospital UCLH and for the first time implanted in a ovine model on May 2013 [2]. It is made of Nitinol and therefore is a retrievable/repositionable stent that let to overcome typical TAV's positioning problems thanks to superelastic and memory form's properties. It was made three different size: 23 mm, 26 mm and 29 mm. In this thesis, we focus our attention on the 26 mm size. Four different views of the 26 mm stent are represented below (Figure 3.2).

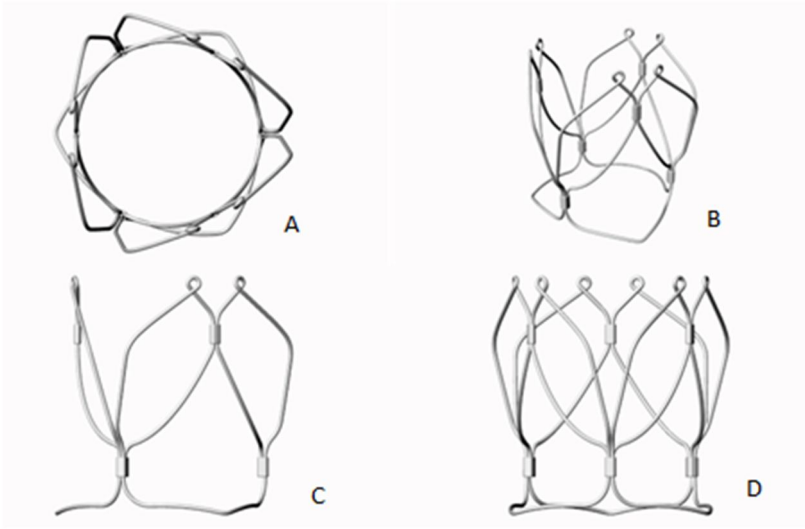

Figure 3.2: Four different views of the 26 mm stent

The stent is realized with a very specific design to match the shape of the leaflets.

In particular, it is possible to divide it in three main part (see Figure 3.3), which are briefly described below:

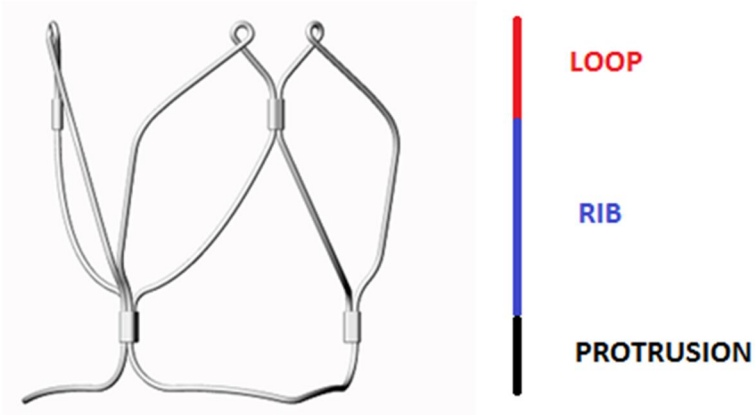

Figure 3.3: Main parts of the stent

- Loops are the upper part of the stent and are specifically designed to minimize the stress concentration. In fact, a very important concept is the stress concentration at the apexes. In the case of, for example, triangular tips, variation of the section lead to an increasing of stress in proximity of the tips that could bring to a structural failure of the material, due to the coefficient of concentration of stress (function of the geometry). Another important function of loops is to facilitate the collapse of the valve into the catheter, during the time of implant.
- Ribs at the top of the stent and Protrusions at the bottom enable the anchor of the valve on the annulus between them, thanks to the shape that is suitable for leaflets.

3.2.3 Stent: mechanical properties

The mechanical properties considered in this thesis from UCL database are:

$$E_A = 50 \text{ kN/mm}^2;$$

$$\nu_A = 0.3;$$

the Young's modulus and the Poisson ratio of the austenite phase are:

$$E_M = 25 \text{ kN/mm}^2;$$

$$\nu_M = 0.3;$$

the Young's modulus and the Poisson ratio of the martensite phase are:

$$\sigma_s^{AS} = 380 \text{ N/mm}^2;$$
$$\sigma_f^{AS} = 400 \text{ N/mm}^2;$$

the starting and the final stress during the phase transformation from austenite to martensite are:

$$\sigma_s^{SA} = 250 \text{ N/mm}^2;$$
$$\sigma_f^{SA} = 220 \text{ N/mm}^2;$$

the starting and the final stress during the phase transformation from martensite to austenite:

$$\epsilon_L = 7\%;$$

where ϵ represents the percentage strain.

All these values are referred to 37 °C.

3.3 Leaflets

3.3.1 Leaflets: material

Regarding the tissue two different pericardium have been tested in order to observe the difference between the 2 valves' performance: a standard pericardium and a decullularized one. We can provide information and properties for the standard pericardium but we can't provide details about the production of the decellularized pericardium, due to industrial secret: in fact, a company developed this tissue and wanted to test it on an aortic valve. It is basically a pericardium without cells, it is biocompatible, blood compatible and without immunological response from the host environment. Furthermore, in order to get the material properties, both of them have been tested through tensile test in the Laboratory (see Figure 3.4).

Figure 3.4: Pericardial specimen during tensile test

Pericardium can be considered as a composite material constituted by an amorphous matrix of proteins and polysaccharides in hydrated macromolecular complexes, containing multidirectional bundles of collagen and elastic fibers having preferential directions [38].

It is clear that this structure implies a certain degree of anisotropy in the mechanical

characteristics of the tissue. Like in other biological soft tissues, orthotropy is a good representation of the behavior, with three principal directions: one along the dominant fiber direction in the plane of the tissue, one across that direction and the last is normal to the tissue. Anatomically, pericardium is a double membrane that, in mammals, encases the heart. Thus, pericardium surrounds the heart in a membrane, whose shape and size correspond to those of the heart itself. It can be grossly divided into two layers: an outer fibrous (fibrous pericardium or pericardial sac) and an inner, serous (serous pericardium) [39]. The latter is made up by two layers: one visceral, closely adherent to the myocardium (called epicardium) and the other one, that is adherent to the fibrous pericardium. The two sheets of the serous pericardium are separated by a virtual space, the cable pericardial, which contains a small amount of yellow viscous liquid (pericardial fluid), whose function is to facilitate the movements of the heart during contraction. It is shown below a representation of the sagittal section (Figure 3.5).

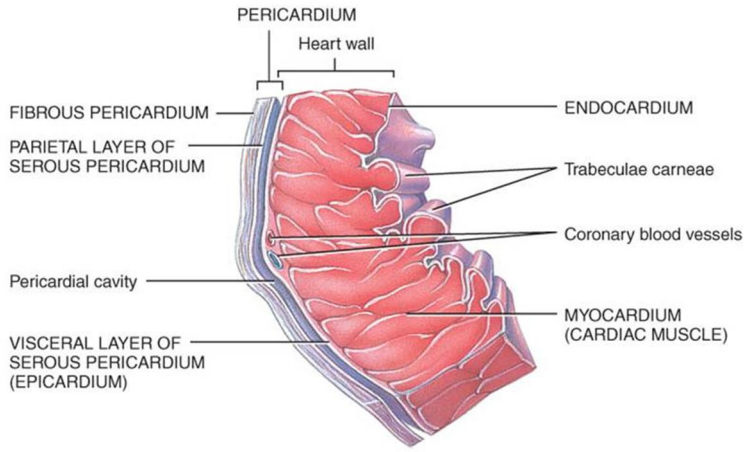

Figure 3.5: Sagittal section of generic pericardium.

3.3.2 Leaflets: Shape

The original shape used for the previous valve by UCL was composed of two separate parts: the leaflet and the wings (Figure 3.6).

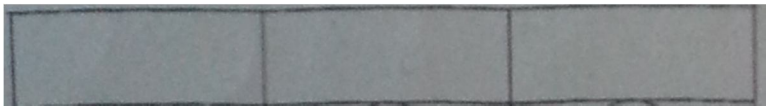

Figure 3.6A: Wings shape

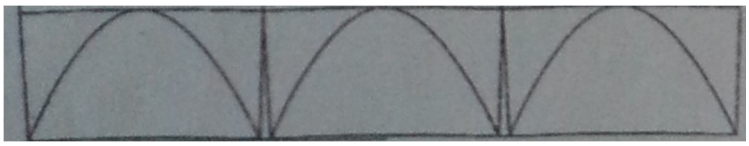

Figure 3.6B: Leaflets shape

The problem of the shapes just depicted was the conjunction between the two parts; in fact, due to the suture spots used to keep together the two main parts, it was possible for the fluid to flow through them more easily than what happens through an entire continuous shape. For this reason, we chose to use a different shape (available at the Department of Mechanical Engineering of UCL), with leaflets and wings included in a unique model (Figure 3. 7).

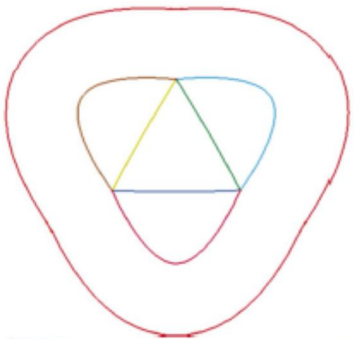

Figure 3.7: Model of leaflets and wings: the three triangles in the middle represent the leaflet whereas the shape around them represents the wings.

This shape tries to reduce the spaces between implanted valve and the aortic root (thanks to its wings) and tries to limit reverse flows of blood to the left ventricle when the leaflets close (thanks to the inflating of the wings). With the purpose to become familiar with sutures, the first leaflets that we realized were made of deer skin; we sutured with needle and thread the leaflet's shape on the deer skin by positioning the paper shape on the tissue and suturing following the path. By water dipping it was possible to remove the paper and get the wanted shape. After that, we used a pair of scissors to cut the deer skin on its boundary to get the wing shape.

The result of this process is shown in Figure 3.8.

.

Figure 3.8: deer shaped leaflet. The three cuts on the outer tissue are useful for folding the tissue on the stent

After practicing with the deer skin that is easier to handle and cheaper than the real tissue, we focalized our attention on pericardial valves.

In order to get the pericardium shaped leaflet, it wasn’t possible to use the same method described above; pericardium, in fact, is very difficult to handle and to keep it steady in the correct position, in order to track the leaflet shape on the tissue.

In fact, the main problems of the pericardium shaping are:

- it's very flexible, so it has to be kept still in the final position it will assume;
- it's a biological material so it has to be kept into the water to keep it wet.

In order to cut the pericardium into the shape depicted in Figure 3.7, a plastic support has been realized using the laser cutter. The CAD software used to convert the model into a

format recognizable by the machine was Adobe Illustrator.

The obtained support is shown in Figure 3.9.

Figure 3.9: Plastic support obtained by laser cutting; all the holes and cuts apart of their function allow water to wet the tissue when dipped into water

This support helped us to keep the tissue still and to suture it on its final shape; furthermore, it was useful to wet the tissue during the suturing. In order to get the leaflet shape, a pericardium patch was placed between two plastic supports (Figure 3.10) and needle and thread were used to track the desired leaflet shape.

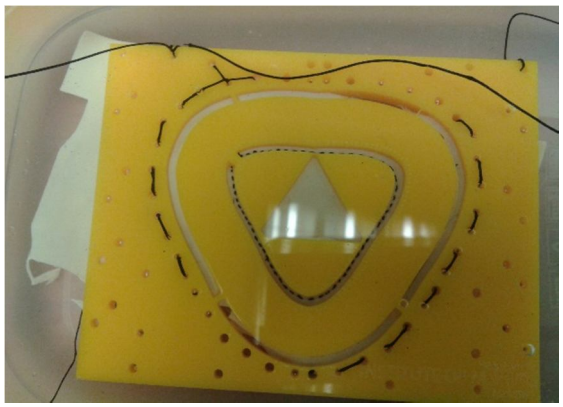

Figure 3.10: Two plastic supports with pericardium between them

It was possible to pass the needle through the supports and to suture the wanted leaflet's shape on pericardium, thanks to the cuts and the holes into the plastic supports. The leaflets' shape obtained is represented in Figure 3.11.

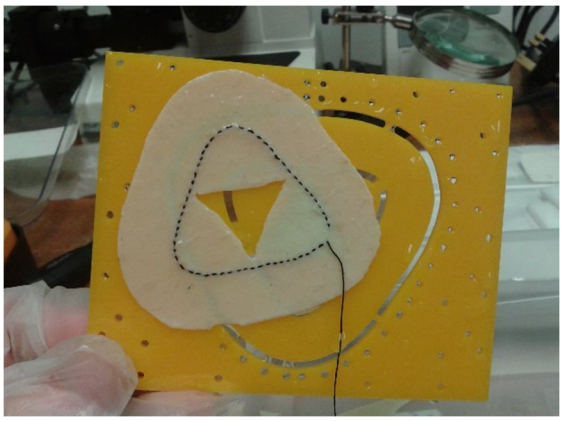

Figure 3.11: leaflets shape

It was very important to have stitches with the form of leaflets on the tissue (Figure 3.11) in order to anchor the tissue to the stent. This procedure will be better described in the following paragraph.

3.4 Enclosing: realization of the valve

The obtained shape has been folded on the stent and stitched to it with needle and thread in order to get the valve. In this paragraph the protocol followed in order to get the decellularized valve is described. The same protocol has been used for the standard pericardial valve and for the deer skin ones.

The tissue has been cleaned up using the salt solution. In the Figure 3.12 is shown the cleaned decellularized pericardium shape.

Figure 3.12: shaped tissue with white thread describing the leaflet shape.

After the cleaning, we folded the tissue on a silicon mold that represented the negative of the valve (Figure 3.13). This helped us to keep the final structure shape during the suturing to the stent (Figure 3.14). With needle and thread we sutured every single stitch to the stent with an Asola suture. This suture guarantees that, even if the thread has cut in one point, the slackness isn't propagated on.

Figure 3.13: tissue on the mold

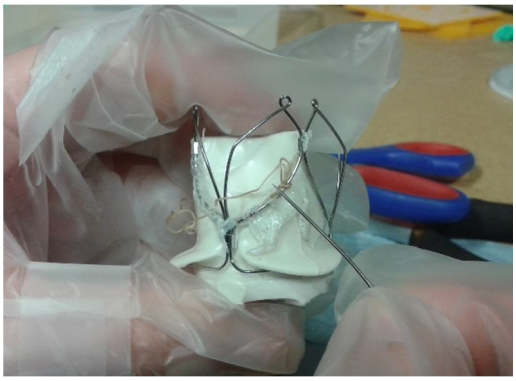

Figure 3.14: suturing of the tissue to the stent

We have first obtained the leaflets stitched to the stent and then the wings (Figures 3.15-3.16).

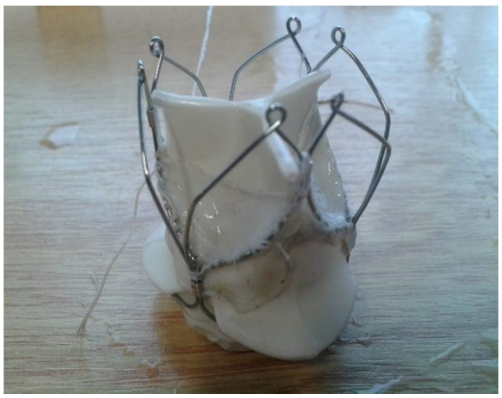

Figure 3.15: leaflets stitched to the stent

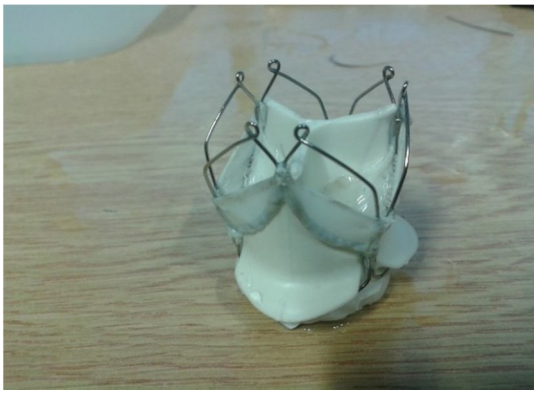

Figure 3.16: wings and leaflets stitched to the stent

Finally, we got the result depicted here (Figure 3.17):

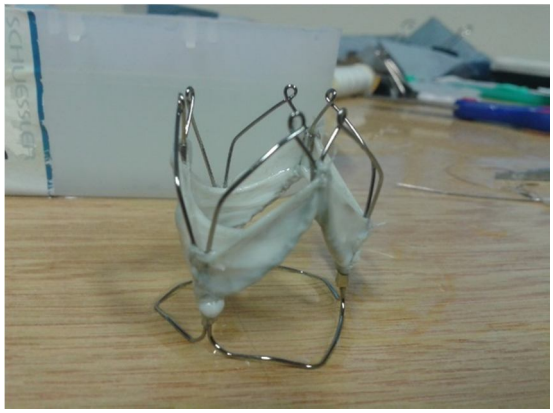

Figure 3.17: dCell pericardium TAV

In Figure 3.18, the pericardial valve obtained with the same method is represented.

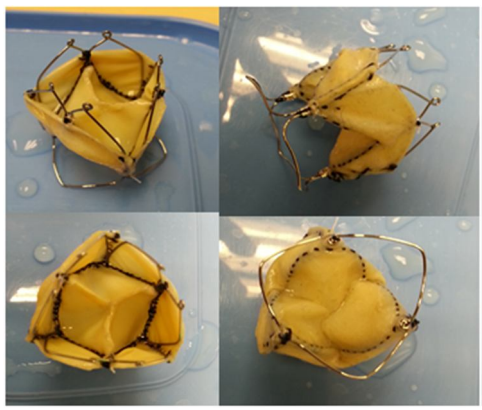

Figure 3.18: pericardial valve from different views

In order to get a better integration with the human root, we put a net cage under the biological tissue. In the following figure, it is possible to observe the net cage on a deer skin valve (Figure 3.19).

Figure 3.19 deer skin valve used for training purpose. It is possible to observe the net cage necessary for a better integration with the living tissue

3.5 Experimental Protocol and ISO Standard for valve testing

3.5.1 Tissue experimentation

In order to investigate the mechanical characteristics of the pericardium, uniaxial tensile tests were performed on more than 35 glutaraldehyde-fixed bovine pericardial specimens prepared from five pericardial samples, and variations in strength and stiffness were determined for two different cutting directions.

3.5.2 Sampling and preparation of tissues

Bovine pericardium samples were obtained immediately postmortem.

The whole complex of the biological tissue included not only pericardium but also fat (Figure 3.20).

Figure 3.20: View of the pericardium with fat

The fatty tissue surrounding the pericardium was delicately removed, obtaining a sheet of pericardium without fat. This operation was carried out with the help of scissors (Figure 3.21).

Figure 3.21: Pericardium without fat

Subsequently to the operation of macroscopic separation, it was necessary to remove the small portions of fat with scalpels, obtaining pieces of pericardium much more smooth and better suited for experimentation (Figure 3.22).

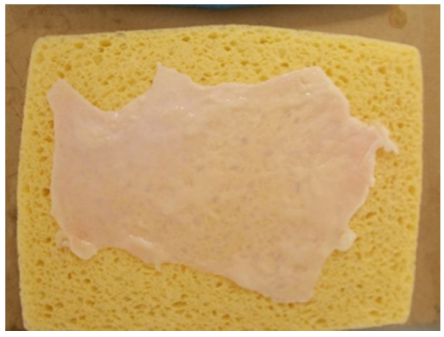

Figure 3.22: Pericardium suited for experimentation

Rectangular pieces of pericardium, approximately 10 x 10 cm or 15 x 15 cm were soaked in physiological solution.

3.5.3 Glutaraldehyde treatment

After the tissue was separated from fat, the leaflets were immersed for 48 h in a saline solution with 0.5% glutaraldehyde. Furthermore, to ensure that the tissue does not wrinkled or rolled up on itself, it was necessary to place it between two sponges soaked in solution and kept in contact via simple magnets (Figure 3.23).

Figure 3.23: Pericardium in the bath of glutaraldehyde

It is well known that fixation with glutaraldehyde stabilizes and cross-links the tissue. Crosslinking reduces the biodegradability and antigenicity of the tissue, modifying its mechanical properties, and reducing its thrombogenicity. At the end of treatment (i.e. after two days) the tissue appeared more clean and homogenous (Figure 3.24).

Figure 3.24: Tissue after the treatment

3.5.4 Samples preparation

The operation was performed using a special machine (Wallace Manual Specimen Preparation Cutter – Figure 3.25), whose operation is similar to that of a press.

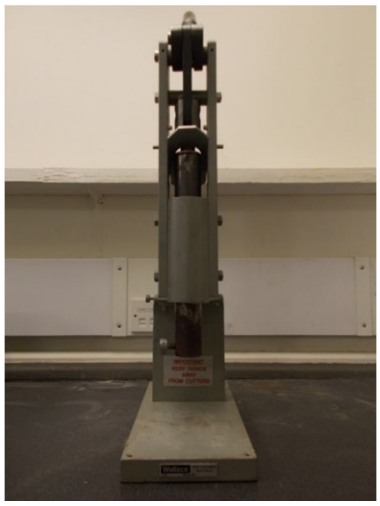

Figure 3.25: Machine used for the sample preparation

A mold was used in order to realize the specimens; they were placed in correspondence of the terminal part of the machinery; the size of the mold in the centerline is 4 mm (Figure 3.26).

Figure 3.26: Mold used for the realization of the specimens

Then, several samples of consecutive portions of pericardium were extracted (Figure 3.27), optimizing the availability of the material and avoiding, as much as possible, wasting of tissue.

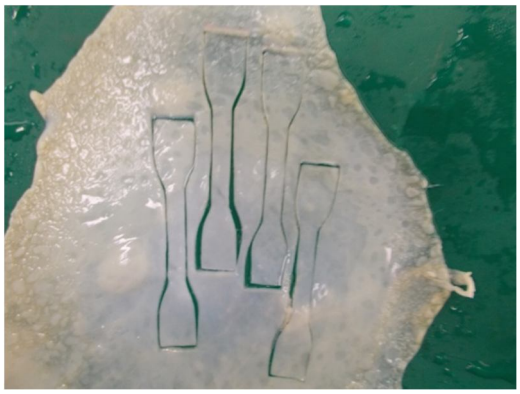

Figure 3.27: Samples of pericardium obtained

Examination of the specimens thickness, performed using a micrometer, showed a mean value of 0.40 mm (Figure 3.28).

Figure 3.28: Specimen obtained

3.5.5 Testing machines and settings test

The samples were tested using a Zwick / Roell Z 5.0 machine (Figure 3.29) and kept in water during the entire duration of the test, in order to avoid dehydration. The constant temperature of 37° C was monitored by a thermocouple soaked in the bath with a cooler. The force and displacement's data were recorded by using the software "testXpert II."

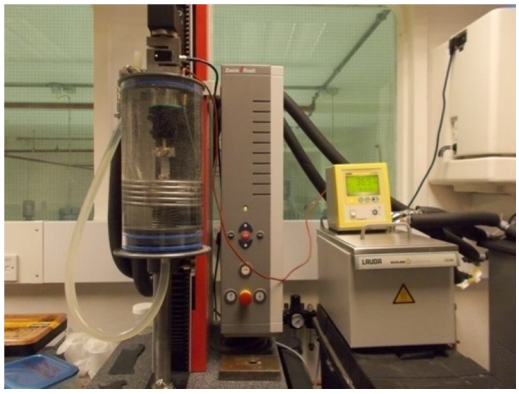

Figure 3.29: Zwick/Roell Z 5.0 machine used for the tensile tests

The experimental procedure started assembling the grip, that was connected to aluminum rods, inserted within the two seals in water, in order to have the two clamps inside the tube.

Before performing the test, the sample was placed on a template (Figure 3.30), which acts as a support to ensure the permanence of the same sample on the desired plane (the one on which act the driving forces of the machine of test), which would be impossible without the aid of the latter.

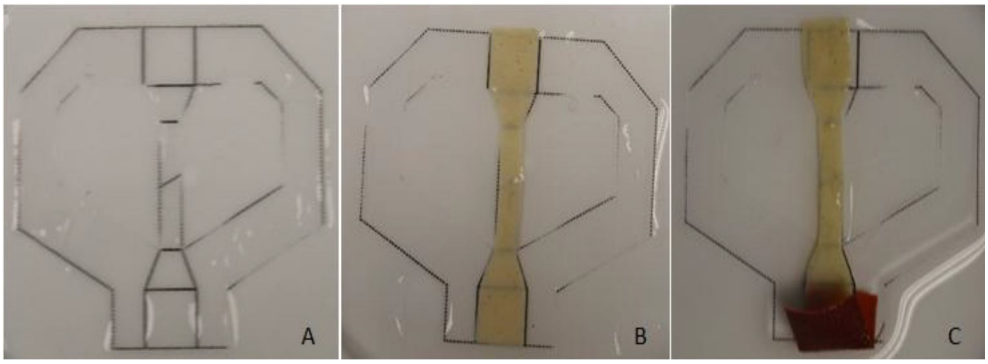

Figure 3.30: Specimens with templates

The portion of pericardium free from the grip is about 5 mm while the other part of the tissue was grasped by the lower clamps (Figure 3.31).

Figure 3.31: Pericardium specimen placed in the machine

Finally, uniaxial tensile tests were performed in a PMMA container filled with water bath. The specimen was then locked in the pliers and the tests were conducted applying an extension rate of 5 mm/min.

3.5.6 Determination of relevant parameters

During each test, the system records the load (N) that develops following the imposed displacement (mm). This data is stored as a text file and then analyzed using Microsoft Excel. The data are essential for the analysis of the mechanical behavior of the tissue in order to obtain, for each sample, the stress-strain curve. Afterwards the data (force and displacement) are converted to stress (MPa, y-axis) and strain (%, x-axis). The tension σ is calculated as the ratio between the load (N) and the section (mm^2):

$$\sigma = \frac{N}{A}$$

The strain ε is calculated using the following equation:

$$\varepsilon = \frac{l - l_0}{l_0}$$

where $l-l_0$ is the change in length obtained directly from the experimental data, l_0 is the initial length of the sample equal to 5 mm. The whole is then multiplied by 100 to obtain the value of deformation in percentage.

Each curve represented the “engineering curve", that is obtained by ignoring the narrowing of the section in the course of elongation of the sample. From this curve it is possible to perform an initial analysis and extract some information of interest. For a more detailed analysis, however, it would be necessary to refer to a curve that takes into account the variations of the section throughout the course of the test. From the stress-strain curve it is possible to derive important quantities such as the elastic modulus and the ultimate voltage, which serve to characterize the mechanical behavior of the tissue.

The parameter elastic modulus expresses the relationship between stress and strain in the case of uniaxial loading conditions and in case of elastic behavior.

The parameter maximal stress is defined as the "maximum stress reached in the test before beginning any damage in the process". For simplicity, that stress corresponds to the last final stress value belonging to the linear phase.

The calculation of biomechanical parameters mentioned can be quite complex, especially when it has to do with biological samples of this type. In this regard and in order to homogenize, as far as possible, the results, samples are grouped for the same pericardium, for the same area and oriented in the same way. The samples belonging to the same pericardium are as homogeneous as possible between them. The elastic modulus and other parameters of each sample are averaged with those of the samples belonging to the other groups, obtaining an average overall value, complete with standard deviation (SD).

3.6 Testing machine and its properties

In order to test the valve in an environment as closer as possible to the human heart we performed the tests on the ViVitro Pulse Duplicator that is widely used in vitro cardiovascular hydrodynamic testing system. It is composed of the ViVitro Model Left Heart, SuperPump and ViViTest data acquisition system.

ViVitro allows to assess the performance of prosthetic heart valves under simulated cardiac conditions. It have been tested 3 valves: the first one was the deer skin one and it was tested for training purpose therefore no data were collected, the second valve was the pericardial one and the third one the decellularized pericardium valve. The same pericardial valve has been tested also with shorter leaflets (trimmed valve). Those valves have been compared with other commercial valves tested in the past on the same machine by the research group.

3.6.1 Description of ViVitro System

A picture of the testing machine is shown below (Figure 3.32).

Figure 3.32: ViVitro Pulse Duplicator

The machine imitates the left part of the heart. The chamber **(1)** on the right side of the above picture represents the atrium. The number **(2)** is a chamber that contains the mitral valve and the number **(3)** is the ventricular that pumps fluid using the pump **(7).** So, the pump rise up the pressure on the chamber; when the pressure is higher than the pressure in the aorta **(5)** the TAVI, that is positioned in the chamber **(4),** opens and lets the fluid goes into the circulation represented by the elements **(6).** It is also possible to regulate the impedance of the body through the control knob **(8)**.

3.6.2 Curves and Data Acquired

The machine is connected with three pressure sensors and one flow sensor. Furthermore, there is a pressure transmitter in each chamber: one in the atrium, one in the ventricle and one in the aorta and the flow meter is just below the aortic valve. Every recorded information goes into the data acquisition box (Figure 3.33) and then to the software.

Figure 3.33: acquisition box

The main 4 curves we are interested in are (Figure 3.34):

- red curve: represents the pressure in the aorta (after the valve);
- yellow curve: represents the ventricular pressure (below the valve);
- light blu curve: represents the atrial pressure;
- dark blu curve: represents the flow.

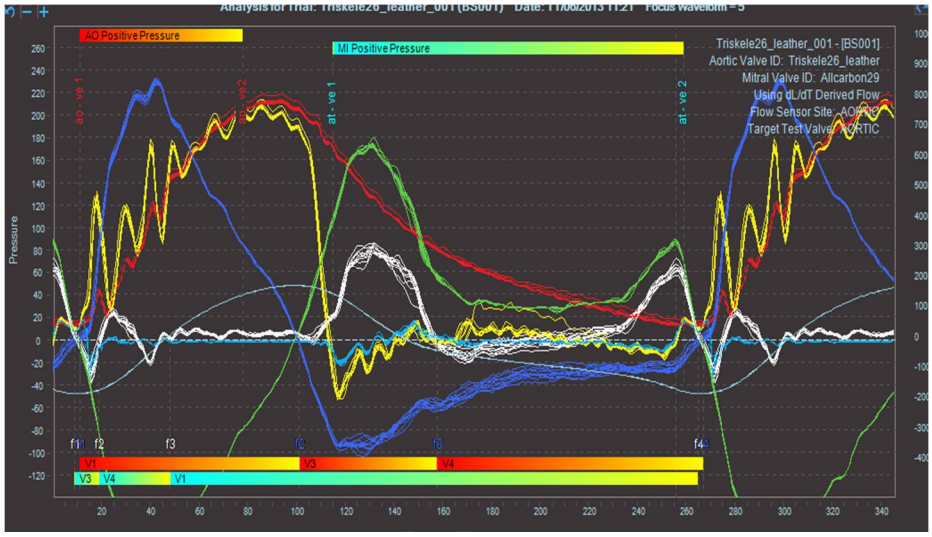

Figure 3.34: example of acquired curves

The software calculates the following pressures:

- trans-aortic pressure as difference between the ventricular and the aortic pressure;
- transmitral pressure as difference between the ventricular and the atrial pressure;
- pump dl/dt: velocity of the piston (l=distance; t=time);
- derive flow: different between the flow meter and the dl/dt of the pump;
- curve for the pump volume.

During the test, the software acquires 10 cycles and then analyzed these cycles in different sections. In the appendix A more details about the machine are explained.

See appendix B for more details.

3.7 ISO Standard: device hydrodynamic performance assessment

Hydrodynamic tests shall be performed in order to provide information about the mechanical performance of the transcatheter heart valve substitute and provide indicators of the valve performance in terms of load to the heart and potential blood damage. The implant shall be deployed into the test fixtures using the loading and deployment steps in accordance with the IFU. The test chamber shall be representative of the critical aspects of the target implant site (e.g. compliance, geometry) for the target patient population. The minimum performance requirements depicted in Figure 3.35 provided as a function of deployed valve diameter (in mm) shall be used as a frame of reference for assessing transcatheter heart valve performance.

Parameter	Deployed valve diameter within implant site mm							
	17	19	21	23	25	27	29	31
A_{EO} (cm^2) greater than or equal to	0,70	0,85	1,05	1,25	1,45	1,70	1,95	2,25
Transvalvular regurgitant fraction (% of forward flow volume) less than or equal to	10	10	10	10	15	15	20	20
Total regurgitant fraction (% of forward flow volume) less than or equal to	15	15	20	20	20	20	25	25

Figure 3.35 Minimum device performance requirements

3.7.1 Valve testing protocol

Aortic hydrodynamic function and ventricular pressures along with the aortic flow rate were measured during the forward and closing flows; this was necessary in order to quantify the mean transvalvular systolic pressure drops, regurgitant and closing volumes, leakage fraction, effective orifice areas (EOA) and energy losses as a function of cardiac output.

The hydrodynamic function parameters (systolic and diastolic characteristics) were plotted against the increasing cardiac outputs (2–7 l/min), therefore for our valves we have performed tests with cardiac output in that range. For other commercial valves tested previously at UCL, tests at 5 l/min according to the ISO standard were performed. In the

Results and Discussions chapter we are going to compare our valves performance utilizing graphs with cardiac output from 2 to 7 l/min and we are going to compare them with commercial valves at cardiac output equal to 5 l/min.

The minimum performance requirements correspond to the following pulsatile flow conditions:
beat rate = 70 cycles/min,
simulated cardiac output = 5,0 l/mm,
mean aortic pressure = 100 mmHg,
systolic duration = 35 %.
These pulsatile flow conditions are based on a healthy normal adult.

It have been tested three valves: the first one was the deer skin one and it was tested for training purpose therefore no data were collected, the second valve was the pericardial one and the third one the decellularized pericardium valve. The same pericardial valve has been tested also with shorter leaflets (trimmed valve).

3.8 Computational analysis

In recent years, the possibility to combine experimental data with numerical simulations has played a very important role to complete information about the operation of the valve with stress and strain analysis; experimental machines used for testing valves, in fact, don't give information about stress and strain.

3.8.1 Finite element method and code

The software used to perform the computational analysis is © LS -DYNA (LSTC , Livermore, CA) , a commercial solver finite element able to model problems of structural dynamics and multi-physics problems, such as fluid-structure interaction (FSI). The analysis will be carried out using the explicit formulation of the solver.

LS-DYNA uses the central difference method, which gives a second order accurate integration, to advance the position of the Lagrangian mesh in time. For every time step Δt,

the algorithm iterates the following steps. First, velocity and displacement values are updated:

$$v_{n+\frac{1}{2}} = v_{n-\frac{1}{2}} + \Delta t_n \cdot a_n$$

$$u_{n+1} = u_n + \Delta t_{n+\frac{1}{2}} \cdot v_{n+\frac{1}{2}}$$

Next, the internal forces f_{int} are computed:

$$\dot{\varepsilon}^{n+\frac{1}{2}} = Bv^{n+\frac{1}{2}}$$

$$\dot{\sigma}^{n+\frac{1}{2}} = F\left(\dot{\varepsilon}^{n+\frac{1}{2}}\right), \sigma^{n+1} = \sigma^n + \Delta t\dot{\sigma}^{n+\frac{1}{2}}$$

$$f_{int}^{n+1} = \int_V B^T \sigma^{n+1} dV$$

where B is the strain-displacement matrix, F(ε) is a function of the strain which depends on the material model adopted and V is the volume of the element.

Subsequently, the external forces f_{ext} are calculated using body loads and boundary conditions.

Lastly, the accelerations are calculated by summing internal and external forces at each node of mass m:

$$a^{n+1} = m^{-1}\left(f_{ext}^{n+1} - f_{int}^{n+1} - cv^{n+\frac{1}{2}}\right)$$

After the new accelerations are calculated, the procedure is iterated.

The time step for the explicit integration is determined according to the Courant-Friedrichs-Lewy condition as the minimum stable time step in any deformable finite element of the mesh, controlled by the element velocity u, the speed of sound in the material c and the characteristic length of the element L_c:

$$\Delta t_{CFL} = f \frac{L_c}{c + u}$$

where f is the time step scale factor, set by default to 0.9.

The choice of this particular software has been made in anticipation of future business development, which will enhance performances on simulations of fluid-structural.

It have been used many different software in order to create the computational model: CAD software for the realization of the geometry and grid computing, Gambit ® *(Ansys Inc., Canonsburg, PA,USA*) and preprocessor standard for LS- DYNA, LSprepost *(LSTC, Livermore, CA*).

In this thesis the numerical simulations involve:

- Simulation of the suturing of leaflets to the stent;
- Structural dynamic simulation of opening and closing of the leaflets in order to get stress fields.

3.8.2 Simulations of leaflets suturing and dynamic

As a first step it was necessary to simulate the positioning of the leaflets onto the stent, linking the leaflets with the stent through the threads. To reach the aim, thermal simulations have been run with materials useful for this purpose. This is the reason why, for the suture simulations, the material assigned to the leaflets wasn't representative of the real properties of the pericardium.

In the following paragraphs we are going to describe the materials and the geometries used for the leaflets, for the stent and for the threads. Furthermore, a detailed report of the simulation protocol will be described.

3.8.2.1 Materials

The elastic plastic thermal was the first material used to describe the leaflets, with a density chosen equal to 1000 Kg/m^3, Poisson's ratio equal to 0,495 and Young's modulus equal to 200 MPa. The choice of using a very high Young's modulus for the leaflets during the

simulations of suturing was due to the oscillations and instabilities observed during the positioning with less stiff tissues. Starting from the positioning obtained with this configuration, in order to refine it, a new simulation has been run with identical material but with a Young's modulus equal to 2 MPa.

For reasons of simplicity, the stent has been supposed rigid (this induces higher values of local stresses than models that include stent movement).

Regarding the material used for the threads, it was chosen to use an elastic plastic thermal material for the possibility to assign thermal properties to the elements. In fact, we assigned to each thread a very high coefficient of thermal expansion (equal to 600 mK^{-1}) and a coefficient of thermal generation equal to -2400 $mJ/s*mm^3$, in order to obtain the shortening of the threads and consequently the positioning of the leaflets. Furthermore, with the purpose to get a great production of heat (negative in sign) inside the threads with a low decreasing of temperature, we set a very high heat capacity, equal to 900 J/K; thus, for great amounts of heat exchanged, the variation of temperature is relatively low, avoiding extreme and unwanted thermal deformations of the threads and, in particular, of the surfaces in contact with them, such as leaflets.

Once obtained the optimal positioning of the leaflets onto the stent, the material assigned to the leaflets during the dynamic simulations was changed from elastic plastic thermal to elastic, with Young's modulus equal to 2 MPa and Poisson ratio equal to 0,495. Nevertheless, the stress induced in the pericardium is non-linearly related to the strain, as explained in the paragraph 4.1. In fact, the response curve exhibits three different patterns:

- a low Young's modulus region, where high extensions correspond to very small tensions;
- a transient region characterized by a rapid stiffening;
- a high stiffness region, with very high stress increments associated with further extension of the tissue.

To describe such a behavior, an Ogden constitutive equation has been used to interpolate the experimental curves obtained from both pericardium tensile test and decellularized pericardium tensile test (Figure 3.36 and 3.37) (see paragraph 4.1). The interpolation has been based on an optimization of the constitutive parameters; at this purpose we have

involved the minimization of a potential defined as function of the mean square deviations calculate from the experimental values of stress.

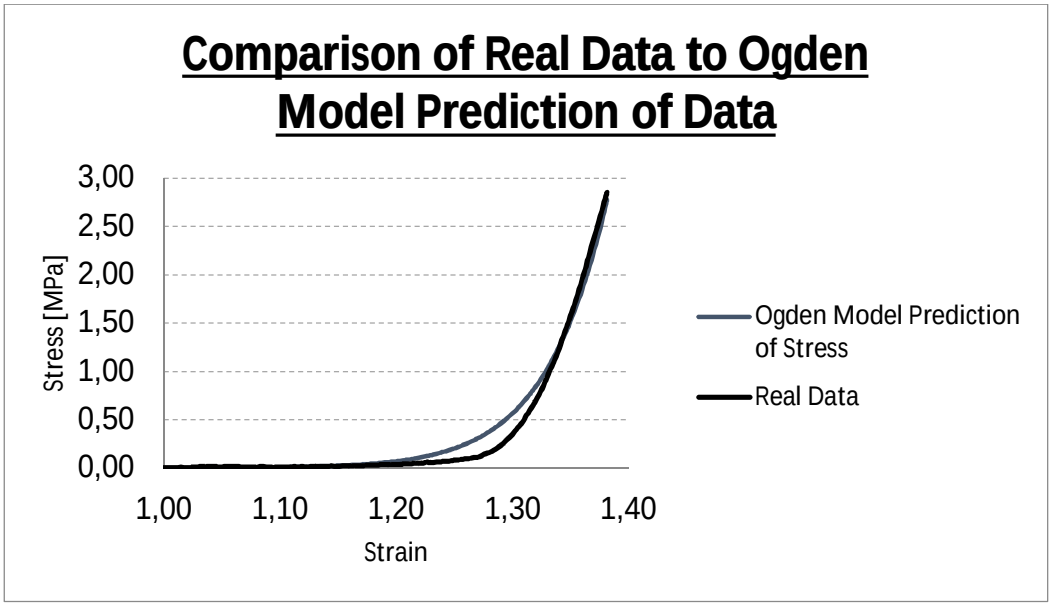

Figure 3.36: Pericardium experimental data at 37°C and Ogden fitting

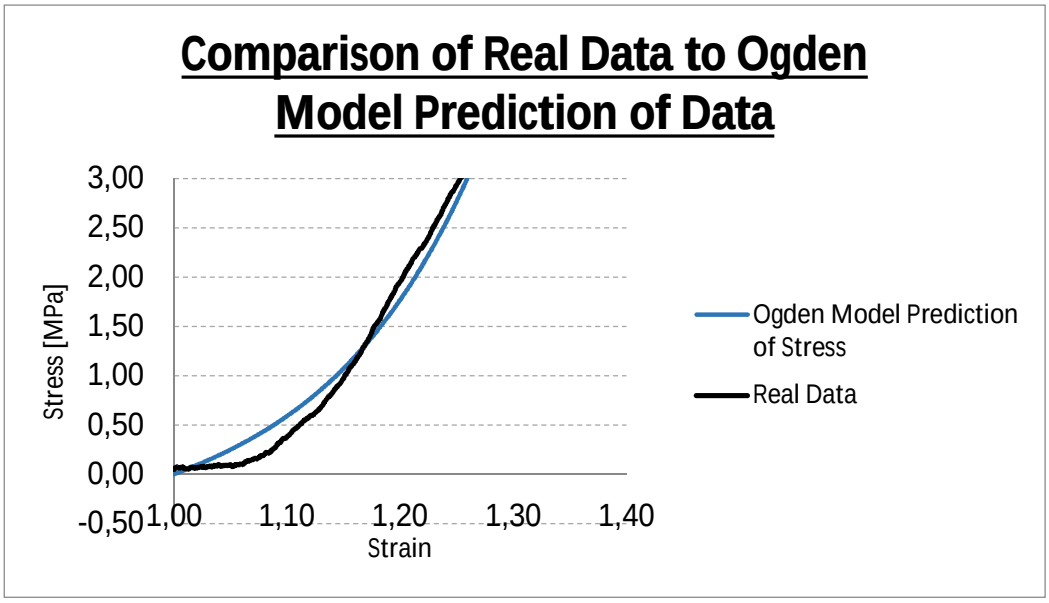

Figure 3.37: Decellularized pericardium experimental at 37°C data and Ogden fitting

Thus, dynamic simulations have been run with three different materials for the leaflets: elastic material, pericardial material (data obtained from tensile tests and fitted with Ogden model) and decellularized pericardial material (data obtained from tensile tests and fitted with Ogden model).

See the appendix C for more details about the procedure used to obtain the results.

3.8.2.2 Model Geometry

The model of leaflets selected for the analysis was the same used for the realization of the valves (Figure 3.38).

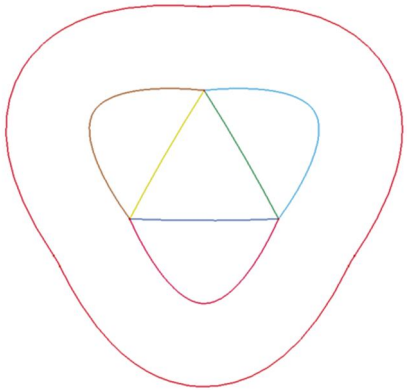

Figure 3.38: Model of leaflets available at the Department of Mechanical Engineering of UCL

The dimensions of the model are suitable for aortic valves with a diameter of the stent equal to 26 mm; however it is possible to scale the model and make it suitable also for 23 mm stent and 21 mm stent.

The model is composed by three leaflets in the inner part and the wings profile in the outer part. For reasons of simplicity and due to the aim of the computational model, the evaluation of stress fields was on the surface of the leaflets; it has been chosen to omit the wings during the realization of the computational geometry.

The obtained model is represented in the Figure 3.39.

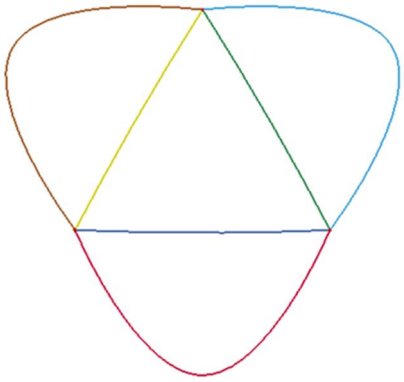

Figure 3.39: Leaflets model without wings. It has been used for the computational model

Regarding the stent, it has been presented only the profile where the leaflets are stitched (Figure 3.40). In the computational model, in fact, the stent is just a reference for the positioning of the leaflets during the suturing simulation. Thus, the geometry involves only three cusps, that are flat on the top, and doesn't consider the whole complexity of the stent, described in paragraph 3.2.

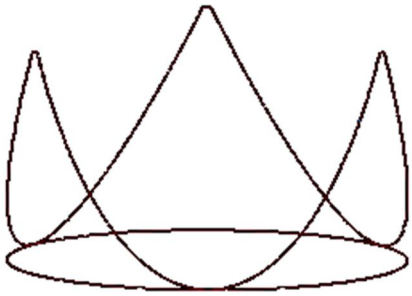

Figure 3.40: Stent profile used in the computational model. This is an exemplification of the real stent because only the shape of the leaflet was considered throughout the computational analysis.

The diameter of the stent is 26 mm whereas the height of the cuspids is 14 mm. The realization was made in Gambit and in LS Pre-post.

For both the leaflets and the stent model, the structural domain was discretized into triangular elements with spacing equal to 1 mm; this choice has been considered the best in

order to maximize the ratio between accuracy and computational time. The meshes obtained are represented in Figure 3.41 and 3.42.

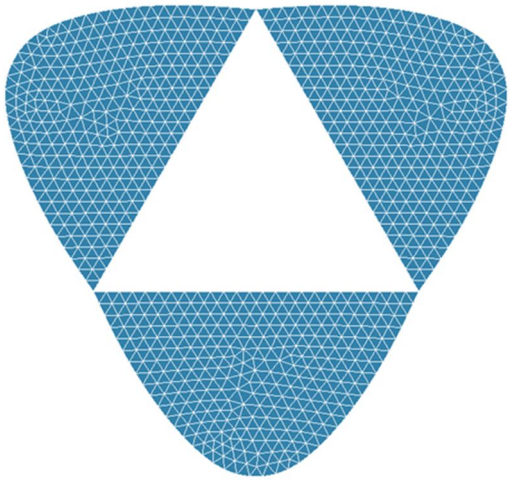

Figure 3.41: Leaflets discretized in triangular elements

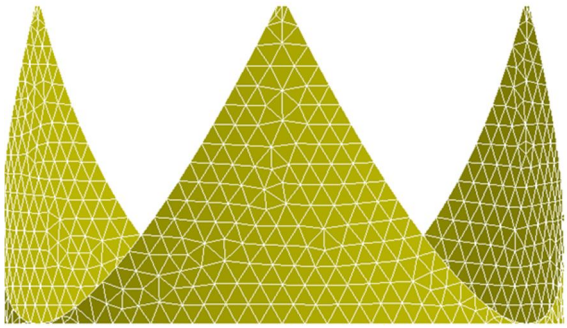

Figure 3.42: Stent discretized in triangular elements

The modelling of the geometries comprises 1595 Belytschko-Tsay triangular shell elements for the leaflets and 1015 Belytschko-Tsay triangular shell elements for the stent; the thickness is uniform and equal to 0,4 mm for the stent whereas two different models with two different thicknesses have been realized for the leaflets: one model, with uniform thickness equal to 0,4 mm, is representative for the standard pericardium tissue whereas a second model with uniform thickness equal to 0,1 mm is representative for the decellularized pericardium. The choice of the thickness is coherent with the features of the

fabric used for the realization of the valves (decellularized pericardium is much thinner than standard pericardium).

The number of integration points through the leaflets thickness is 2 (default for Ls-Dyna).

3.8.2.3 Simulation protocol

In this paragraph a detailed report of the simulations settings is shown. The simulations have been run at the Department of Mechanical Engineering of UCL and at the Bioengineering Department of Politecnico di Milano.

The first step in order to simulate the sutures between leaflets mesh and stent's, consisted in linking the stent geometry with the leaflets geometry, described in the previous paragraph (3.8.2.2). So, we chose solid elements with 4 duplicated nodes (Figure 3.43) for the possibility to assign thermal properties in order to get the shortening of the threads.

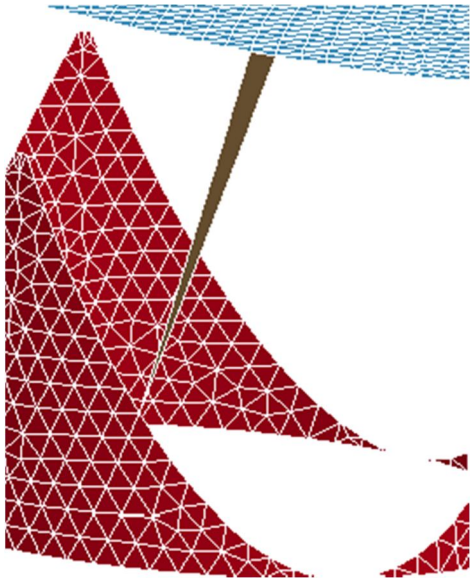

Figure 3.43: Example of thread that links stent and leaflets together

The creation and the definition of the solid elements have involved the following steps:

- identification (but not attribution) of the nodes suitable for threads bestowing; in particular, for each thread, we have chosen one node from the stent and three node from the leaflets (three apexes of one discretized element), except for the commissure zones: in

those parts, in fact, we have chosen to use three elements from the stent and one from the leaflets, due to the small size of the leaflets in the commissures zone (Figure 3.44); for reasons of simplicity, the distance between each threads was 4 mm;

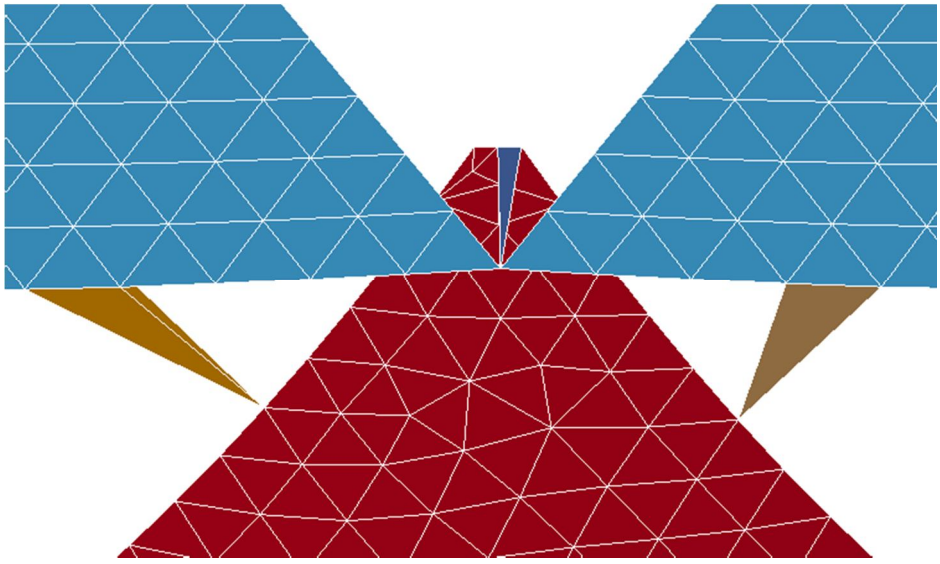

Figure 3.44: Enlargement of threads; in particular it is possible to observe the geometric difference between the commissure thread (shown in the middle) and the other threads. The nodes bestowed to the threads are the duplicated ones.

- duplication of the selected nodes; using the command *Node editing*, new nodes perfectly overlapped with the already existing nodes have been created;
- attribution of the new nodes to the threads in the solid element definition;

The duplication of nodes is essential to avoid a very common problem in thermal simulations that involve contact between parts subjected to heat generation and parts without heat generation; in that case, in fact, the heat transfer may causes the deformation of the contact zone. This problem is particularly evident observing the temperature profile shown in Figure 3.45.

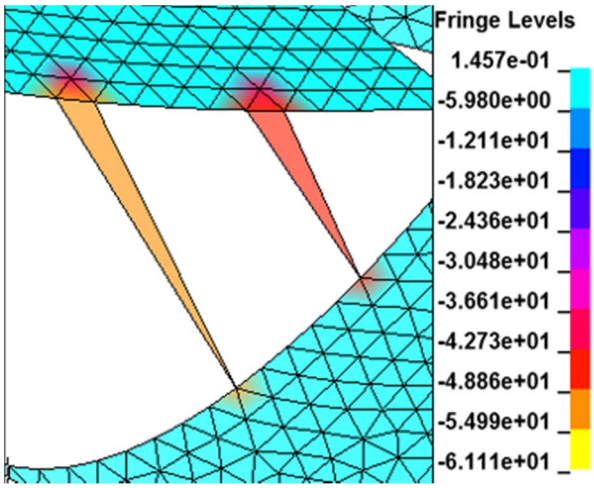

Figure 3.45: Temperature profile without using duplicate nodes. The contact zones between the leaflets and the threads and between the stent and the threads are subject to a drastic cooling

Thus, the duplication of nodes, associates with opportune management of the contact (see paragraph 3.8.2.4) is a good way to avoid the problem just explained.

In order to avoid distortions and oscillations of both threads and leaflets during the simulation (Figure 3.46), the keyword DAMPING was added at the input file. In particular, a time depending curve for damping was defined (oscillations and distortions increased with time) (Figure 3.47).

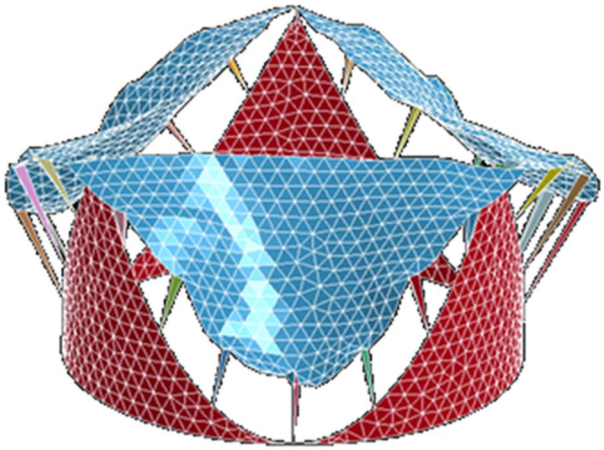

Figure 3.46: Shape distortions on the surface of the leaflets during the simulation

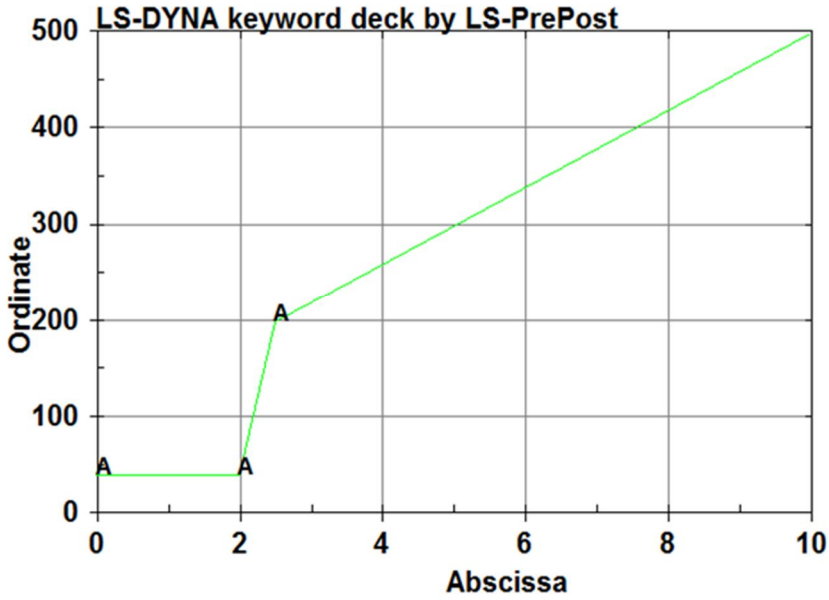

Figure 3.47: Damping coefficient as function of time

The positioning obtained with the suture simulation shows a significant gap between the leaflets and the stent, as shown below (Figure 3.48).

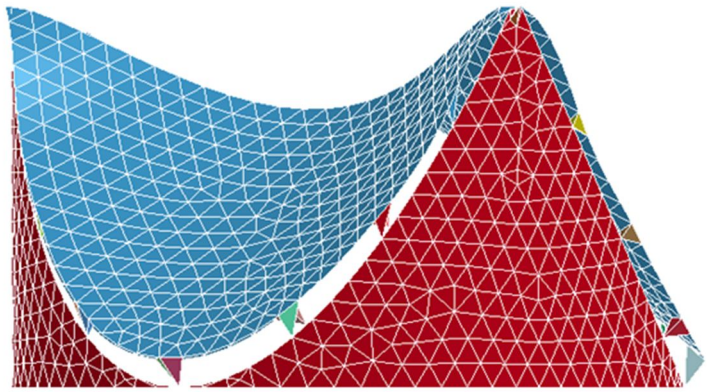

Figure 3.48: First positioning showing gaps between the stent and the leaflets

To optimize the shape that the valve has when it's completely opened, another simulation has been run starting from the geometry obtained from the previous one. Thus, the elements and the nodal coordinates have been exported and a new simulation was run, setting a Young's modulus for the leaflets equal to 2 MPa and thermal generation rate for the threads equal to -4000 mJ/s*mm^3.

All the other setting remained unchanged from the previous simulation.

The positioning obtained from this simulation is shown in Figures 3.49-3.50.

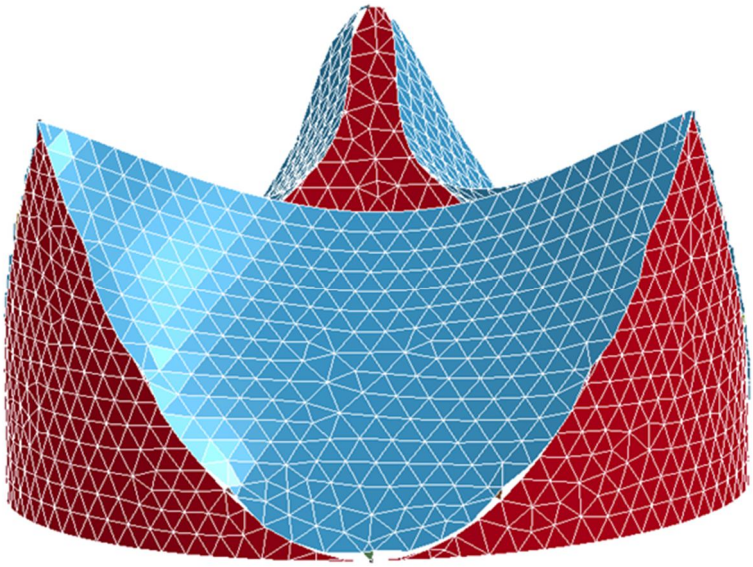

Figure 3.49: Final leaflets positioning

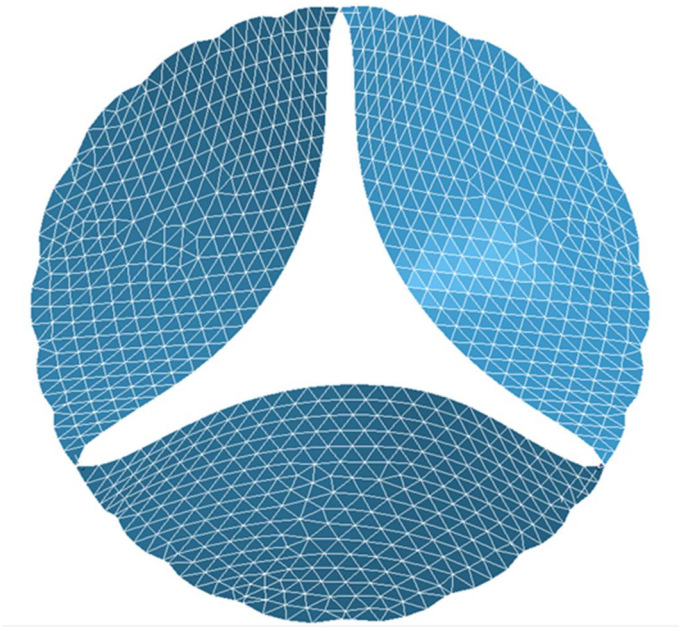

Figure 3.50: View from the top of the leaflets

The positioning of the valve shown in Figure 3.49-3.50 is representative of the valve's nominal shape. However, implanted valves in the body and tested valves in laboratory are always crimped against the walls: this means that the valve's disposition is quite different from the disposition assumed outside the aortic root. At this purpose, we have chosen to

represent, in a simplified manner, the valve in two different configurations: the one corresponding to a 23 mm root placement (Crimp23 valve) and the one corresponding to a 21 mm root placement (Crimp21 valve).

Starting from the initial disposition of the valve and threads described above, the stent and the nodes where the threads are linked with the stent have been scaled first with a factor equal to 0,8846 and second with a factor equal to 0,8077, obtaining, as result of the suture simulation, the Crimp23 valve and the Crimp21 valve respectively.

Starting from the positioning obtained with the suture simulations for all the valve's configurations (valve with nominal shape, Crimp23 and Crimp21), the elements and the nodal coordinates have been exported in new input files. The purpose was to analyze the opening and the closing dynamic of the valve. The threads and the stent have been removed (they were useful just during the positioning of the leaflets) and a pressure curve has been applied on the surface of the leaflets (Figure 3.51): in particular, it reached the diastolic value equal to 0,01333 MPa (100 mmHg) in 0,3 s and remained constant for 0,5 s when reached the systolic value equal to -0.001333 MPa (-10 mmHg).

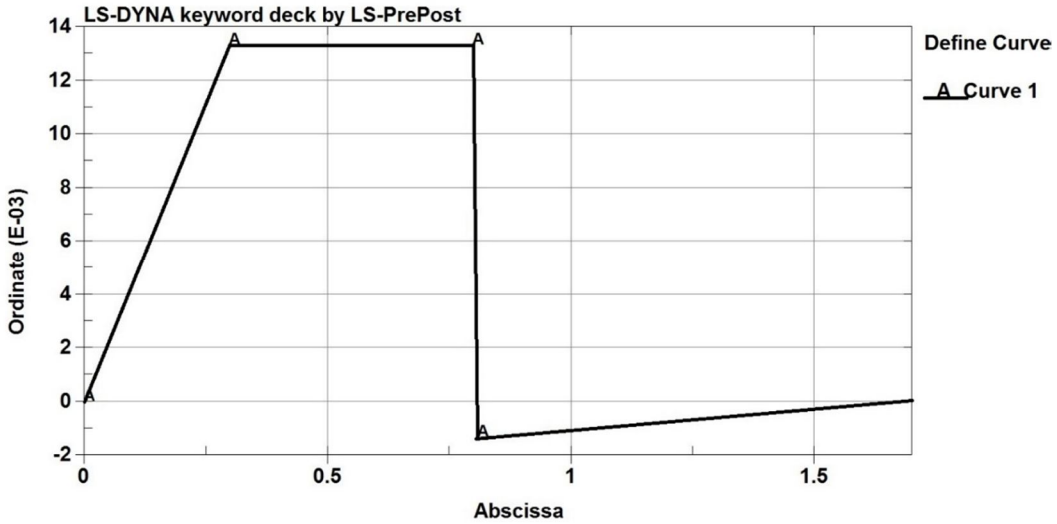

Figure 3.51: Time varying pressure applied to the leaflets

The use of the full pressure (100 mmHg) caused some distortions and oscillations during the coaptation of the leaflets; in order to obtain significant results the analysis used a

damping coefficient equal to 5; shapes comparable with the experimental ones were obtained.

3.8.2.4 Contacts

As explained in the previous paragraph, the duplication of nodes has played an important role in the setting of the suturing simulation. The purpose of that operation was obtaining threads defined without using leaflets' nodes; this means that threads and leaflets are separated entities after the duplication. Thus, it was necessary to confer contacts between threads and leaflets in order to obtain the positioning of the leaflets pulled by the threads. This was possible following these two steps:

- First of all, for each thread one set of nodes containing the duplicated nodes placed on the leaflets surface has been defined;
- second, a contact keyword has been added at the input file. In particular we have chosen a contact node to surface. In the definition of this contact, it was necessary to allocate each set of nodes as slave and each thread as master.

Regarding the dynamic simulations, in order to allow the leaflets to coapt without passing through one another during the closure (Figure 3.52), it has been added at the input file a contact one way surface to surface, setting the leaflets as slave part. During the analysis the code applies a penalty force that restores the contact for those nodes that are predicted to interpenetrate during the incremental solution.

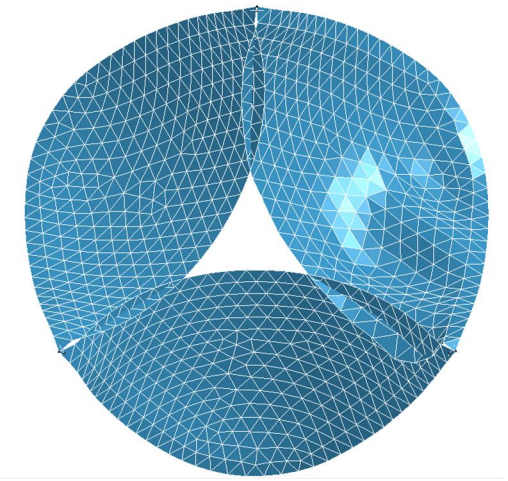

Figure 3.52: Penetration of the leaflets during the closure, without any contact keyword (26 mm valve).

3.8.2.5 Boundary conditions

In the real valves, the external profile of the leaflets is stitched with the stent profile and, consequently, it remains fixed onto the stent. In order to reproduce the attachment during the suture simulations, boundary conditions have been used to constraint all the translations and rotations of the threads' nodes placed on the stent surface.

Regarding the dynamic simulations, as explained in the paragraph 3.8.2.3, the threads were removed from the model; with the purpose to keep the leaflets still anchored at the base, it was necessary to constrain the translations of the leaflets' external nodes. All the rotations have been allowed as happens, although in a more complicated way, for the leaflets' points stitched with the stent in the real valves.

Chapter 4: Results and Discussions

4.1 Pericardium results from tensile tests

In this paragraph are shown the experimental results only for the standard pericardium tissue; in fact, even if we tested also the decellularized one, we haven't been authorized to publish all the results obtained but only the results strictly necessary such as the stress-strain results shown in figure 4.8. In Figure 4.1 the mean values of strength (N), displacement (mm), ultimate tensile stress (σ), strain (%), Young's modulus are summarized in the low stress–strain zone (E_1) and in the high stress–strain zone (E_2). Moreover it is reported the strength-strain ratio (P/L). For each the code number and the orientation are mentioned. It is to note that samples number 10, 21 and 25-28 do not appear in the table because were discarded. The response of the tissue is non-linear and there are differences among strips oriented along different directions. These results are related to the standard pericardium.

Code number	Strain [mm]	P [N]	σ [MPa]	Strain [%]	E_1 [MPa]	E_2 [MPa]	P/L [N/mm]	Orientation
1	11,02	14,01	21,90	68,91	1,58	82,89	1,27	Parallel
2	11,31	22,58	21,71	70,70	2,34	69,22	2,00	Parallel
3	9,68	12,01	20,02	60,51	1,98	83,80	1,24	Parallel
4	12,97	26,26	21,88	81,04	1,05	63,34	2,03	Perpendicular
5	9,46	28,00	25,00	59,12	1,51	79,45	2,96	Perpendicular
6	11,97	19,59	18,14	74,82	0,68	65,40	1,64	Perpendicular
7	16,20	16,85	16,85	101,22	2,66	59,21	1,04	Parallel
8	11,00	17,67	18,41	68,75	2,66	97,22	1,61	Parallel
9	8,50	23,51	23,23	53,11	0,86	103,47	2,77	Parallel
11	8,29	22,26	18,99	51,84	1,36	77,93	2,68	Parallel
12	8,52	18,66	14,90	53,22	1,36	66,04	2,19	Parallel
13	11,09	12,91	10,21	69,29	2,12	33,97	1,16	Perpendicular
14	9,24	15,69	12,94	57,72	2,19	63,94	1,70	Perpendicular
15	11,19	16,96	11,37	69,91	1,42	29,20	1,52	Perpendicular
16	10,49	14,57	10,72	65,59	2,34	43,32	1,39	Perpendicular
17	10,29	27,85	18,82	64,32	3,13	90,86	2,71	Parallel
18	10,49	42,48	23,60	65,57	3,73	97,35	4,05	Parallel
19	11,83	24,00	14,64	73,92	1,35	50,13	2,03	Parallel
20	9,92	21,68	14,81	61,99	1,61	53,49	2,19	Parallel

22	9,25	37,26	24,97	57,79	0,59	116,42	4,03	Parallel
23	10,12	23,31	15,10	63,26	1,09	31,27	2,30	Parallel
24	6,49	22,09	16,43	40,57	1,66	72,38	3,40	Perpendicular
29	10,24	26,32	15,82	64,01	0,22	63,10	2,57	Parallel
30	8,30	29,67	15,78	51,89	2,12	42,66	3,57	Perpendicular
31	8,48	32,85	20,23	53,02	1,91	73,81	3,87	Perpendicular
33	11,02	16,09	10,32	68,89	4,20	47,52	1,46	Perpendicular
34	9,74	20,38	11,58	60,86	2,04	46,08	2,09	Perpendicular
35	10,67	15,10	11,01	66,67	7,81	54,52	1,42	Perpendicular
36	11,97	25,40	25,40	74,82	0,91	69,87	2,12	Parallel
Average	**10,34**	**22,28**	**17,41**	**64,60**	**2,02**	**66,48**	**2,24**	
dev. St.	1,79	7,24	4,79	11,21	1,43	22,00	0,88	

Figure 4.1. A screenshot of summarized data.

As in most other soft tissues, the stress induced in pericardium is non-linearly related to the strain (Figure 4.2). The response curve exhibits three different regions [40]:

- Region I: **low-modulus region**, where high extensions correspond to very small tensions. In this phase a small elongation, that represent the elongation of the collagen fibers, can be observed. At first it is possible to appreciate a low stiffness due to the fact that the fibrous structures are still in rippled configuration, where the inter-and intra-fibrillar bonds are not fully tensioned and the fibers still show the typical wavy structure; then this behavior could be governed by the elastin/matrix part of the tissue during which time the collagen is uncoiling.

- Region II: **high stiffness region**, characterized by a rapid stiffening and very high stress increments associated with further extension of the tissue.

After the elbow, this zone corresponding to the linear section, where the fibers are aligned in the direction of load application. In this region, when there is an increase of the strength applied to the tissue, there is also an increasing of the stiffness of the material. This happens because, at the microstructural level, we are proving the complete relaxation of inter-and intra-fibrillar and the unwinding of the collagen fibers that reach the so-called "crimped" configuration;

- Region III: **damage region**, characterized by a breakup of the structures that make up the tissue. In this region it is possible to observe the breaking of inter-and intra-fibrillar, resulting in deterioration of the mechanical properties of the material. The modulus of elasticity decreases drastically and phenomena of plasticity and damage occur, that cannot

be recovered at the time of unloading of the specimen.

This qualitative behavior remains after chemical treatment such as glutaraldehyde fixation and mechanical conditioning, even though these factors modify the actual response curve.

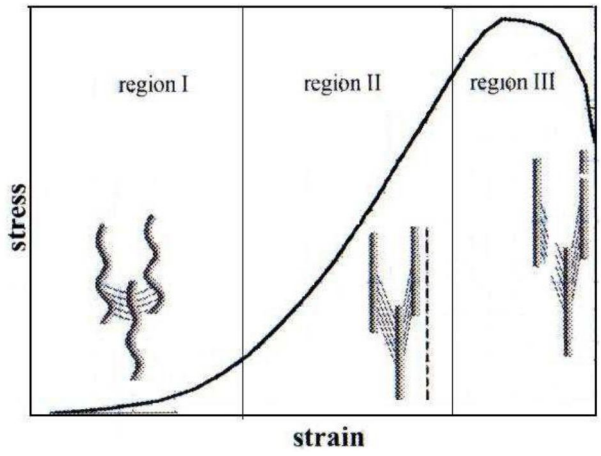

Figure 4.2. Typical stress-strain graph of biological tissue.

The elastic modulus is extrapolated from the linear part of the curve (Region I and II), in which the behavior of tissue can be assumed elastic.

The Figure 4.3 reports a graph (referred to the first linear region) that shows a comparison between the elastic modulus of samples tested along the fibers and perpendicular to them. Moreover, in the same graph, the mean value of the two configurations is showed. It can be observed that the perpendicular samples strips have a higher elastic modulus. However, paying attention to the standard deviation, it is clear that this behavior is not statistically relevant. All specimens have shown a very initial compliant region with low loads (from 1 MPa to 4 MPa) producing large deformation. The following results have been obtained by an average of 15 specimens. It has been performed a tStudent test to verify the statistical relevance of the data.

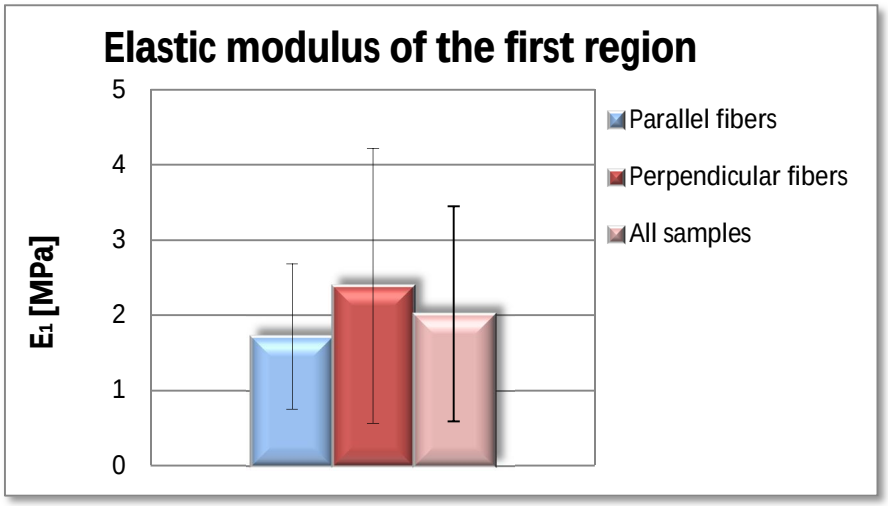

Figure 4.3. Comparison of Elastic modulus (1st region). According to a tStudent test, the difference between the parallel fibers' average and perpendicular ones' average is not significant.

Considering the second linear region (Figure 4.4), the elastic modulus mean values reaches higher values (from 4 MPa to almost about 80 MPa) than those to the previous branch. The behavior changes from one direction to another according to the orientation of the sample but, in this linear region, the difference is more pronounced (from about 50 MPa for perpendicular samples to almost 80 MPa for parallel samples). Also in this case the standard deviation is very high, as common for biological tissue.

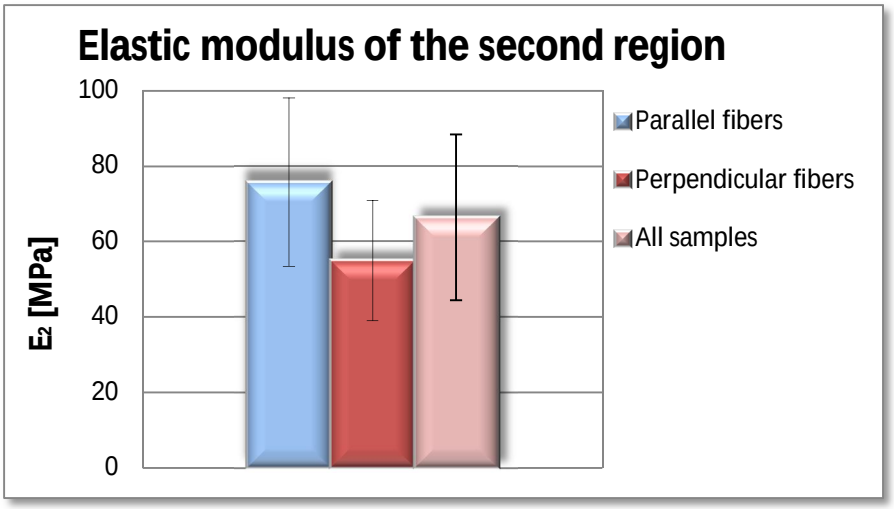

Figure 4.4. Comparison of Elastic modulus (2nd region). According to a tStudent test, the difference between the parallel fibers' average and perpendicular ones' average is significant with p equal to 0,89%

In the graph shown in Figure 4.5 it is immediately noticeable that samples with fibers parallel to direction of load have a higher tensile strength (almost 20 MPa compared to about 15 MPa for perpendicular samples) and this difference is statistical relevant with p equal to 1.37%. This is probably due to the fact that parallel samples are able to withstand higher loads because they have many collagen fibers along their tensile axes, as compared to the other directions.

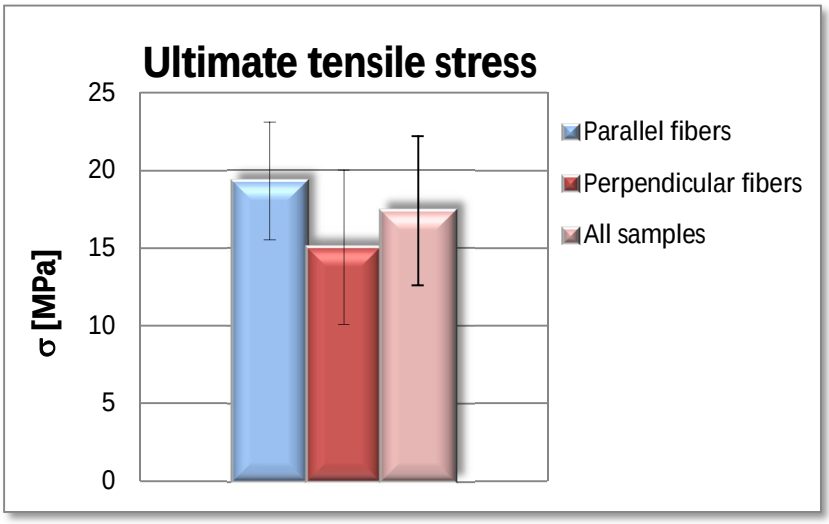

Figure 4.5. Comparison of ultimate tensile stress. According to a tStudent test, the difference between the parallel fibers' average and perpendicular ones' average is significant with p equal to 1.37%

In Figure 4.6, data are similar and there are not statistical differences in terms of strain.

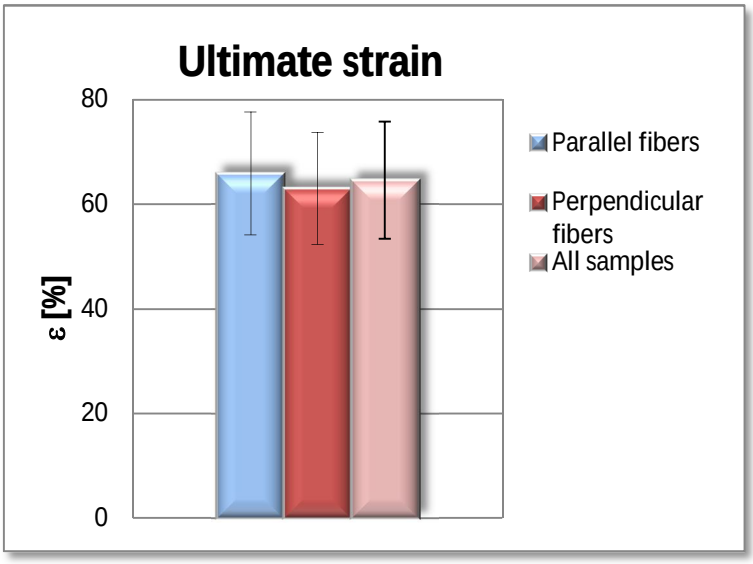

Figure 4.6. Comparison of ultimate strain. According to a tStudent test, the difference between the parallel fibers' average and perpendicular ones' average is not significant.

The stress and strain graphs obtained from the tensile test are presented in Figures 4.7 and 4.8.

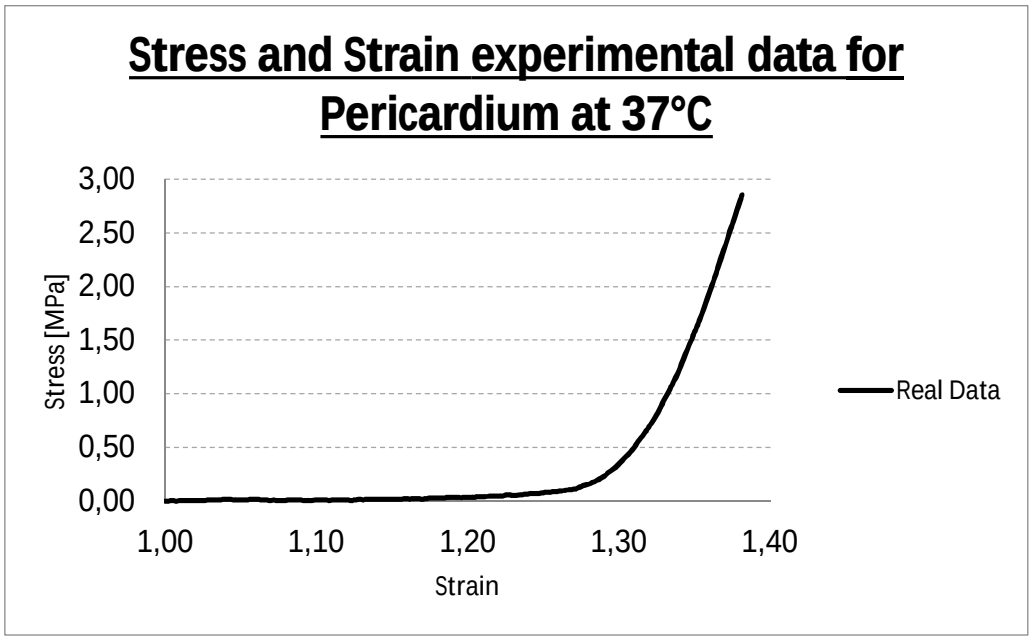

Figure 4.7: Pericardium experimental data at 37°C (1 sample)

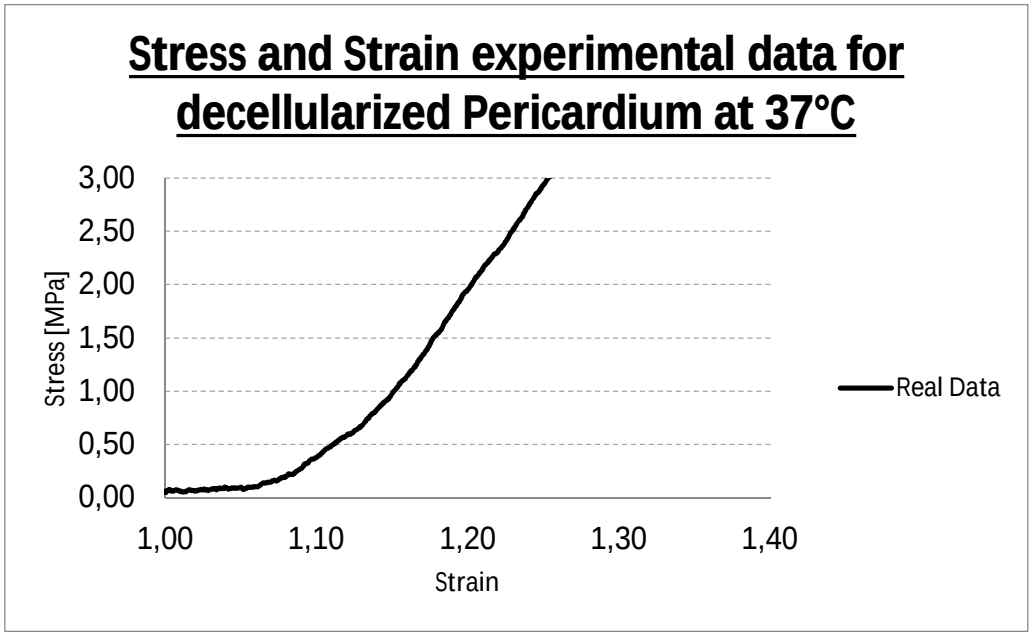

Figure 4.8: Decellularized pericardium experimental at 37°C data (1 sample)

4.2 Graphs and trends for experimental analysis

Comparisons between different types of valves and between the same valves placed in different root size have been assessed in order to compare transvalvular pressure drop, leakage volume, total regurgitant fraction, EOA and leakage, forward and total energy losses, closing regurgitant volume and its energy loss. For getting the results has been used the ViVitro machine. In particular we compared the valves realized with the commercial ones. We wanted also to see if the length of leaflets changes the valve performance. In order to do so we trimmed therefore the pericardial valve to get shorter leaflets but still enough long to close. The valves have been tested in root with diameter equal to 21 mm and 23 mm. Only the dCell valve hasn’t been tested in the root 23 due to the leaflets length, not suitable for that root (as we explained, the decellularized pericardium patch was too small). A tStudent test has been executed in order to check if the difference between the control valves' average and pericardium valve's average is significant.

4.2.1 Transvalvular Pressure Drop

In this paragraph the results regarding the Transvalvular pressure drop are shown for the pericardial valve, the dCell valve and the trimmed valve; furthermore, the comparisons of these valves with the commercial ones are shown. One experiment has been performed for each valve.

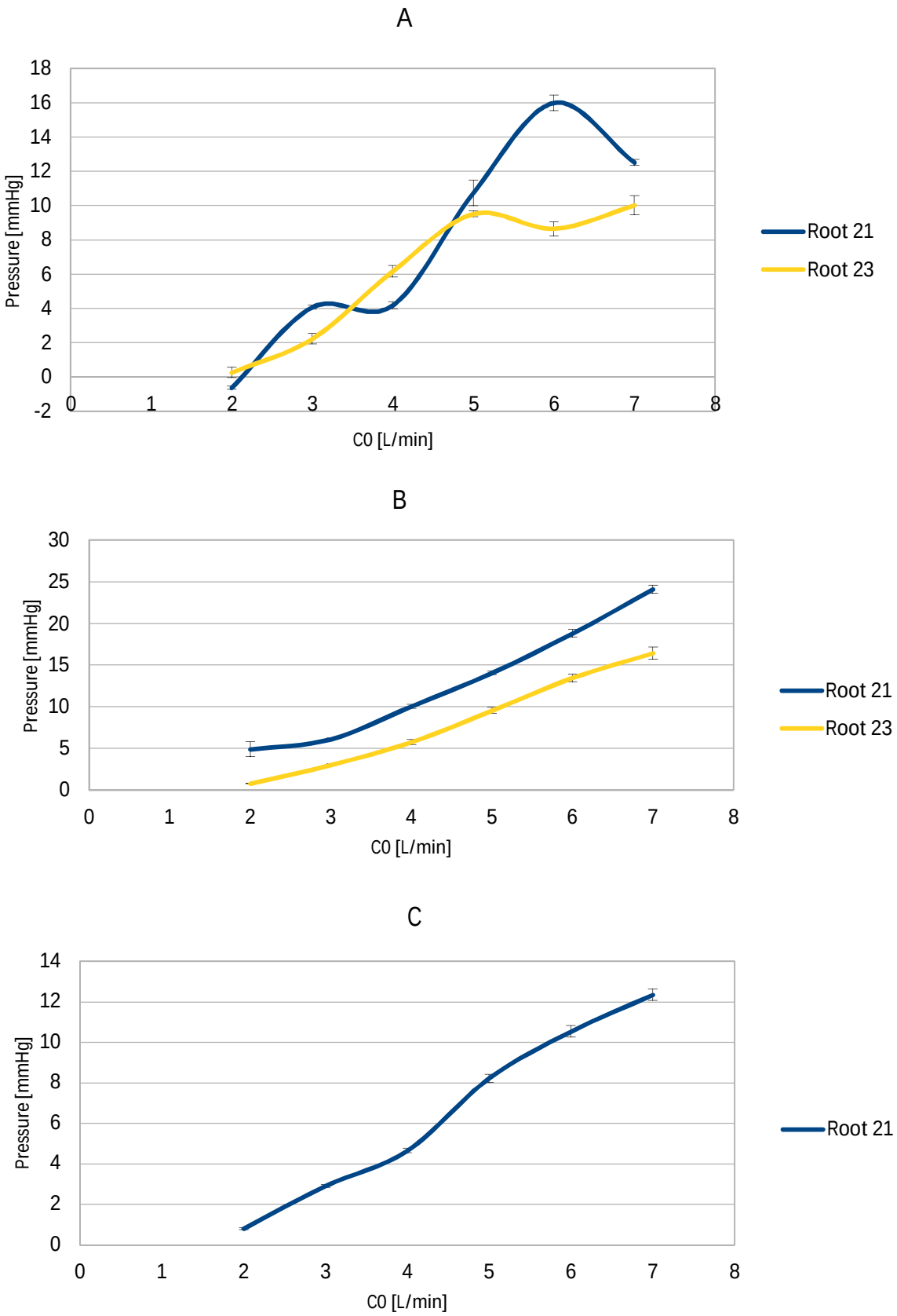

Figure 4.9 Transvalvular Pressure Drop - A: Pericardial Valve, B: trimmed pericardial valve, C: dCell Valve

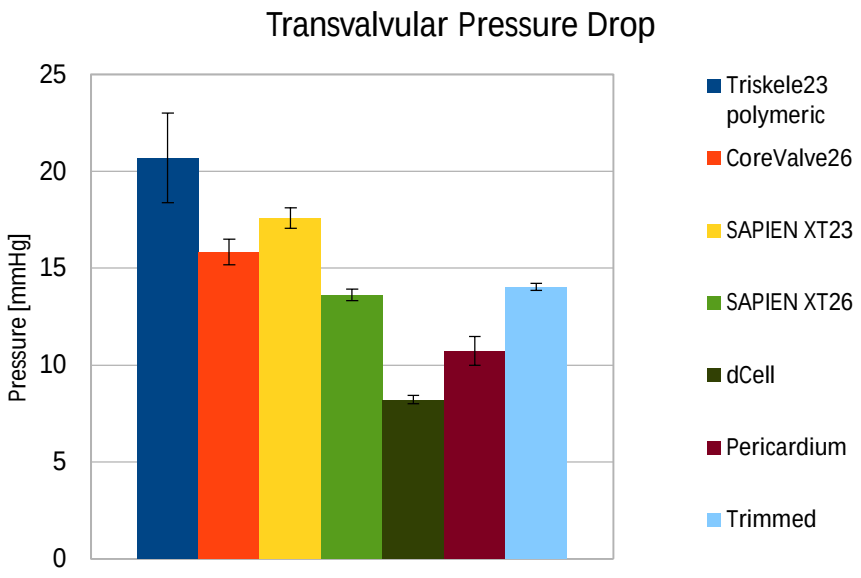

Figure 4.10 Transvalvular Pressure Drop - 21 mm at CO= 5l/min. According to a tStudent test, the difference between the control valves' average and pericardium valve's average is significant with p equal to 4.64%

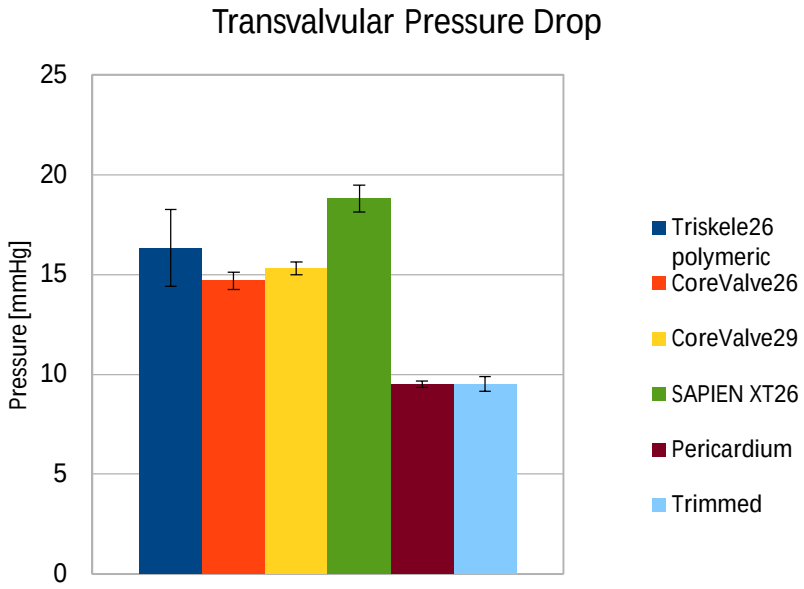

Figure 4.11 Transvalvular Pressure Drop - 23 mm at CO= 5 l/min. According to a tStudent test, the difference between the control valves' average and pericardium valve's average is significant with p equal to 0.75%

Regarding the two pericardial valves, the Root 23 globally exhibited a significantly lower transvalvular pressure drop compared to the Root 21.The mean pressure gradient across the valves rose as the cardiac output increased, reaching 16 mmHg at 6 l/min for Root 21, but it did not exceed 10 mmHg for Root 23. Although variation between the 2 valves was small, Root 23 demonstrated the lowest amount of pressure drop compared to Root 21.

This trend is linear for the dCell valve as the cardiac output increased.

The pericardial valve achieved a lower transvalvular systolic pressure drop (compared to the control) indicating a considerably reduced resistance against the forward flow. This difference is even between Root 21 and 23 where the last one is even lower due to its bigger diameter. The same trend has been obtained by the trimmed pericardial valve. It reachs 12,346 mmHg at 7 l/min. Regarding the dCell valve the pressure drop is even lower than the pericardial valve thanks to its tissue that is thinner than the standard pericardium obstructing even less the fluid flow. Compared to the control valve (Triskele23 polymeric, CoreValve26, SAPIEN XT23 and SAPIEN XT26) our three valves have shown a lower pressure drop at 5 l/min of cardiac output, with statistically significant differences according to the tStudent test.

4.2.2 Closing Volume

In this paragraph the results regarding the closing volume are shown for the pericardial valve, the dCell valve and the trimmed valve; the comparisons of these valves with the commercial ones are shown. One experiment has been performed for each valve.

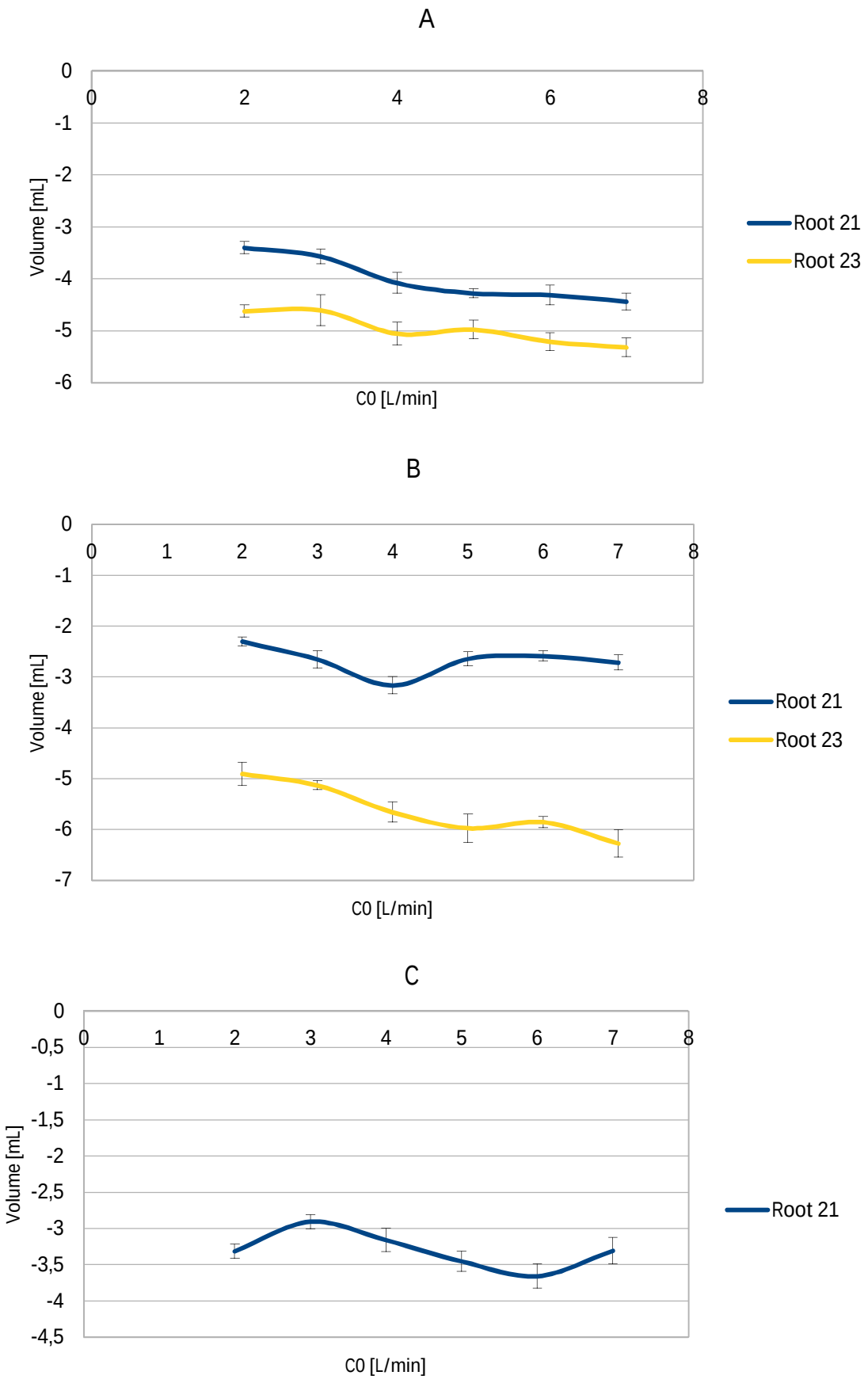

Figure 4.12 Closing Volume - A: Pericardial Valve, B: trimmed pericardial valve, C: dCell Valve
dCell Valve

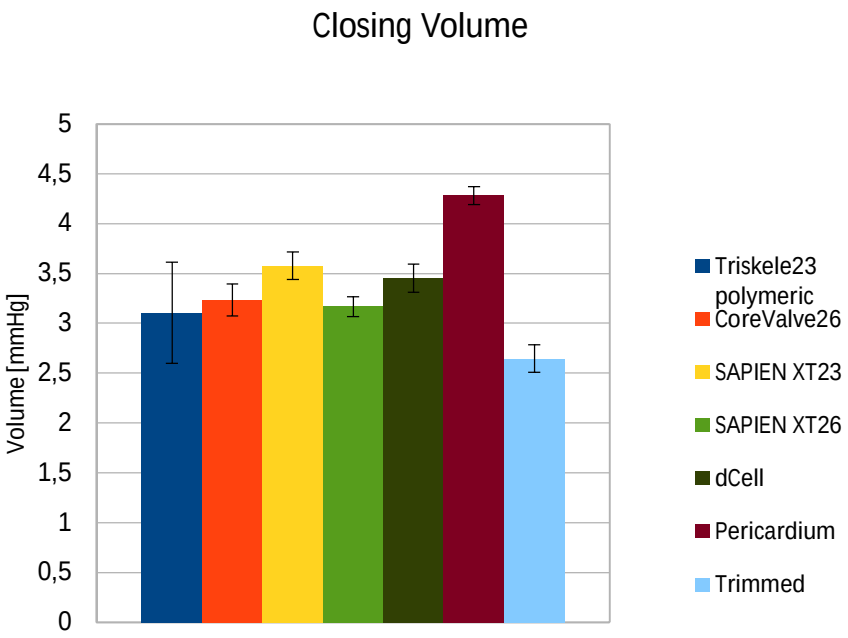

Figure 4.13 Closing Volume - 21 mm at CO = 5 l/min. According to a tStudent test, the difference between the control valves' average and pericardium valve's average is not significant

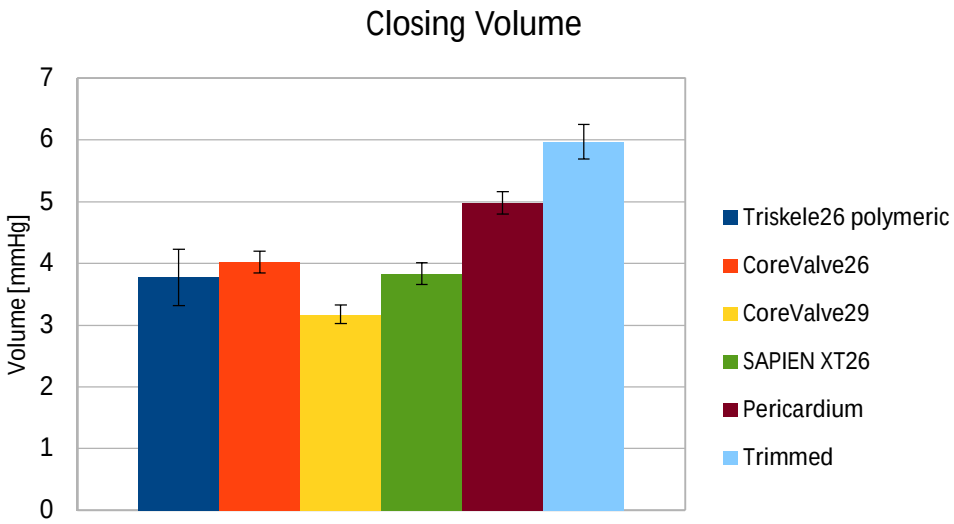

Figure 4.14 Closing Volume - 23 mm at CO = 5l/min. According to a tStudent test, the difference between the control valves' average and pericardium valve's average is significant with p equal to 1.23%

The Root 23 exhibited a significantly higher closing volume compared to the Root 21, but globally the trend is similar between them. The closing volume rose as the cardiac output increased (reaching 4,44 mL at 7 l/min for Root 21 and 5,325 mL at 7 l/min for Root 23).

Also for the trimmed one the closing volume rose as the cardiac output increased, reaching 3,16 mL at 4 l/min for Root 21 and 6,27 mL at 7 l/min for Root 23. These considerations are true for both pericardial valves. For the dCell valve the graph exhibited an oscillated trend between -2,9 ml and -3,65 ml.

The lowest closing volume has been obtained by the Trimmed one (Root 21). This is due to the fact that the leaflets closes much better and let less blood flows back to the ventricular. The highest value has been reached by the same valve is in the 23 root configuration due to the fact that the leaflets were not enough long to close each other in the proper way. The other valves and configurations show an average behavior that remain constant on -3 ml.

Compared to the control valves, the Trimmed valve has a better behavior than any valve in Root 21 and worse than other in Root 23 due to the reasons explained before. The pericardial valve (21) has shown the worst result compared to other valves in 23 Root. This can be due to the leaflets' length that was too long to let the valve close properly. dCell valve has the same value of the control valves.

4.2.3 Aortic Leakage and Aortic Regurge Fraction

In this paragraph the results regarding the Aortic Leakage and the Aortic Regurge Fraction are shown for the pericardial valve, the dCell valve and the trimmed valve; the comparisons of these valves with the commercial ones are shown. One experiment has been performed for each valve.

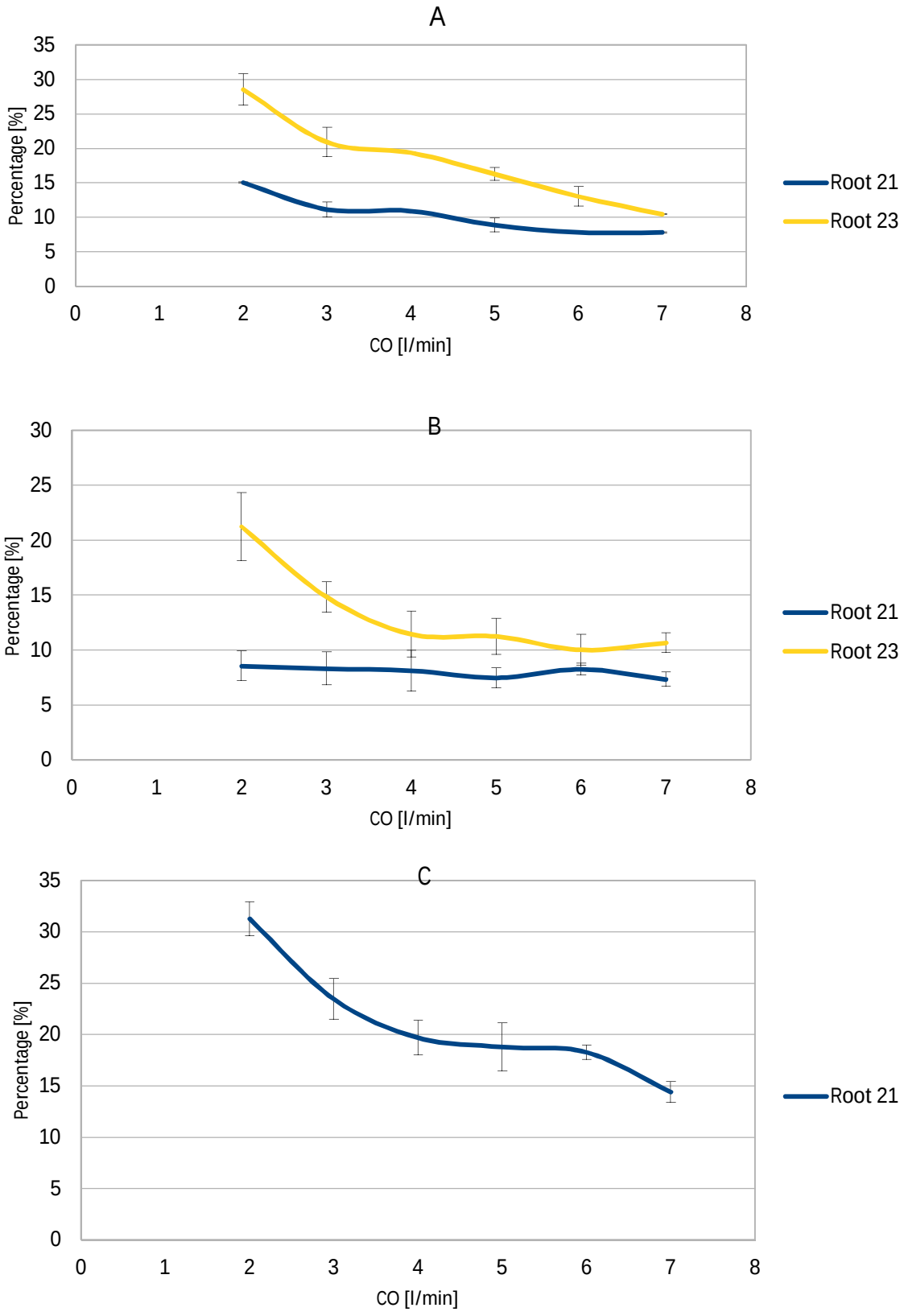

Figure 4.15 Aortic regurge fraction – A: Pericardial Valve, B: trimmed pericardial valve, C: dCell Valve

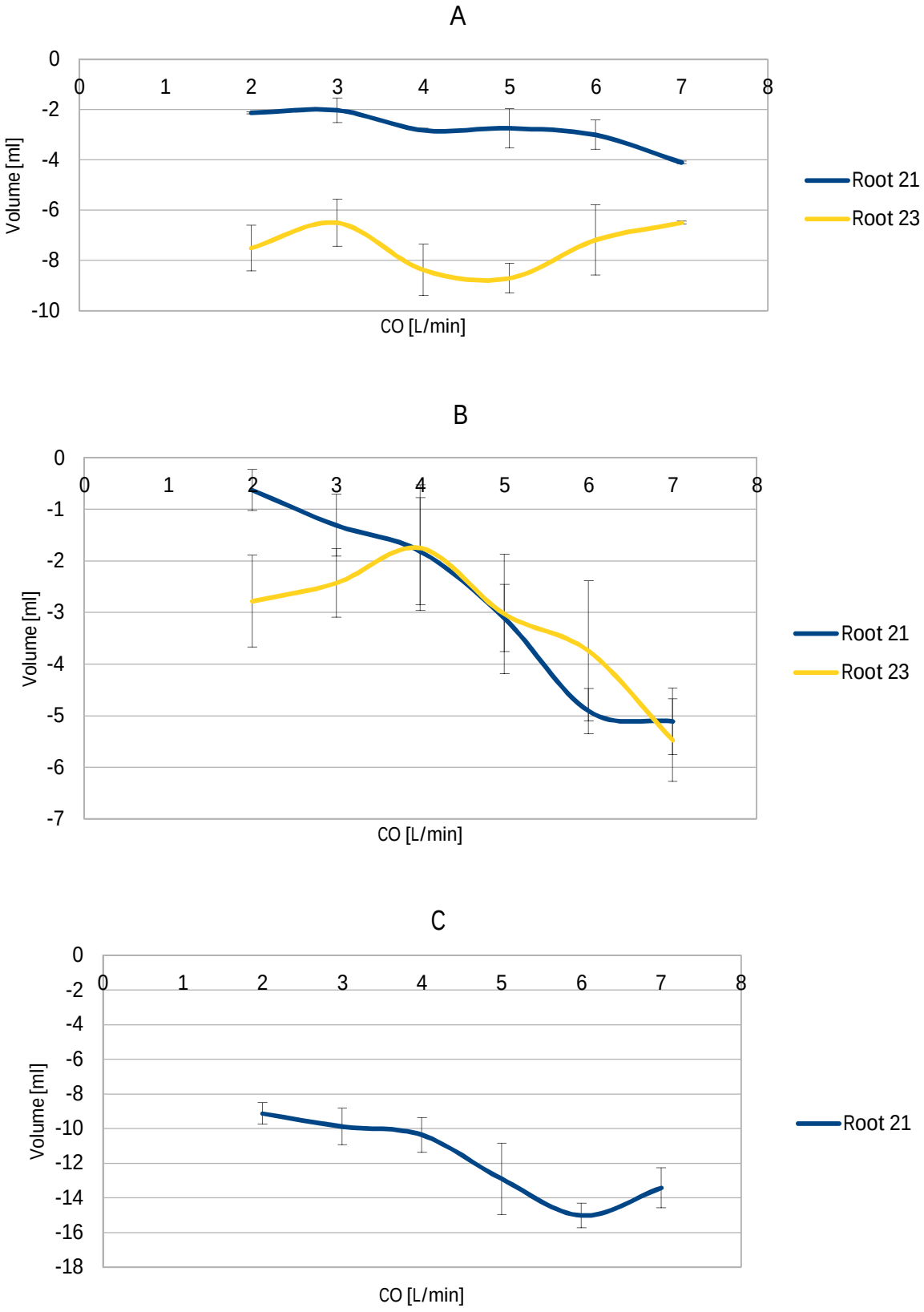

Figure 4.16 Aortic leakage – A: Pericardial Valve, B: trimmed pericardial valve, C: dCell Valve

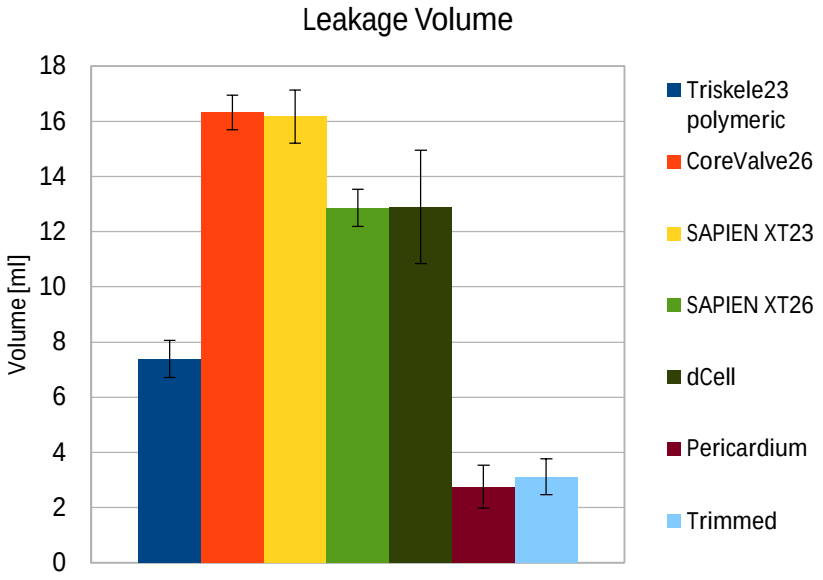

Figure 4.17 Leakage volume - 21 mm a CO = 5 l/min. According to a tStudent test, the difference between the control valves' average and pericardium valve's average is significant with p equal to 3.08%

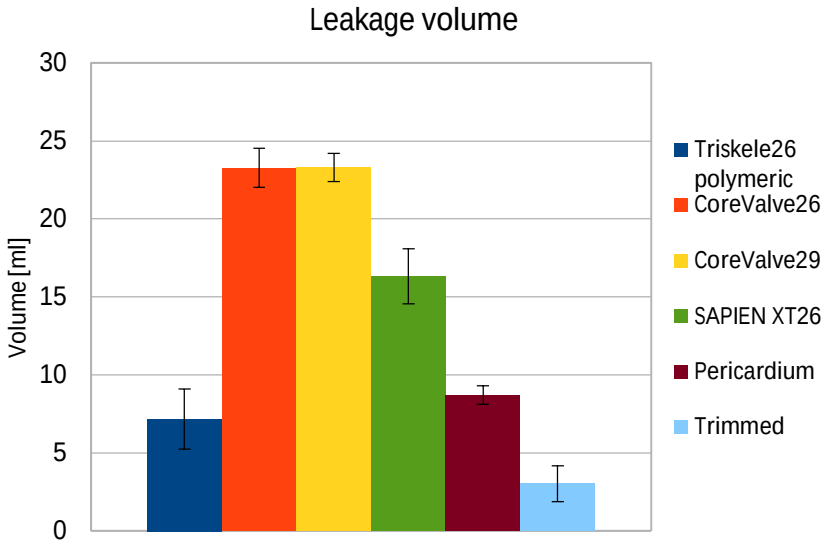

Figure 4.18 Leakage volume - 23 mm a CO = 5 l/min.
According to a tStudent test, the difference between the control valves' average and pericardium valve's average is significant with p equal to 12.39%

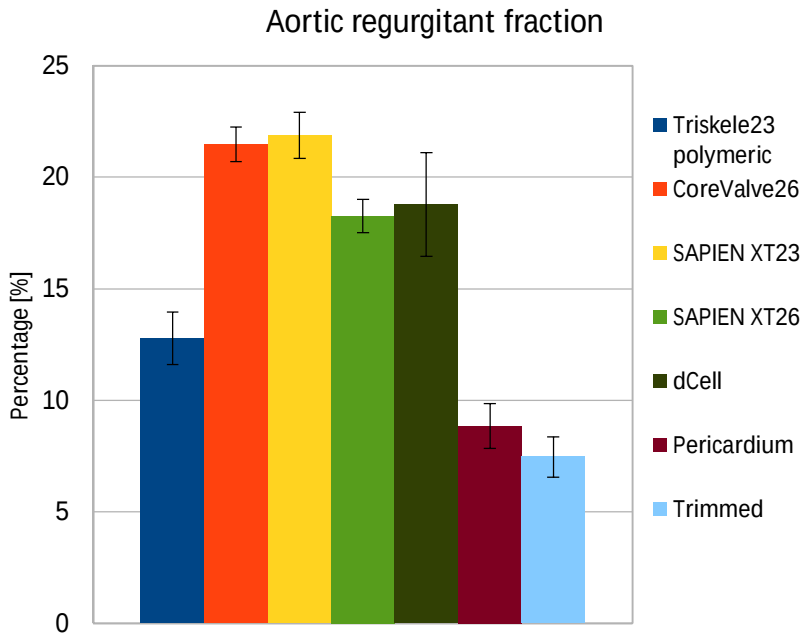

Figure 4.19 Total regurgitant fraction - 21 mm a CO = 5 l/min. According to a tStudent test, the difference between the control valves' average and pericardium valve's average is significant with p equal to 3.05%

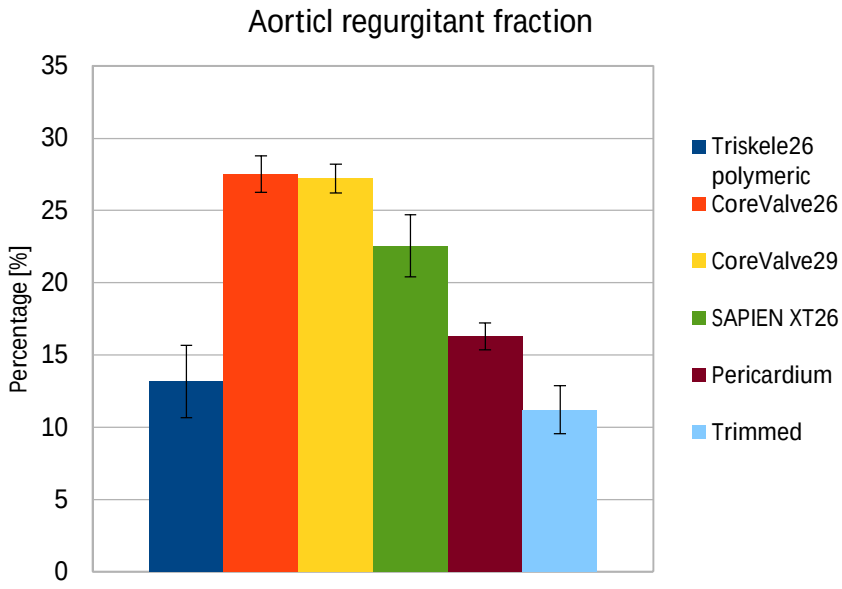

Figure 4.20 Total regurgitant fraction - 23 mm a CO = 5 l/min. According to a tStudent test, the difference between the control valves' average and pericardium valve's average is significant with p equal to 16.7%

Regurgitation or leakage volume represented the amount of backward flow volume during the diastolic phase of a cardiac cycle. This is directly related to the valve size and the normal configuration of the leaflets in absence of flow pressure. According to previous studies [41], porcine bioprosthetic valves have superior diastolic characteristics (e.g. regurgitation) benefiting from their relatively close leaflet configuration.

This trend has been reflected by the aortic regurge fraction graph.

In the pericardial valve, Root 23 configuration exhibited a significantly higher aortic leakage and aortic regurge fraction compared to Root 21 (it reaches -4,108 mL at 7 l/min for Root 21), showing an oscillating trend as the cardiac output increased,

whereas Root 23 (it reaches -8,708 mL at 5 l/min) exhibited an higher aortic regurge fraction compared to Root 21 until 5l/min and a lower regurge up to 7 l/min for what regards the trimmed ones. For the dCell one, the aortic leakage has a decreasing trend as the cardiac output rise up. This trend has been reflected by the aortic regurge fraction graph shown below.

For trimmed pericardial valve, Root 23 exhibited an higher aortic regurge fraction compared to Root 21 until 5l/min and a lower regurge up to 7 l/min. The aortic leakage reaches -5,11 mL at 7 l/min for Root 21 and -5,47 mL at 7 l/min for Root 23.

As described before, the same trend has been shown by the aortic regurge fraction's graph with better performance for Root 21. In the dCell valve, the aortic leakage has a decreasing trend as the cardiac output rise up. The same trend has been shown by the aortic regurge fraction's graph.

The aortic leaked obtained with pericardial valve is the lowest in any configuration compared with control valves. This is a very good achievement of this work. We have got leakage of about 2 ml for the pericardial valve against the 16 ml of CoreValve26 and Sapien XT23 for both root configurations This trade is also reflected on the Total Regurgitant Fraction of 7/8% for our pericardial valves against more than 20% of Sapien and CoreValve26. This is valid for both 21 and 23 configuration even if the 21 configuration presents less values due to its lower diameter that helps to keep leakage lower. Even in this case, the trimmed valve has got better results compared to the not-trimmed. The dCell valve has got comparable value with the control valve even if it has the same shape of the Pericardium Valve. This is because of some leakage in the tissue that we noticed during the experimental trials. In fact the tissue is very fragile especially close to

the stitch where there are holes that let the blood goes back when the valve is closed. Another reason was the presence of a hole in the middle of the valve where leaflets are supposed to close; this is due to the small dimension of the patch used for the realization of the leaflets (the factory that provided us with, gave us one patch that was smaller than expected). Even the wings around the stent were slightly smaller so another portion of fluid escaped due to the presence of free space.

Unfortunately it wasn't possible to get more tissue from the company and realizing another valve.

4.2.4 Aortic Orifice Area (EOA)

In this paragraph the results regarding the EOA are shown for the pericardial valve, the dCell valve and the trimmed valve; the comparisons of these valves with the commercial ones are shown. One experiment has been performed for each valve.

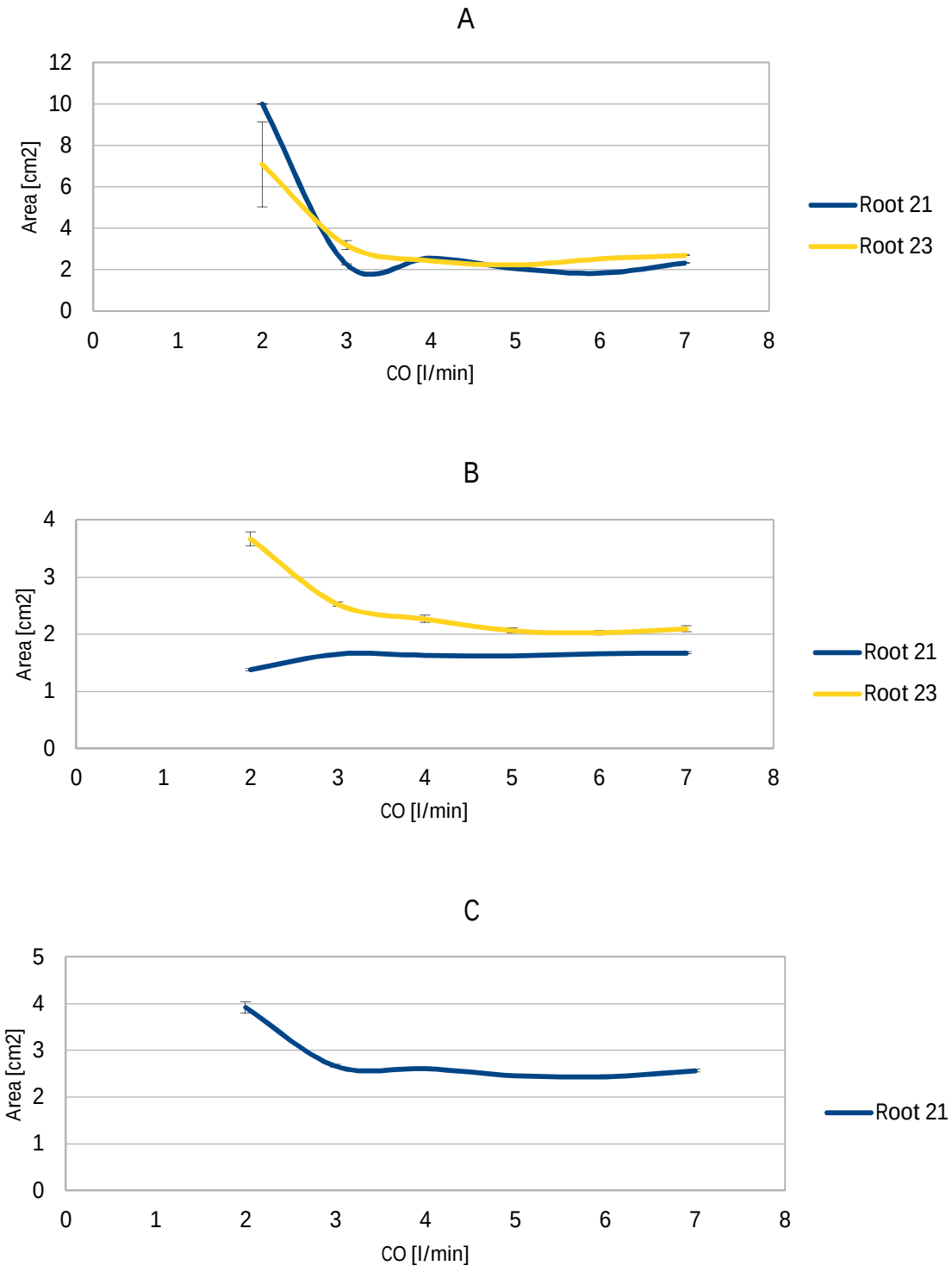

Figure 4.21 Aortic orifice area [EOA] - A: Pericardial Valve, B: trimmed pericardial valve, C: dCell Valve

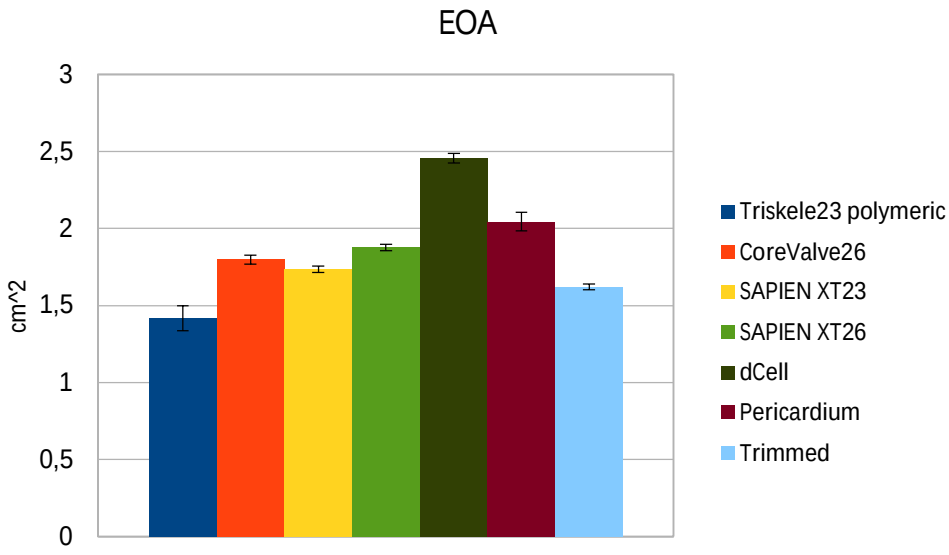

Figure 4.22 EOA - 21 mm at CO = 5 l/min. According to a tStudent test,
the difference between the control valves' average and pericardium valve's average is not significant

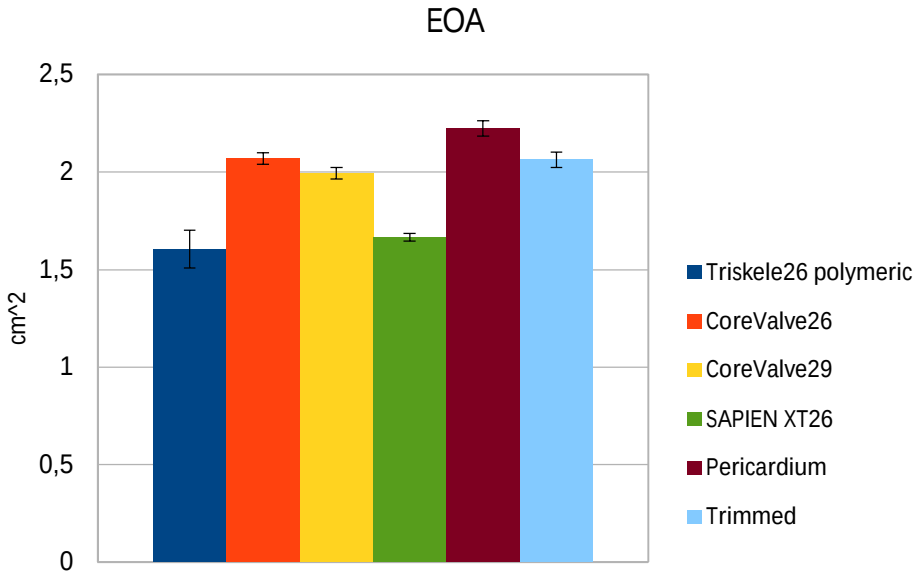

Figure 4.23 EOA - 23 mm at CO = 5 l/min.
According to a tStudent test, the difference between the control valves' average
and pericardium valve's average is significant with p equal to 16.12%

The valves tested in the Root 21 and in the Root 23 exhibited a similar trend, which remained constant as the cardiac output increased, except for low cardiac output because of the Gorlin Formula's limitations at cardiac output lower than 3/l/min. For both roots, the effective orifice area is in a range between 1,827 cm^2 and 2,697 cm^2.

Regarding the trimmed valve's version, Root 21 and Root 23 exhibited a similar trend (except for the 2 l/min value where the formula can't be applied), which remained constant as the cardiac output increased. dCell valve exhibits a constant trend (except for the 2 l/min value where the formula can't be applied). This trend is maintained as the cardiac output rise up.

Our valves have a wider effective orifice area (2.5 cm^2 for dCell against less than 1.5 for Triskele23). Wider EOA was obtained with all our valves, confirming their design efficiency in achieving improved systolic flow. Errors of the EOA measurements in cardiac output lower than 3/min and higher than 7 l/min is mainly due to inefficiency of the Gorlin's formula in calculating EOA [42]. The fundamental function of a heart valve is to facilitate the unidirectional blood flow while maximizing flow rate and minimizing flow resistance. Transvalvular pressure gradient and EOA are inter-related factors which allow to quantify the valve resistance to forward flow. The EOA is an issue especially when aortic annulus size is small, since it is critical to ensure that the prosthetic valve will have an adequate functional valve area for the patient's body size to avoid patient prosthetic valve mismatch [43].

As shown previously, our valve's pressure drop was lower than the control valves and this fact has also been confirmed by a bigger EOA (they are inter-related factor as discussed above).

4.2.5 Transaortic Forward Energy Loss

In this paragraph the results regarding the Transaortic Forward Energy Loss are shown for the pericardial valve, the dCell valve and the trimmed valve; the comparisons of these valves with the commercial ones are shown. One experiment has been performed for each valve.

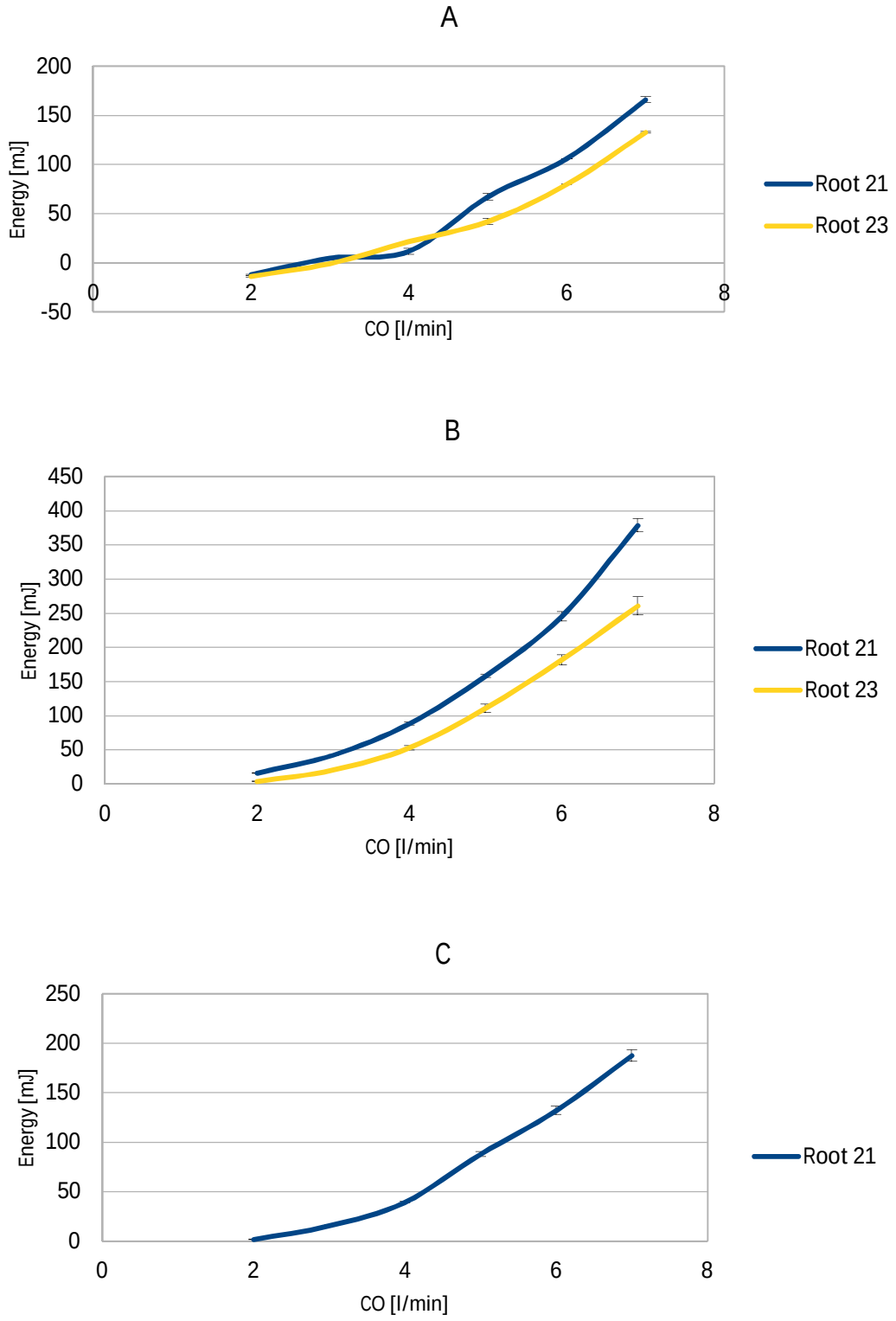

Figure 4.24 TransAortic Forward energy loss - A: Pericardial Valve, B: trimmed pericardial valve, C: dCell Valve

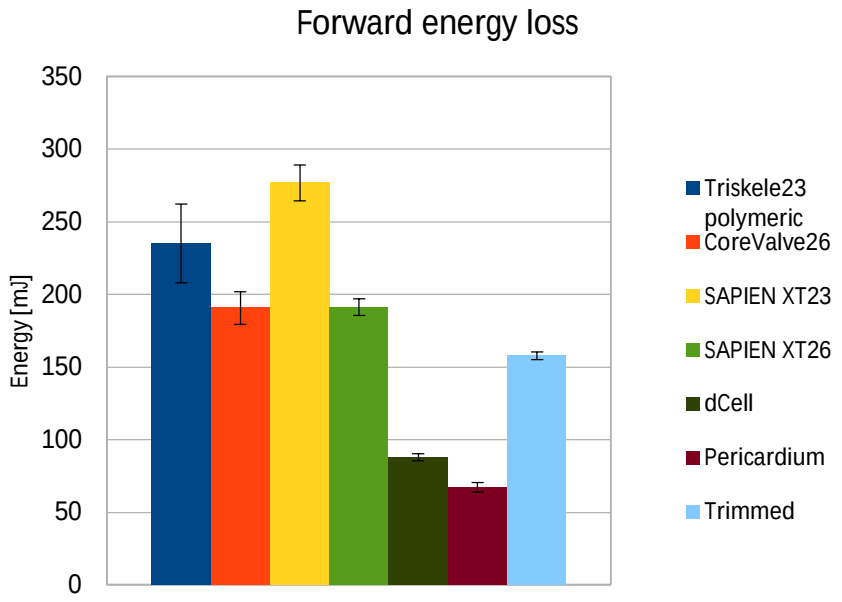

Figure 4.25 Forward energy loss - 21 mm at CO = 5 l/min.
According to a tStudent test, the difference between the control valves' average and pericardium valve's average is significant with p equal to 5.58%

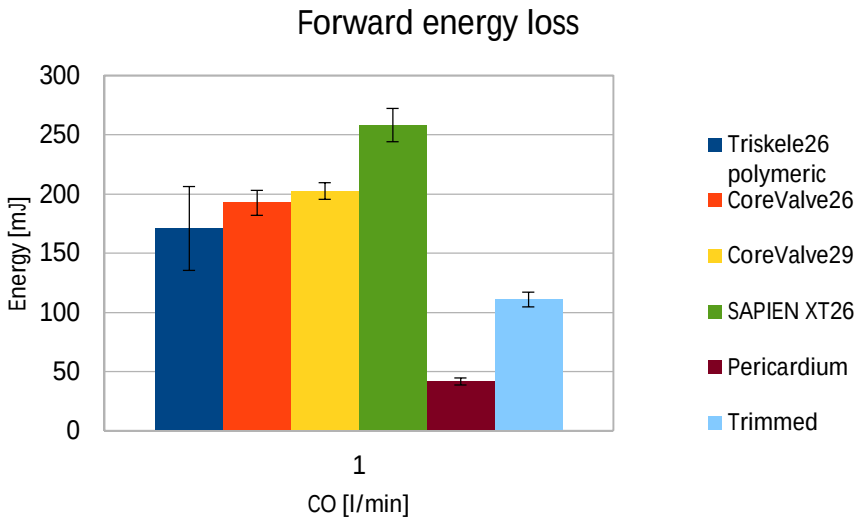

Figure 4.26 Figure 30 Forward energy loss - 23 mm at CO = 5 l/min.
According to a tStudent test, the difference between the control valves' average and pericardium valve's average is significant with p equal to 2.07%

The pericardial and dCell valves exhibited improved function in terms of energy losses. The quantification of the energy loss parameter allows the assessment of both systolic and diastolic characteristics of the heart valves and provides information about the impact of

valve function on myocardial performance [42]. All our valves were characterised by lower values of the energy loss, all over the operating range, confirming their better performance in terms of reduced ventricular workload.

For both pericardial valves and dCell one, Root 21 and Root 23 exhibited a similar trend, which increased as the cardiac output increased. The trends are related to the transvalvular pressure drop; in particular, the bigger is the orifice, the smaller is the pressure drop and consequently the transaortic forward energy loss.

For the pericardial valve, Root 23 globally exhibited a significantly higher TransAortic leakage energy loss compared to Root21. The trends are globally constant as the increased of the cardiac output. On the other hand, Root 23 globally in the trimmed one exhibited a comparable TransAortic leakage energy loss with Root21.

Finally, Root 21 that host the dCell valve has globally a linear trend (increasing up to 6 l/min and decreasing after that).

Overall, the best energy index obtained has been the Leakage energy loss for both pericardial valves in both root configurations. We have got values as low as 40 mJ for both valves compared to 200 mJ of Triskele and CoreValve26. This is in agreement with low Leakage volume as discussed previously. Furthermore, we got high leakage energy loss for dCell valve because of leakage as discussed above (paragraph 4.2.3).

4.2.6 Transaortic Closing Energy Loss

Here are shown the results regarding the Transaortic Closing Energy Loss for the pericardial, dCell and trimmed valve and the comparisons of these valves with the commercial ones. One experiment has been performed for each valve.

In this paragraph the results regarding the Transaortic Closing Energy Loss are shown for the pericardial valve, the dCell valve and the trimmed valve; the comparisons of these valves with the commercial ones are shown. One experiment has been performed for each valve.

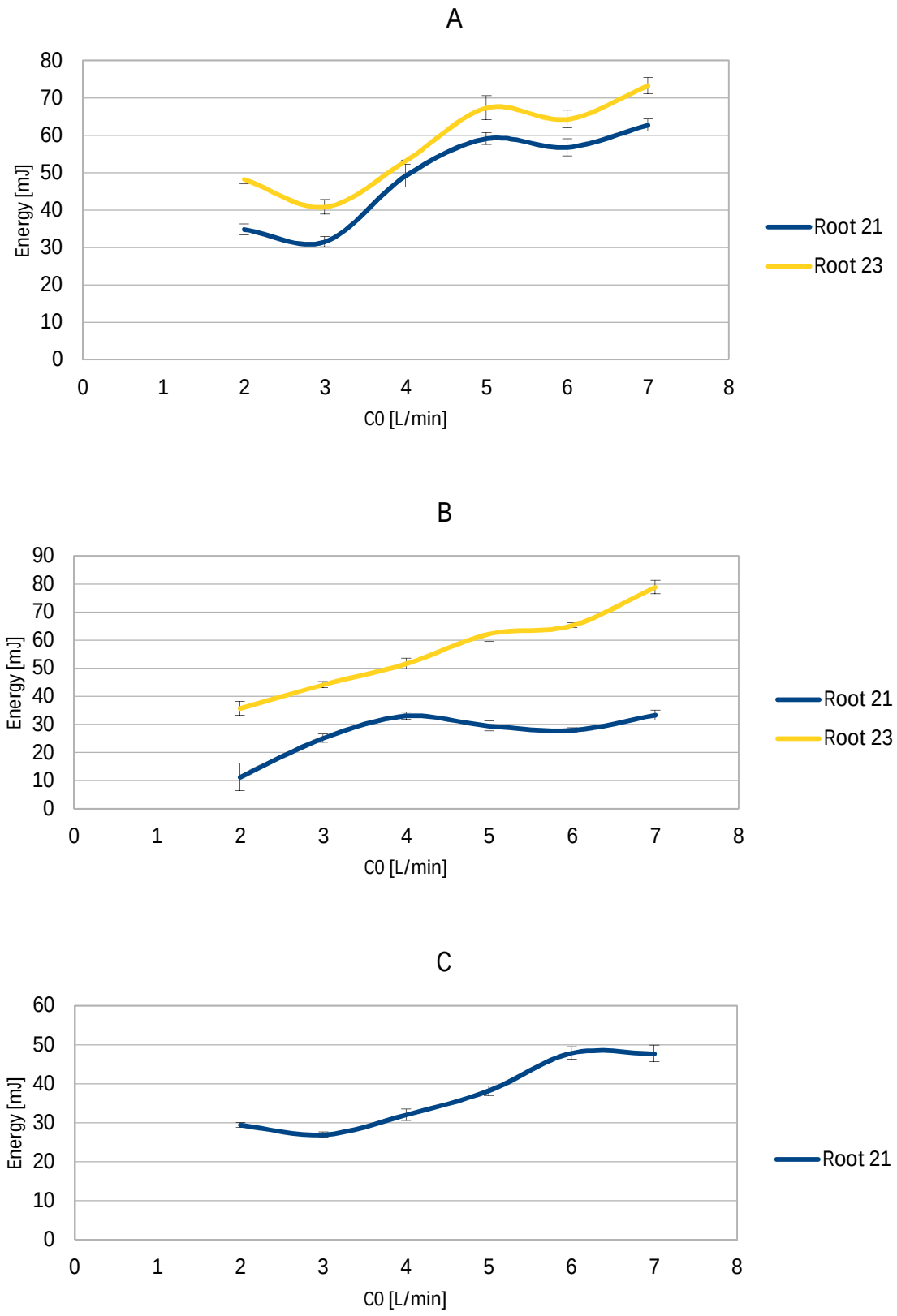

Figure 4.27 TranAortic closing energy loss - A: Pericardial Valve, B: trimmed pericardial valve, C: dCell Valve

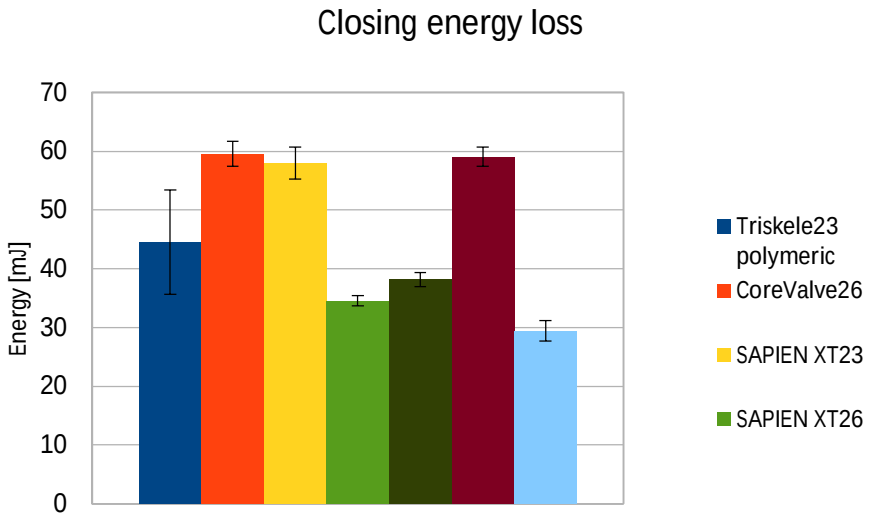

Figure 4.28 Closing energy loss - 21 mm at CO = 5 l/min.
According to a tStudent test, the difference between the control valves' average and pericardium valve's average is not significant

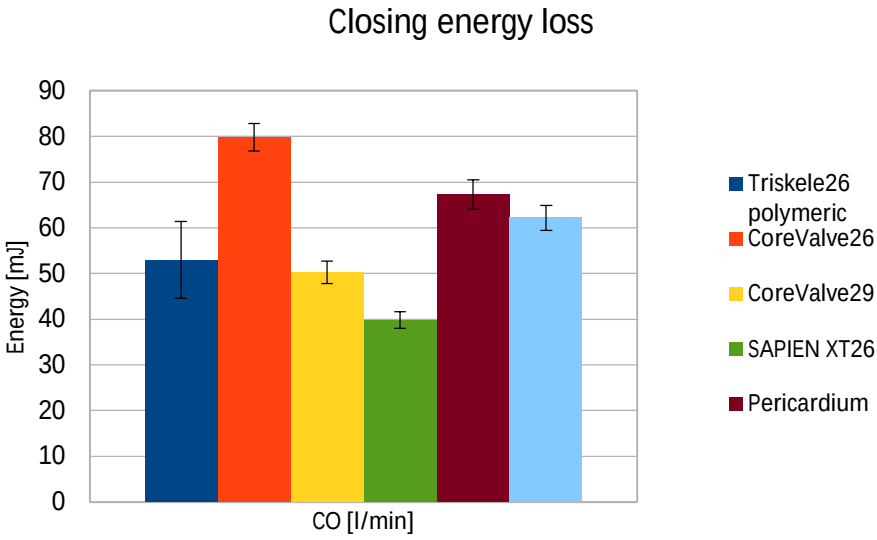

Figure 4.29 Closing energy loss - 23 mm at CO = 5 l/min.
According to a tStudent test, the difference between the control valves' average and pericardium valve's average is not significant

The trends are related to the aortic closing volume; in particular, as the cardiac output increased, the closing volume increased and consequently the energy losses.

For both pericardial valves, the Root 21 and the Root 23 exhibited a similar trend, which increased as the cardiac output increased. Regarding the trimmed one, after 4 l/min both

curves continues to rise but with different slope.

Closing energy loss has the same trend shown above for the Closing Regurgitant Volume. These energy losses are lower than the other valves for the 21 Root configuration and a little bit higher for the 23 ones. This is due to the diameter of the 21 root that is lower than the 23 one; this size difference helps to close the valve more effectively.

4.2.7 Transaortic Leakage Energy Loss

In this paragraph the results regarding the Transaortic Leakage Energy Loss are shown for the pericardial valve, the dCell valve and the trimmed valve; the comparisons of these valves with the commercial ones are shown. One experiment has been performed for each valve.

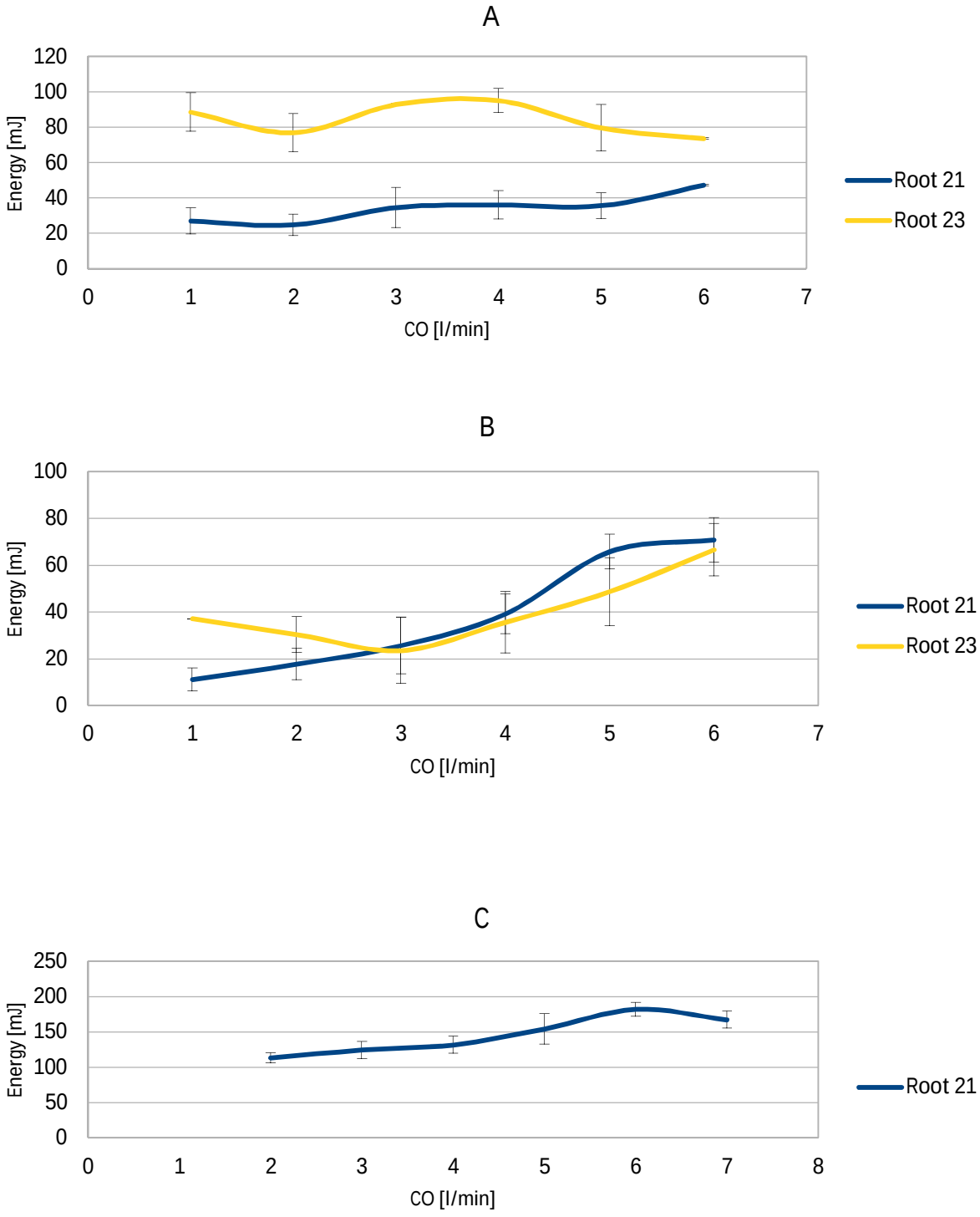

Figure 4.30 TransAortic leakage energy loss - A: Pericardial Valve, B: trimmed pericardial valve, C: dCell Valve

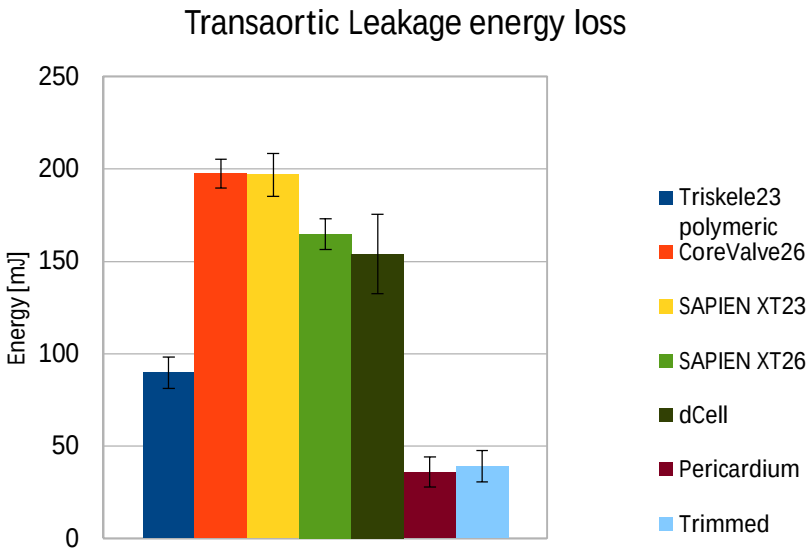

Figure 4.31 Transaortic Leakage energy loss - 21 mm at CO = 5 l/min. According to a tStudent test, the difference between the control valves' average and pericardium valve's average is significant with p equal to 3.05%

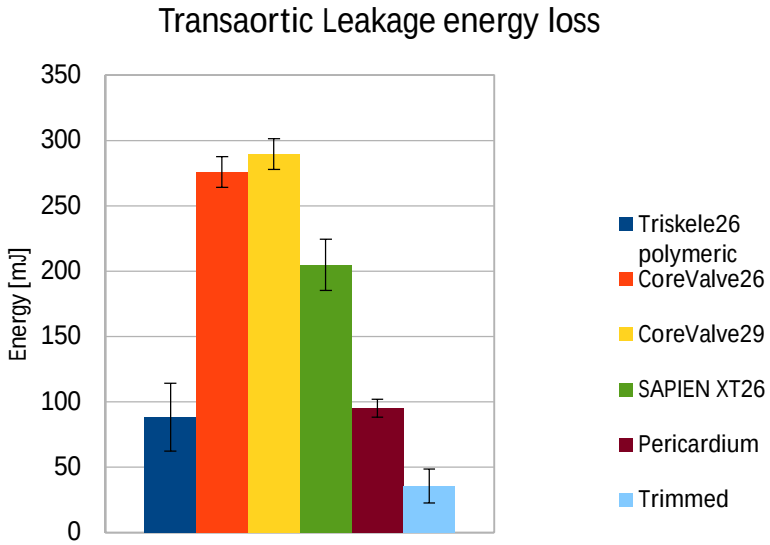

Figure 4.32 Transaortic Leakage energy loss - 23 mm at CO = 5 l/min. According to a tStudent test, the difference between the control valves' average and pericardium valve's average is significant with p equal to 10.48%

For both pericardial valves, the Root 23 globally exhibited a significantly higher Transaortic leakage energy loss compared to the Root21. The trends are globally constant as the increased of the cardiac output for the no-trimmed one and globally linear with the increased of the cardiac output for the trimmed variant and for the dCell valve (increasing

up to 6 l/min and decreasing after that).

This index reflexes the trade of Transvalvular Pressure Drop: in fact, as the transvlavular pressure drops, the transaortic leakage energy losses are much better in our valves than in the control one. A lower forward energy loss means a less obstruction for the flow that passes through the valve when it is opened. This is due to the fact that the shape of the leaflet has been studied to have less obstruction for the fluid and minimal amount of space into the stent once opened.

The gap between our valves and the control ones in terms of losses are lower and lower as Root width becomes bigger and bigger.

4.2.8 Transaortic Total Energy Loss

Here are shown the results regarding the Transaortic Total Energy Loss for the pericardial, dCell and trimmed valve and the comparisons of these valves with the commercial ones. One experiment has been performed for each valve.

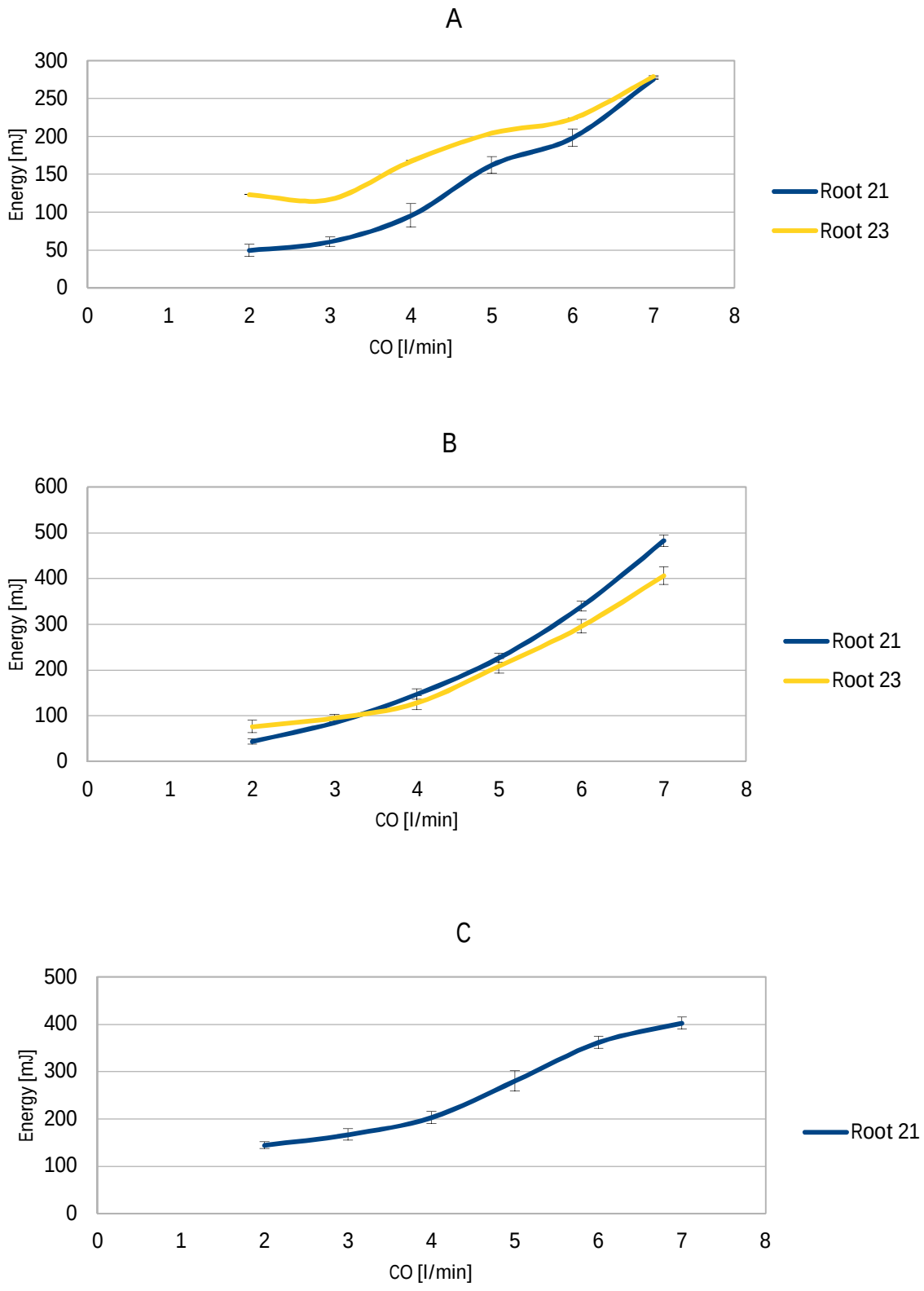

Figure 4.13 TransAortic total energy loss - A: Pericardial Valve, B: trimmed pericardial valve, C: dCell Valve

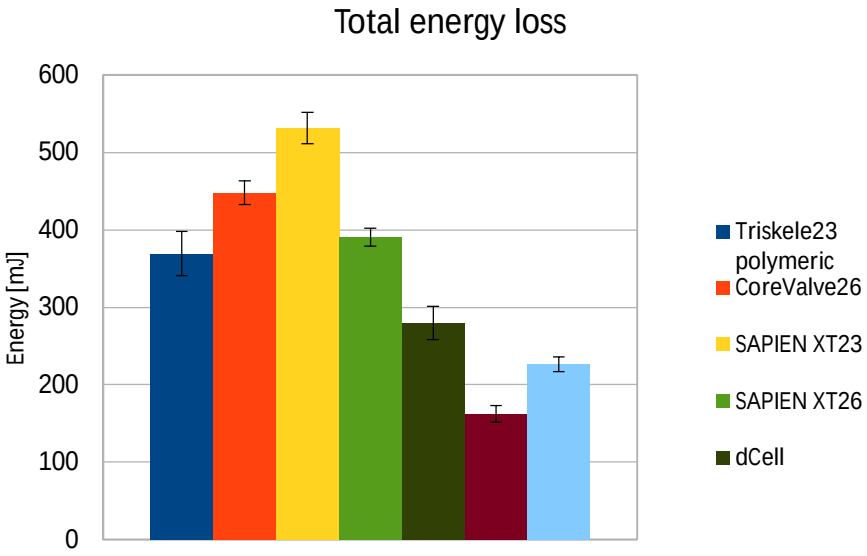

Figure 4.34 Total energy loss - 21 mm at CO = 5 l/min.
According to a tStudent test, the difference between the control valves' average and pericardium valve's average is significant with p equal to 1.41%

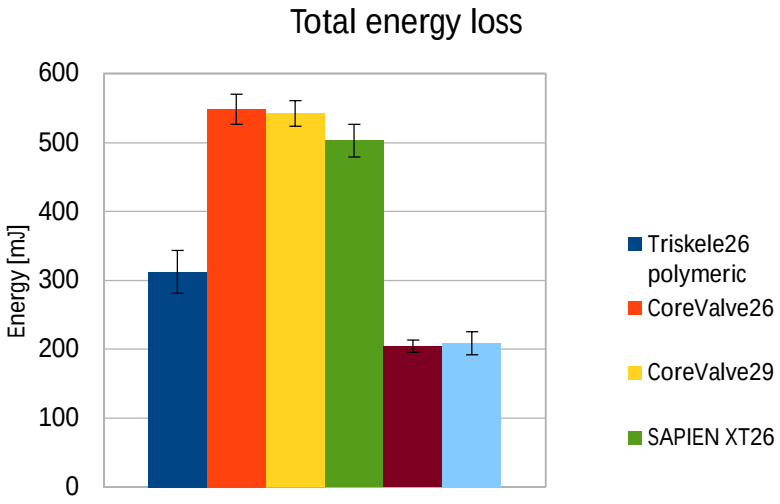

Figure 4.35 Total energy loss - 23 mm at CO = 5 l/min.
According to a tStudent test, the difference between the control valves' average and pericardium valve's average is significant with p equal to 3.2%

For pericardial and dCell valves, the transaortic total energy loss is a global index of the performances of the valve. Root 21 and Root 23 exhibited a trend which increased as the cardiac output increased. Overall the Total Energy Loss regarding our valves is lower than

the control ones because this is a sum of the other energies (that are still lower than the control ones). This allows the heart to spend less energy to move the fluid on.

4.3 Experimental results conclusions

Almost all the parameters have been improved: transvalvular pressure drop, leakage volume, total regurgitant fraction, EOA and leakage. Forward and total energy losses are the ones with the best improvements. Closing regurgitant volume and its energy loss are the only two that are equal or worse than the control one. The main reason was the excessive leaflets length for the no-trimmed pericardium and the short leaflets lenght for the dCell valve. For both pericardial valve and dCell valve, the wings inflate when the leaflets close; this allows less blood to return back to the left ventricle; wings are tall enough to close any open space between the aorta annulus and the implanted valve; this has also been shown by a less aortic leakage and leakage energy loss. In fact, the native valve is typically not removed but it is crushed by the bioprosthesis against the aorta annulus; this fact can results in an incomplete seal between the bioprosthetic valve and aortic annulus, with subsequent occurrence of paravalvular leak (PVL).

Moreover, the ISO recommendations regarding the minimum device performance requirements for EOA and total regurgitant fraction have been fulfilled.

In fact, according to the ISO standard (Figure 4.36), the total regurgitant fraction has to be lower than 20% for both root configuration analyzed. Both configurations in pericardium and trimmed pericardium have values equal to 7-8% (much lower than those obtained by Sapien and CoreValve, that are bigger than 20%).

Parameter	**Deployed valve diameter within implant site** mm							
	17	**19**	**21**	**23**	**25**	**27**	**29**	**31**
A_{EO} (cm^2) greater than or equal to	0,70	0,85	1,05	1,25	1,45	1,70	1,95	2,25
Transvalvular regurgitant fraction (% of forward flow volume) less than or equal to	10	10	10	10	15	15	20	20
Total regurgitant fraction (% of forward flow volume) less than or equal to	15	15	20	20	20	20	25	25

Figure 4.36 Minimum device performance requirements, ISO standard

Even the dCell valve has got value lower than 20% even considering the problems encountered with this tissue described in the previous paragraphs.

The EOA of our valves fulfils the ISO standard; the dCell shows the higher value equal to 2.5 $cm^{2,}$ that is much higher than 1.05 cm^2 (ISO minimum value) and bigger even than Sapien (equal to 1.737 cm^2).

4.4 Computational analysis: results and discussions

An explicit finite element code has been used to perform the analyses; explicit schemes are often more efficient than implicit ones in the solution of problems with large numbers of nodes. They operate by dividing the event into a finite number of time-steps and formulating the equations of motion of every node of the mesh at each time-step. The resulting accelerations are then integrated to evaluate the velocities and the displacement increments. Once this has been done, the nodes are moved to their next position, the model is updated and the procedure repeats for the next time increment. The forces acting on the nodes come from the element stresses, which are calculated from the current values of strains and/or strain rate through whatever constitutive equations represent the material. The advantage over implicit codes comes from the fact that, since each nodal displacement is available directly at every increment of the solution, explicit formulations do not need any global inversion of the stiffness matrix. The price to be paid is a time-step that is small enough to avoid problems of numerical instability. The control of this is usually the time taken for a sound wave to cross the smallest element dimension [4].

In order to study the stress typically involved in possible failure, the maximum and minimum principal stress distribution for all the models, at time equal to 0,34 s, are shown below; in particular, it has been chosen to show the stress fields obtained for the Crimp21 valve and for the Crimp23 valve, more realistic than the nominal valve (see paragraph 3.8.2.3).

4.4.1 Stress distributions

In Figures 4.37, 4.38 and 4.39 the stress distributions are shown at time 0,34 s on the surface of the Crimp23 valve's leaflets, using, respectively, elastic material, Ogden fitting for pericardium and Ogden fitting for decellularized pericardium. The highest stress during closure of all the models are produced during the coaptation of the leaflets. During this stage, the apexes of the leaflets and the commissures zones exhibited the maximum concentration of stresses.

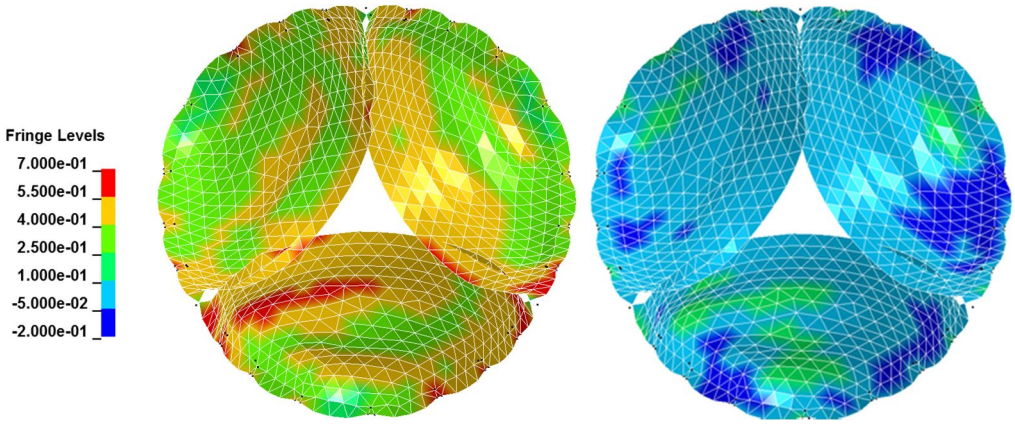

Figure 4.37: Maximum and minimum principal stress distribution at 0.34 s (Crimp23 valve). The material for leaflets is ELASTIC. The values are expressed in MPa

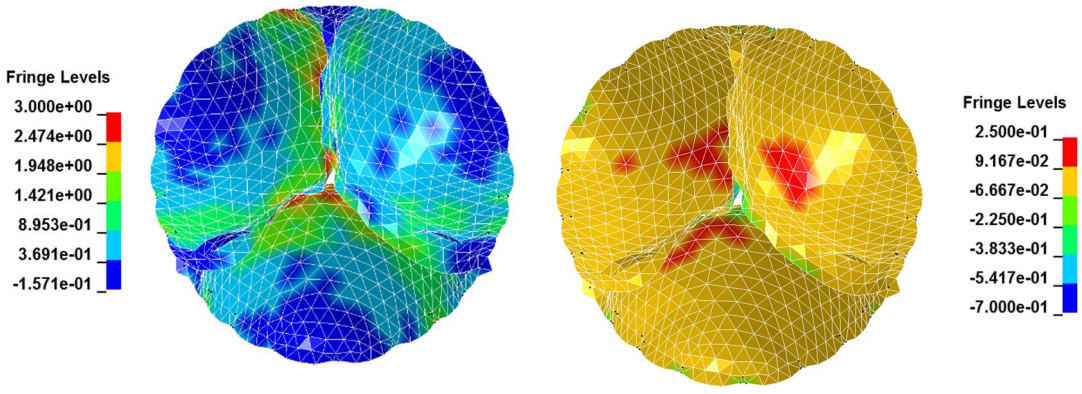

Figure 4.38: Maximum and minimum principal stress distribution at 0.34 s (Crimp23 valve). The material for leaflets is pericardium fitted with Ogden model. The values are expressed in MPa

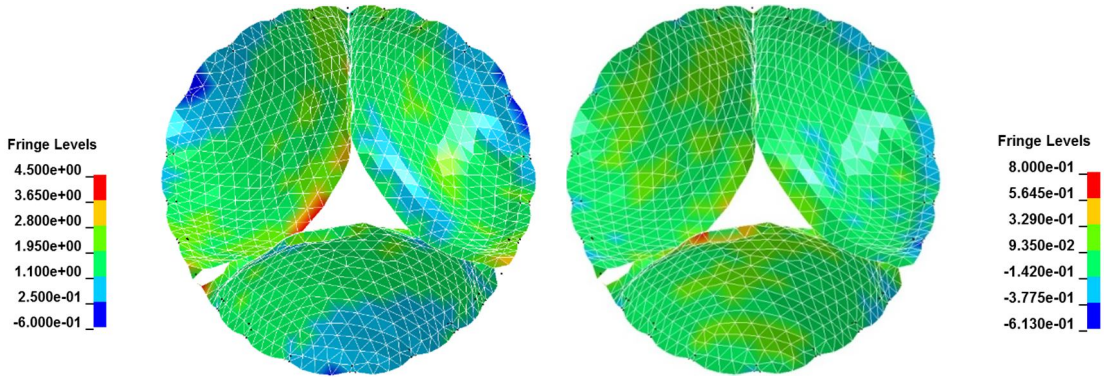

Figure 4.39: Maximum and minimum principal stress distribution at 0.34 s (Crimp23 valve). The material for leaflets is pericardium decellularized fitted with Ogden model. The values are expressed in MPa

As shown in Figures 4.37, 4.38 and 4.39, for the elastic material the maximum stress reached on the surface of the leaflets is 0,7 MPa whereas for the Ogden models the maximum stresses are substantially higher: in particular, for the decellularized pericardium fitted with Ogden model, the maximum stress reaches 4,5 MPa; this value, that is 1,5 MPa higher than the pericardial valve, can be an index of less life expectancy; in fact, the most common forms of failure in pericardial bioprostheses are perforations, often found in association with calcification, caused by fatigue mechanism, common at the sites of high stress concentration [44]. It has been observed that calcification is dominant in the zones of high compression and flexion; for this reason, a good valve design that tends to minimize local concentrations of stress is a good step to improve durability (that represents, in fact, the biggest disadvantage of biological valves) [45][46]. Furthemore, for the leaflets made with decellularized pericardium the closing dynamic is peculiar: due to the absence of cells inside and the very low thickness of the leaflets (0,1 mm for decellularized pericardium against 0,4 mm for elastic model and pericardium model), the closing of the valve is faster than the other materials used for leaflets; for example, the Crimp23 pericardial valve is completely closed at 0,33s whereas the decellularized Crimp23 valve is completely closed at 0,17s (Figure 4.40). This means that for the valve made with decellularized pericardium it is necessary just a pressure equal to 55 mmHg to get it closed.

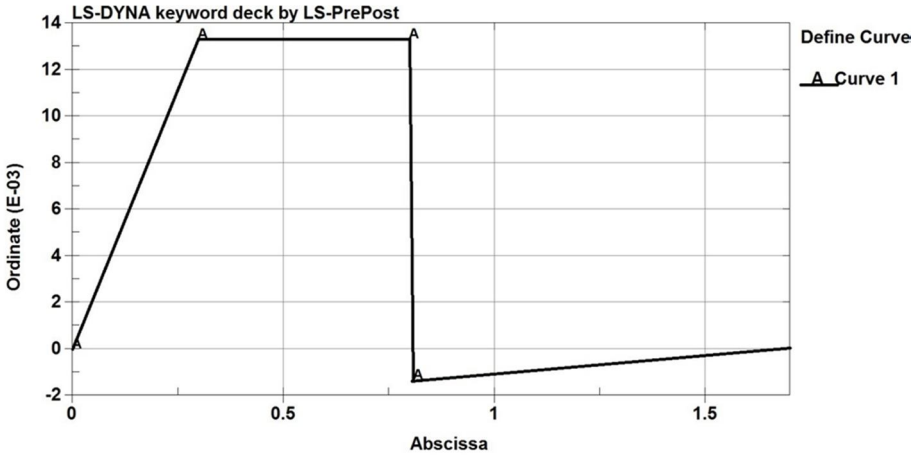

Figure 4.40: Pressure curve used in the dynamic simulations: ordinate expressed in MPa and Abscissa in sec.

Those significant differences in the stress values and in the closing dynamic are associated to different configurations assumed by the leaflets during the coaptation: in the decellularized model, the coaptation takes place at lower height than the standard pericardium. The behavior just described may be quantified with the measure of the coaptation heights, shown in the table 4.1 at time t= 0,34s. They correspond to the axial distance between the nodules of Aranzio and the aortic annulus.

	Coaptation height (mm)
Pericardium	8,215
Dcell Pericardium	5,477

Table 4.1: Coaptation heights at t=0,34 s

In Figures 4.41, 4.42 and 4.43 the stress distributions are shown at time 0,34 s on the surface of the Crimp21 valve's leaflets, using, respectively, elastic material, Ogden fitting for pericardium and Ogden fitting for decellularized pericardium.

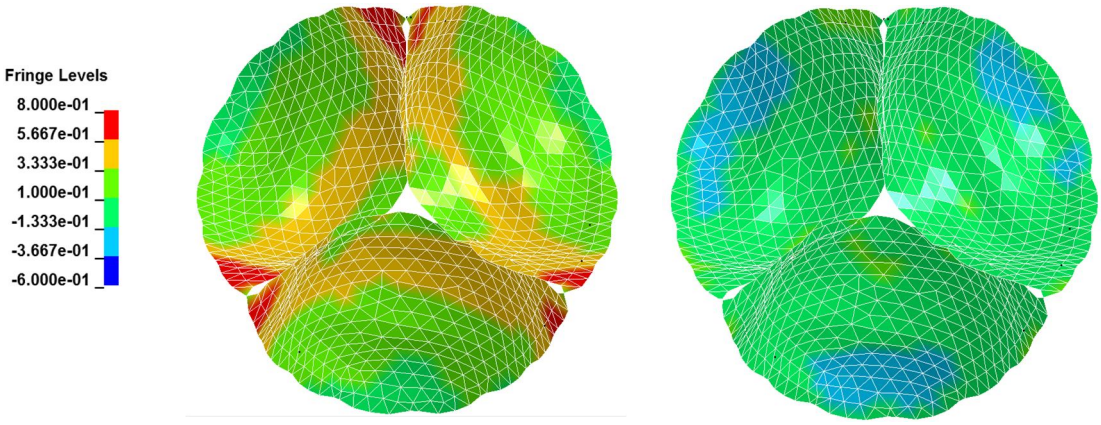

Figure 4.41: Maximum and minimum principal stress distribution at 0.34 s (Crimp21 valve). The material for leaflets is ELASTIC. The values are expressed in MPa

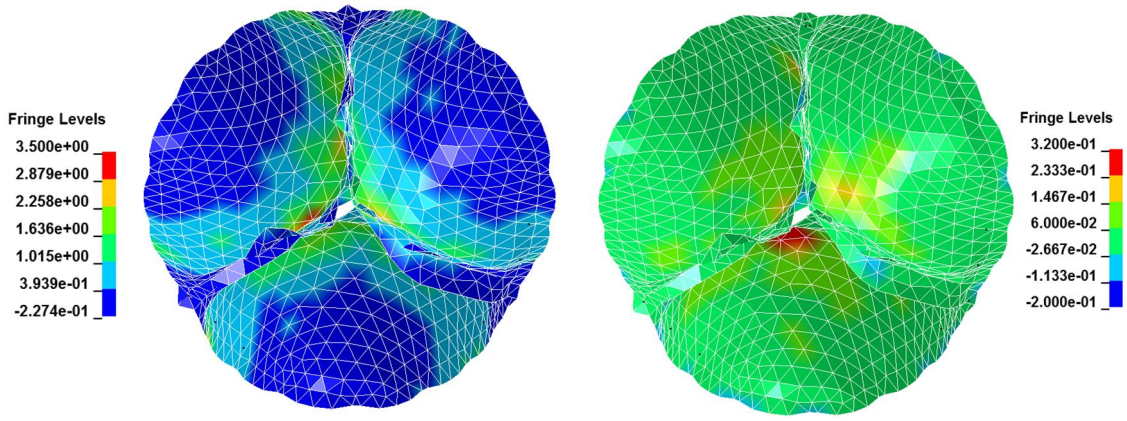

Figure 4.42: Maximum and minimum principal stress distribution at 0.34 s (Crimp21 valve). The material for leaflets is pericardium fitted with Ogden model. The values are expressed in MPa

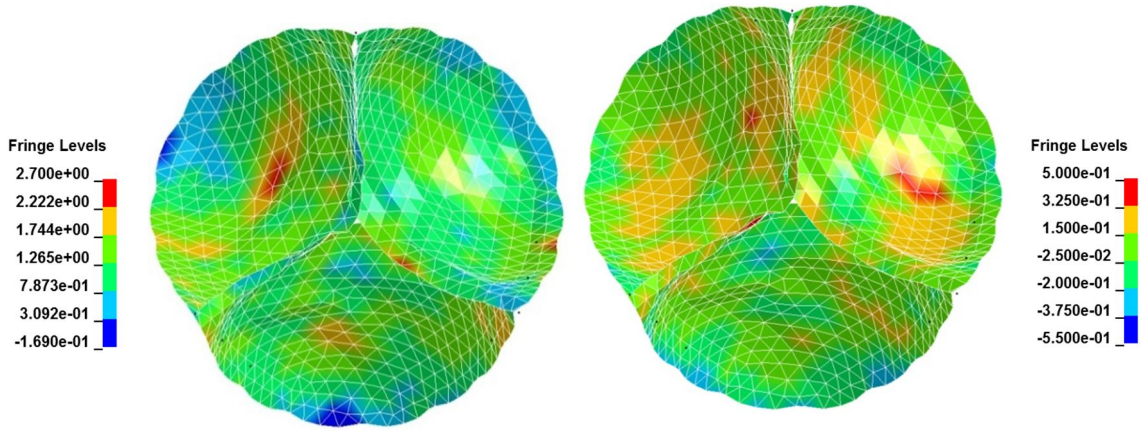

Figure 4.43: Maximum and minimum principal stress distribution at 0.34 s (Crimp21 valve). The material for leaflets is pericardium decellularized fitted with Ogden model. The values are expressed in MPa

As in the Crimp23 valve, the maximum stress reached on the surface of the leaflets are substantially higher with standard and decellularized pericardium than with elastic material.

In both the valves (Crimp23 and Crimp21), during the closure of all the models, the compressive stresses are not very different, in absolute value, from the tensile stresses whereas, at the end of the coaptation, tensile stresses are ten times greater than compressive stresses; at this time the maximum tensile stresses concentrate at the commissures and at the base of leaflets. The average of the maximum principal stresses on the surface of the leaflets shows that, overall and for all the materials, the Crimp23 valve is more stressed than the Crimp21 valve (Table 4.2); furthermore, due to fabric thickness and mechanical properties, the decellularized pericardium shows average stress significantly higher than standard pericardium; this value may be an index of less life expectancy, as explained before.

	Crimp21 valve	**Crimp23 valve**
Elastic	0,289	0,313
Pericardium	0,287	0,437
Dcell Pericardium	0,990	1,250

Table 4.2: Average of maximum principal stresses on the surface of the leaflets at t=0,34 s. Values expressed in MPa

Regarding the coaptation heights during the closure phase, for the Crimp21 valve the values are larger than the Crimp23 valve due to the different crimping of the leaflets, as shown in table 4.3.

	Coaptation height (mm)
Pericardium	8,999
Dcell Pericardium	6,326

Table 4.3: Coaptation heights at t=0,34 s

Decreasing the aortic annulus diameter from 23 mm to 21 mm, increases the coaptation height and consequently the coaptation area, which could lead to improved coaptation and better valve performance [48]. In particular, an increased coaptation area is correlated to reduced insufficiency problems.

Qualitative analysis of the middle hole that is possible to see at the end of the coaptation suggests the importance of the valve crimping with the aim to reduce the regurgitation: in all the models, the hole in the Crimp21 valve is smaller than in the Crimp23 one. This observation suggests the importance to use the correct size of the valve, depending on the valve's design and depending on the specifications of use.

Chapter 5:

Conclusion and Future Developments

A new generation of heart valves has been developed in order to improve the hemodynamic function and reduce the energy absorbed during the operating cycle. The enhanced hydrodynamic function of the pericardial and dCell valves suggests that the proposed valve design is a promising breakthrough in the development of heart valves with potential clinical application. Almost all our valve's performance index have been improved compared to the commercial valve's performance index presented before: transvalvular pressure drop, leakage volume, total regurgitant fraction, EOA and leakage; forward and total energy losses are the ones with the best improvements. Closing regurgitant volume and its energy loss are the only two that are equal or worse than the control ones; the main reason for was the excessive leaflets length for the no-trimmed pericardium and the short leaflets length for the dCell valve.

The valve takes the advantages of both structure: stent and leaflet.

Due to the self-expanding nature of the Nitinol frame of the Stent, it can be deployed in stages allowing for subtle adjustments in position during the deployment phases. In contrast, other valves such as the Sapien Valve are rapidly deployed with a single balloon expansion that does not allow repositioning either during or after deployment. The self-expanding design offers many others potential advantages over a balloon expandable device. First and most important, a self-expanding percutaneous aortic valve may minimize the occurrence of paravalvular leaks and enable the treatment of patients with aortic regurgitation. Secondly, by avoiding balloon trauma to the valve leaflets, the self-expanding design may theoretically prolong valve durability.

Furthermore, the pericardium tissue used for the leaflets can be better tolerated by the human body than polymeric materials.

In order to evaluate the life-time durability of the valves, high-cycled accelerated physiological flow tests will start soon (Figure 5.1).

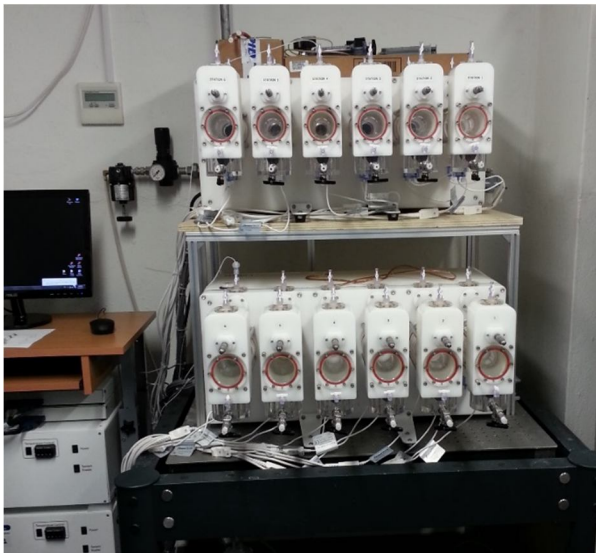

Figure 5.1: High cycles test machine

Due to the limitation observed with the dCell valve (especially for what related with regurgitation, where the dCell valve has shown not such a good behavior), a bigger pericardium patch would be better in order to obtain a valve that could closing completely and showing performances comparable with the pericardial valves.

Regarding the realization of the valves, the choice of using a plastic mold to obtain and suture the shape of the valve was a successful choice but we haven't had the control on the leaflets length; in fact, we cut the triangle in the middle of the valve (Figure 5.2) by hands without any guide throughout the process. During the manufacturing, a good improvement to ensure the correct leaflets length would be the development of another guide, in order to cut the leaflet in the proper way.

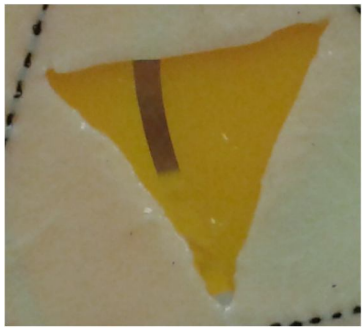

Figure 5.2: Middle leaflets profile showing irregularities

Regarding the computational model, a thicker stitches distribution (for example one stitch every 1 mm) could be useful. More stitches would be preferable in order to make the leaflets follow better the stent profile; furthermore, for the representation of the threads, shell elements could be used instead of solid elements in order to avoid the constraints of the external elements during the dynamic simulation.

Moreover, a crimping simulation that allows the valve to be crimped before the dynamic simulation would be an important step towards a more realistic analysis: in fact, in this work, the Crimp21 configuration and the Crimp23 configuration have been simply obtained by scaling the stent profile and the position of the threads base towards the center. The simulations obtained give an idea of what to expect from those size valves in the final root configuration but they don't take into account the real crimped geometry of the stent and the stress generated by the crimping. Therefore, it should be followed a crimping procedure like what described in Dimasi's thesis [47], applying pressure on different portions of the stent.

At a later stage, it should be useful to utilize the whole geometry of the stent, in order to analyze the stress generated on the aortic root.

Finally, the fluid evaluation should be included in the model in order to get a more realistic simulation.

APPENDIX A

Pericardial valve index results

	Root 21	Root 23	Test
TransAortic mean pressure [mmHg]	-0,644	0,254167	2
	4,063	2,221	3
	4,176	6,161	4
	10,727	9,507	5
	15,985	8,646	6
	12,509	10,012	7

	Root 21	Root 23	Test
Aortic closing volume [ml]	-3,405	-4,625	2
	-3,576	-4,609	3
	-4,084	-5,06	4
	-4,282	-4,98	5
	-4,318	-5,214	6
	-4,44	-5,325	7

	Root 21	Root 23	Test
TransAortic closing energy loss (mJ)	34,793	48,206	2
	31,507	40,786	3
	49,144	53,112	4
	59,081	67,314	5
	56,752	64,259	6
	62,721	73,261	7

	Root 21	Root 23	Test
Aortic leakage volume [ml]	-2,138	-7,509	2
	-2,034	-6,506	3
	-2,825	-8,384	4
	-2,753	-8,708	5
	-3,014	-7,187	6
	-4,108	-6,505	7

	Root 21	Root 23	Test
Aortic regurge fraction (%)	15,022	28,541	2
	11,129	20,891	3
	10,914	19,369	4
	8,859	16,293	5
	7,803	13,022	6
	7,797	10,439	7

	Root 21	Root 23	Test
TransAortic leakage energy loss (mJ)	26,911	88,487	2
	24,668	76,853	3
	34,58	92,759	4
	35,994	95,039	5
	35,569	79,542	6
	47,173	73,486	7

	Root 21	Root 23	Test
Aortic orifice area [PF] (cm2) EOA	9,99	7,078	2
	2,24	3,172	3
	2,556	2,429	4
	2,045	2,224	5
	1,827	2,514	6
	2,314	2,697	7

	Root 21	Root 23	Test
TransAortic forward energy loss (mJ)	-12,337	-13,936	2
	4,527	-0,829	3
	11,608	21,401	4
	66,994	41,912	5
	105,836	79,649	6
	165,7	132,507	7

	Root 21	Root 23	Test
TransAortic total energy loss (mJ)	49,367	122,757	2
	60,702	116,81	3
	95,332	167,271	4
	162,069	204,264	5
	198,157	223,45	6
	275,594	279,254	7

APPENDIX B

Testing machine

Main Parts of the testing machine:

- Pressure readings from atrium, ventricle, and aorta flow can be measured directly at the aortic or mitral sites;
- Optically clear view ports permit ultrasound transmission for flow assessment allows hydrodynamic testing of heart valve replacements in order to assess mechanical and hemodynamic performance;
- Ventricle membrane to replicate the natural chamber flow for testing other implantable cardiac devices.

The ViViTest control system inputs a waveform to the SuperPump while the data acquisition system captures and analyzes physiological pressures and valve flow rates.

Accessories of the machine

- Viscoelastic Impedance Adapter (VIA) The VIA consists of a unique combination of resistive and compliance elements to replicate the viscoelastic properties of the ventricle. It works with the SuperPump to produce realistic waveforms. The dp/dt ratio can be adjusted to produce both physiological and diseased cardiac models.
- The ViVitro heat exchanger is a highly efficient add-on to the ViVitro Pulse Duplicator. It allows the heating of test fluid with minimal interference of the fluid flow. An isolated inflow and outflow metal heat conducting channel transfers heat to the solution maintains testing solution to desired temperature ± 0.5°C.

Software

The software consists of four primary processes: Waveform Acquisition, Waveform Analysis, Waveform Comparison, Waveform Review and one secondary utility: Sensor Calibration.

Process Display

Displays the activity of information gathered.

- a multi-axis graph typically showing both pressure and flow data over a 1.35 pump cycle
- most recent pressure sensor values for most recent ADC analysis
- multiple valve cycles

Figure 41: explanatory graph

A legend bar indicating the meaning of the various colored graph traces. These can be turned on/off to highlight specific data to be viewed:

- RED line – Aortic Pressure
- YELLOW line – Ventricular Pressure
- BLUE line – Atrial Pressure

- PINK line – Transaortic Pressure
- ORANGE line – Transmitral Pressure
- WHITE line – Derived Flow
- GREEN line – Pump dL/dT
- DARK BLUE line – Flow meter
- GREY line – Pump Volume

Machine's Processing Output Parameters

The software uses a number of various calculations to output accurate and relevant information.

$$EOA = \frac{Q_{rms}}{51.6\sqrt{\frac{\Delta p}{\rho}}}$$

Equation 1 formula for the calculation of the Effective Orifice Area

$$Q_{rms} = \sqrt{\frac{\int_{t1}^{t2} Q(t)^2 \, dt}{t_2 - t_1}}$$

Equation 2 formula for the calculation of the average flow

Crossover points are defined as follows	
F1 - Flowrate - Beginning of systole Forward Flow	P1 - Pressure Drop - Beginning of Systole Positive Pressure Drop
F2 - Flowrate - End of systole forward flow	P2 - Pressure Drop - End of Systole Positive Pressure Drop
F3 - Flowrate – Outflow Valve Closing, leakage begins	P3 - Pressure Drop - Beginning of Diastole Positive Pressure Drop
F4 - Flowrate - End of Leakage/Cycle	P4 - Pressure Drop - End of Diastole Positive Pressure Drop
(P) Calculated between Positive pressure markers (F) Calculated between Flow markers (H) Calculated between first Pressure and second Flow marker	

Table 1: crossover point on the graph

General parameters

Cardiac Output (Liters per Minute):

Mean Flowrate (F1 to F4)

Heart Rate (beats per min):

(60 (sec/min)) / Total Period (sec)

Total Period = total points between F1 to F4 / sample Rate (samples/sec)

Total Period (sec):

#samples between F1 to F4/sample Rate (samples/sec)

Flow parameters

Pump Stroke Volume (ml):

(Maximum Position signal – Minimum Position signal)* Cross-sectional Area of piston.

Calculated Stroke Volume (ml):

Cardiac Output (l/min) *1000 (ml/l) / Heart rate (beats/min)

Systolic percent of time

#samples between maximum and minimum position signal/# points between F1 and F4

Forward flow time

#samples between f1 to f2/ sample Rate (samples/sec) [F3 to F4 for Mitral]

RMS Forward Flow (ml/sec):

(RMS Flowrate (f1 to f2) *1000)/60 (sec/min) [F3 to F4 for Mitral]

Mean Forward Flow (ml/sec):

Mean Flowrate (f1 to f2) *1000)/60 (sec/min) [F3 to F4 for Mitral]

Forward Flow Volume (ml):

Flowrate Area (F1 to F2)*1000(ml/Liter)/60(sec/min) [F3 to F4 for Diastolic FF volume]

Closing Volume (ml):

(flowrate Area (F2 to F3))*1000(ml/Liter)/60(sec/min) [F1 to F2 for Mitral]

Leakage Volume (ml):

(flowrate Area (F3 to F4))*1000(ml/Liter)/60(sec/min) [F2 to F3 for Mitral]

Regurgitant Fraction (RF) (%):

(closing volume + leakage Volume)*100/Forward Volume

Forward Flow Ratio (%):

Forward Flow time *100 / Sample rate (samples/sec)

Mean Leakage Flowrate (ml/sec):

-1* (Mean Flowrate (F3 to F4)) [F2 to F3 for Mitral]

Pressure parameters

Mean Pressure Drop [P] (mmHg):

(Mean of pressure difference between outflow and inflow of points between P1 to P2) [P3 to P4 for Mitral]

Mean Pressure Drop [F] (mmHg):

(Mean of pressure difference between outflow and inflow of points between F1 to F2) [F3 to F4 for Mitral]

Back Pressure (mmHg):

-1* (Mean Pressure Drop (F3 to F4))

Maximum Pressure Drop (mmHg):

Maximum Pressure Drop value between Points P1 to P2

Mean Aortic Pressure (mmHg):

Mean Aortic/Proximal/Pulmonary Pressure between P1 to P4 without compensation

RMS Aortic Pressure (mmHg):

RMS of aortic pressure F1 to F4 without compensation

Peak Aortic Pressure (mmHg):

Peak Aortic Pressure between P1 to P2 [Mitral between P3 to P4]

Mean Vent Pressure (mmHg):

Mean Vent Pressure between P1 to P4

Peak Vent Pressure (mmHg):

Peak Vent Pressure between P1 to P4

Parameters based on pressure and flow

E.O.A. (cm^2):

RMS Forward Flow (ml/sec)/51.6*(Square Root (Mean Pressure Drop/Density))

Parameters based on Energy

Energy loss is calculated by integrating the flow times the transvalvular pressure over a relevant flow interval. A conversion factor of 0.1333 is applied to convert the energy from mmHg*ml to millijoules (mj).

Ventricular energy is computed using the following integral

$$VE = Conversion\ factor * \int_{F1}^{F4} P_{vent} * DL\_Dt(\frac{ml}{s}) * dt$$

Forward Energy (FE) (mj):

$$FE = Conversion\ factor * \int_{F1}^{F2} \Delta P * flow\ (\frac{ml}{s}) * dt$$

Closing Energy (CE) (mj):

$$CE = Conversion\ factor * \int_{F2}^{F3} \Delta P * flow\ (\frac{ml}{s}) * dt$$

Leakage Energy (LE) (mj):

$$LE = Conversion\ factor * \int_{F3}^{F4} \Delta P * flow\ (\frac{ml}{s}) * dt$$

Total Energy (mj):

Forward Energy+Closing Energy+Leakage Energy

APPENDIX C

Ogden Material Model: Experimental Data to LS-Dyna Model

Theory

In the Ogden material model, the strain energy density (W) is expressed in terms of the principal stretches: λ_1 λ_2 λ_3, see Fig.7.

$$\text{stretch or extension ratio} = \frac{\text{final length}}{\text{original length}}$$

$$\text{stretch or extension ratio} = \lambda = \frac{l}{L_0}$$

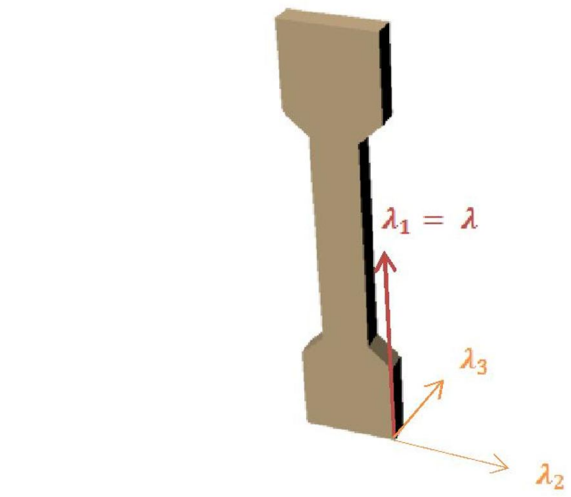

Fig.7: *Uniaxial tensile test specimen; orientation of principle stretches*

$$W(\lambda_1, \lambda_2, \lambda_3) = \sum_{p=1}^{N} \frac{\mu_p}{\alpha_p} (\lambda_1^{\alpha_p} + \lambda_2^{\alpha_p} + \lambda_3^{\alpha_p} - 3)$$

Where N, μ_P, α_P are materials constants.

Isotropic behaviour is when a material has the same material properties in all directions. This will be assumed to be true for pericardium and so:

$\lambda_{2=} \lambda_3$

incompressible behaviour means there is no change in volume and so the determinant of the deformation gradient tensor F must be equal to the Jacobian (J) and equal to 1.

The deformation gradient tensor F:

$$F = \begin{bmatrix} \lambda_1 & 0 & 0 \\ 0 & \lambda_2 & 0 \\ 0 & 0 & \lambda_3 \end{bmatrix}$$

$$\det(F) = 1$$

(using isotropic relationship)

$$\lambda_1 \lambda_2 \lambda_3 = \lambda_1 \lambda_2^2 = 1$$

$$\lambda_2 = \frac{1}{\sqrt{\lambda_1}}$$

So:

$$\lambda_1 = \lambda_1$$

$$\lambda_2 = \frac{1}{\sqrt{\lambda_1}}$$

$$\lambda_3 = \lambda_2 = \frac{1}{\sqrt{\lambda_1}}$$

Writing it more simply: (now relevant for uniaxial tensile test data with one extension measurement

$$\lambda_1 = \lambda$$

$$\lambda_2 = \frac{1}{\sqrt{\lambda}}$$

$$\lambda_3 = \frac{1}{\sqrt{\lambda}}$$

Substituting:

$$W(\lambda) = \sum_{p=1}^{N} \frac{\mu_p}{\alpha_p} (\lambda^{\alpha_p} + \left(\frac{1}{\sqrt{\lambda}}\right)^{\alpha_p} + \left(\frac{1}{\sqrt{\lambda}}\right)^{\alpha_p} - 3)$$

In general the shear modulus results from:

$$2\mu = \sum_{p=1}^{N} \mu_p \alpha_p$$

RUBBERS N=3

NEO-HOOKEAN SOLID N=1, α=2

MOONEY-RIVLIN MATERIAL N=2, α_1=2, α_2=2

With the constrained condition: $\lambda_1 \lambda_2 \lambda_3 = 1$

Using the Ogden material model, the three principle values of the Cauchy stresses can now be computed as; the cauchy stress is:

$$\sigma = \begin{bmatrix} \sigma_{11} & \sigma_{12} & \sigma_{13} \\ \sigma_{21} & \sigma_{22} & \sigma_{23} \\ \sigma_{31} & \sigma_{32} & \sigma_{33} \end{bmatrix}$$

$$\sigma_{11} = p + \lambda_1 \frac{\partial W}{\partial \lambda_1}$$

$$\sigma_{22} = p + \lambda_2 \frac{\partial W}{\partial \lambda_2}$$

$$\sigma_{33} = p + \lambda_3 \frac{\partial W}{\partial \lambda_3}$$

For membranes α_{33}=0 therefore;

$$\sigma_{33} = p + \lambda_3 \frac{\partial W}{\partial \lambda_3} = 0$$

$$p = -\lambda_3 \frac{\partial W}{\partial \lambda_3}$$

So;

$$\sigma_{11} = \lambda_3 \frac{\partial W}{\partial \lambda_3} + \lambda_1 \frac{\partial W}{\partial \lambda_1}$$

$$\sigma_{22} = \lambda_3 \frac{\partial W}{\partial \lambda_3} + \lambda_2 \frac{\partial W}{\partial \lambda_2}$$

$$\sigma_{33} = 0$$

$$\lambda_1 = \lambda$$

$$\lambda_2 = \frac{1}{\sqrt{\lambda}}$$

$$\lambda_3 = \frac{1}{\sqrt{\lambda}}$$

Implementation in Excel

A four parameter Ogden material model that best fits experimental data can be derived using excel.

Input Values

Extension (measured by the Zwick tensile testing machine)

Original Length = 20 mm

Experimental Stress = $\alpha_{11,exp}$

Equations

Stretch: $\lambda = \frac{extension+20}{20}$

$$\lambda_2 = \frac{1}{\sqrt{\lambda}}$$

$$\lambda_3 = \frac{1}{\sqrt{\lambda}}$$

$$W = \left(\frac{\mu_1}{\alpha_1}\right)\left(\lambda_1^{\alpha_1} + \lambda_2^{\alpha_1} + \lambda_3^{\alpha_1} - 3\right) + \left(\frac{\mu_2}{\alpha_2}\right)\left(\lambda_1^{\alpha_2} + \lambda_2^{\alpha_2} + \lambda_3^{\alpha_2} - 3\right)$$

$$\frac{\partial W(\lambda)}{\partial \lambda} = \mu_1\left(\lambda_1^{(\alpha_1-1)}\right) + \mu_2(\lambda_1^{(\alpha_2-1)})$$

$$p = \mu_1\left(\lambda_3^{(\alpha_1-1)}\right) + \mu_2(\lambda_3^{(\alpha_2-1)})$$

This resulted in the output values shown below.

Output values

$$\sigma_{11} = \lambda_1 \left(\frac{\partial W(\lambda)}{\partial \lambda} \right) + p$$

$$\textbf{Shear Modulus } [MPa] = \mu_1 \alpha_1 + \mu_2 \alpha_2$$

When the above equations were implemented in excel, the parameters were found such that the sum of the squared differences was minimised, see evaluation below.

Evaluation

$$\Delta\sigma^2 = (\sigma_{11,exp} - \sigma_{11})^2$$

$$\textbf{SUM}(\Delta\sigma^2) = sum\ of\ all\ \Delta\sigma^2\ values$$

Bibliography:

[1] Boudjemline Y., Bonhoeffer P., « Images in cardiovascular medicine. Percutaneous aortic valve replacement in animals. », *Circulation*, 109:e161, 2004.

[2] Rahmani B., Burriesci G., Mullen M., Seifalian A., Tzamtzis S., Yap J., « A New Generation Transcatheter Heart Valve with a Novel Nanocomposite Material and Fully Retrievable Design. »,*Cardiovascular Interventions*, 60(17), B34, 2013.

[3] Forrest J.K., « Transcatheter aortic valve replacement: design, clinical application, and future challenges », *Yale J Biol Med.*, 85(2):239-47, 2012.

[4] Burriesci G, Howard I.C., Patterson E.A., « Influence of anisotropy on the mechanical behaviour of bioprosthetic heart valves », *Journal of Medical Engineerign and Technology*, vol 23, pp. 203-215, 1999.

[5] Underwood M.J., El Khoury G., Deronck D., Glineur D., Dion R., « The aortic root: structure, function, and surgical reconstruction », *Heart*, 83, pp. 376-380, 2000.

[6] Nkomo V.T., Gardin J.M., Skelton T.N., Gottdiener J.S., Scott C.G., Enriquez-Sarano M. « Burden of valvular heart diseases: a population-based study », *Lancet*, 368, pp. 1005-1011, 2006.

[7] Michaels A.D., Lederman R.J., MacGregor J.S. « Cardiovascular involvement in AIDS », *Curr Probl Cardiol*, 22, pp. 109–148, 1997.

[8] Hojnik M., George J., Ziporen L., « Heart valve involvement (Libman-Sacks endocarditis) in the antiphospholipid syndrome », *Circulation*, 93, pp. 1579-1587, 1996.

[9] Soler-Soler J., Galve E., « Worldwide perspective of valve disease », *Heart,* 83, pp.721–725, 2000.

[10] Coasts L., Bonhoeffer P., « New percutaneous treatments for valve disease», Heart, 93, pp. 639–644, 2007

[11] Hopkins R., « From cadaver harvested homograft valves to tissue-engineered valve conduits », *Prog Pediatr Cardiol*, 21, pp. 137-152, 2006.

[12] Friedewald V.E., Bonow R.O., Borer J.S., « The editor's roundtable: cardiac valvesurgery. » *Am J Cardiol*, 99, pp. 1269–1278, 2007.

[13] Grube E., Laborde J., Gerckens U., « First experience with a new self expanding aortic valve prosthesis for percutaneous treatment of aortic valve disease in high risk patients. » *Am J Cardiol*, 96, 50H, 2005.

[14] Iung B., Baron G., Butchart E.G., « A prospective survey of patients with valvular heart disease in Europe: The Euro heart survey on valvular heart disease. » *Eur Heart J,* 24, pp. 1231–1243, 2003.

[15] Barnett S.D., Halpin L.S., Speir A.M., « Postoperative complications among octogenarians after cardiovascular surgery. » *Ann Thorac Surg,* 76, pp. 726–731, 2003.

[16] Colon G., Perez C.M., Guzman M. « Perioperative outcomes in octogenarians undergoing cardiac surgery in Puerto Rico. » *P R Health Sci,* J 19, pp. 115–122, 2000.

[17] Walther T., Falk V., Mohr F.W. « Minimally invasive surgery for valve disease. » *Curr Probl Cardiol,* 31, pp. 399–437, 2006.

[18] Sakata Y., Syed Z., Salinger M.H., « Percutaneous balloon aortic valvuloplasty: antegrade transseptal vs. conventional retrograde transarterial approach. » *Catheter Cardiovasc Interv,* 64, pp. 314–321, 2005.

[19] Cribier A., Eltchaninoff H., Tron C., « Treatment of calcific aortic stenosis with the percutaneous heart valve: mid-term follow-up from the initial feasibility studies: the French experience. » *J Am Coll Cardiol,* 47, pp. 1214–1223, 2006.

[20] Boudjemline Y., Bonhoeffer P. « Steps toward percutaneous aortic valve replacement. » *Circulation,* 105, pp. 775–778, 2002.

[21] Davidson M.J., White J.K., Baim D.S., « Percutaneous therapies for valvular heart disease. » *Cardiovasc Pathol,* 15, pp. 123–129, 2006.

[22] Neale T., « Vascular Problems Affect TAVI. » *Perelman School of Medicine at the University of Pennsylvania*, 2012.

[23] Di Marco F., Gerosa G., « Percutaneous aortic valve replacement: which patients are suitable for it? A question for a controlled use. » *J Thorac Cardiovasc Surg,* 133, pp. 294–298, 2007.

[24] Attmann T., Jahnke T., Quaden R., « Advances in experimental percutaneous pulmonary valve replacement. » *Ann Thorac Surg,* 80, pp. 969–975, 2005.

[25] Attmann T., Quaden R., Jahnke T., « Percutaneous pulmonary valve replacement: 3-month evaluation of self-expanding valved stents. » *Ann Thorac Surg,* 82, pp. 708–714, 2006.

[26] Attmann T., Lutter G., Quaden R., « Percutaneous valve replacement: significance of different delivery systems in vitro and in vivo. » *Cardiovasc Intervent Radiol,* 29, pp. 406–412, 2006.

[27] Lutter G., Ardehali R., Cremer J., « Percutaneous valve replacement: Current state and future prospects. » *Ann Thorac Surg*, 78, pp. 2199–2206, 2004.

[28] Cribier A., Eltchaninoff H., Tron C., « Early experience with percutaneous transcatheter implantation of heart valve prosthesis for the treatment of end-stage inoperable patients with calcific aortic stenosis. » J Am Coll Cardiol, 43, pp. 698–703, 2004.

[29] Zegdi R., Khabbaz Z., Borenstein N., « A repositionable valved stent for endovascular treatment of deteriorated bioprostheses. » *J Am Coll Cardiol*, 48, pp. 1365–1368, 2006.

[30] Salahieh A., Brandt B., Morejohn D., « Repositionable heart valve and method. » *US patent 20050137688*, 2005.

[31] Meine T.J., Harrison J.K. « Should we cross the valve: The risk of retrograde catheterization of the left ventricle in patients with aortic stenosis. » *Am Heart J*, 148, pp. 41–42, 2004.

[32] Quaden R., Klaws G.R., Theisen-Kunde D., « Percutaneous aortic valve replacement: first endovascular resection of human aortic valves in situ. » *Eur J Cardiothorac Surg*, 31, pp.305, 2007.

[33] Eltchaninoff H., Nusimovici-Avadis D., Babaliaros V., « Five month study of percutaneous heart valves in the systemic circulation of sheep using a novel model of aortic insufficiency. » *Euro Interv*, 1, pp. 438–444, 2006.

[34] Eltchaninoff H., Tron C., Babaliaros V., « Treatment of calcific aortic stenosis with the Edwards percutaneous heart valve: Mid-term follow-up from the initial feasibility studies. » *J Am Coll Cardiol*, 47:11B, 2006.

[35] Attmann T., Quaden R., Freistedt A., « Percutaneous heart valve replacement: histology and calcification characteristics of biological valved stents in juvenile sheep. » Cardiovasc Pathol, 16, pp. 165–170, 2007.

[36] Ferreira M., Luersen M.A., Borges P.C., « Nickel-titanium alloys: A systematic review. » *Dental Press J Orthod.*, 17(3), pp. 71-82, 2012.

[37] Duerig, Pelton, Stoeckel,«An Overview of Nitinol Medical Applications.», *Materials Science and Engineering*, A273-275, pp.149-160, 1999.

[38] Ishihara T., Ferrans V.J., Jones M., Boyce S.W., Roberts N.C., « Structure of bovine parietal pericardium and of unimplanted Ionescu-Shiley pericardial valvular bioprostheses.» *Journal of Thoracic and Cardiovascular Surgery*, 81, 747, 1981.

[39] Elias H., Boyd L.J., « Notes on the anatomy, embriology and the histology of the pericardium. » *Journal of New York Medical College*, 2, 50, 1960.

[40] Sanchez-Arevalo F.M., Farfan M., Covarrubias D., Zenit R., Pulos G., « The micromechanical behaviour of lyophilized glutaraldehyde-treated bovine pericardium under uniaxial tension. » *Journal of the Mechanical Behaviour of Biomedical Materials*, 3(8), pp. 640-646, 2010.

[41] Bakhtiary F., Dzemali O., Steinseiffer U., Schmitz C., Glasmacher B., Moritz A., Kleine P., « Opening and closing kinematics of fresh and calcified aortic valve prostheses: an in vitro study. »*The Journal of Thoracic and Cardiovascular Surgery*, 134, pp. 657–662, 2007.

[42] Akins C.W., Travis B., Yoganathan A.P., « Energy loss for evaluating heart valve performance. » *The Journal of Thoracic and Cardiovascular Surgery*, 136 (4), pp. 820–833, 2008.

[43] Apostolakis E., Baikoussis N.G., Papakonstantinou N.A., Goudevenos J., « Patient-prosthesis mismatch and strategies to prevent it during aortic valve replacement. » *Hellenic Journal of Cardiology*. Hellenike Kardiologike Epitheorese, 52, pp. 41–51, 2011.

[44] Schuster P. R., Wagner J. W., « A preliminary durability study of two types of low-profile pericardial bioprosthetic valves through the use of accelerated fatigue testing and flow characterisation, » *J Biomed Mater Res*, 23(2), pp. 207-222, 1989.

[45] Thubrikar M.J., Deck J.D., Aouad J., Nolan S.P., « Role of mechanical stress in calcification of aortic bioprosthetic valves, » *J Thorac Cardiovasc Surg.*,86(1), pp. 115-25, 1983.

[46] Nolan S. P., « Role of mechanical stress in calcification of aortic bioprosthetic valves. » *Journal of Thoracic Cardiovascular Surgery*, 86, pp. 115-125, 1983.

[47] Dimasi A., « Modelli computazionali per la valutazione dell'effetto delle calcificazioni della valvola aortica sull'esito dell'impianto di una valvola aortica percutanea, » Tesi di Laurea Magistrale: Politecnico di Milano, 2013.

[48] Marom G., Rami H.A., Rosenfeld M., Schafers H.J., Raanani E, «Aortic root numeric model: Annulus diameter prediction of effective height and coaptation in post–aortic valve repair», The journal of thoracic and cardiovascular surgery, 2012.

[49] Mano Thubrikar, «The aortic valve», Library of Congress USA, 1990.